THE KINETICS AND MECHANISM OF SUPEROXIDE REDUCTION BY TWO-IRON SUPEROXIDE REDUCTASE FROM *DESULFOVIBRIO VULGARIS*

by

JOSEPH PATRICK EMERSON

(Under the direction of Donald M. Kurtz, Jr.)

ABSTRACT

Superoxide reductase (SOR) has been recently found in anaerobic bacteria and archaea, and is proposed to be involved in a pathway of oxidative resistance. The sulfate reducing-anaerobic bacterium *Desulfovibrio vulgaris* expresses an SOR, which contains two non-heme iron centers. A novel [Fe(NHis)$_4$(SCys)] site is proposed to interact with superoxide, and a rubredoxin-like, [Fe(SCys)$_4$] site is presumably involved in electron transfer. In order to better understand the oxidative stress resistance pathway within anaerobic bacteria, a detailed kinetic study of the reaction of the *D. vulgaris* 2Fe-SOR, along with several engineered variants are studied as they interact with several reactive oxygen species. Identification of a transient species produced from the reaction of SOR with superoxide is described, as well as the kinetics associated with formation and decay are elaborated upon. The role of the [Fe(SCys)$_4$] site is explored by characterization of a [Fe(SCys)$_4$] deficient variant of *D. vulgaris* 2Fe-SOR.

INDEX WORDS: Superoxide reductase, *Desulfovibrio vulgaris*, Oxidative stress, Oxidative stress resistance, Pulse radiolysis, Stopped-flow, Transient, Reactive oxygen species, Dioxygen, Superoxide, Hydrogen peroxide

THE KINETICS AND MECHANISM OF SUPEROXIDE REDUCTION BY TWO-IRON SUPEROXIDE REDUCTASE FROM *DESULFOVIBRIO VULGARIS*

by

JOSEPH PATRICK EMERSON

B.S., The University of Wisconsin-Eau Claire, 1999

A Dissertation Submitted to the Graduate Faculty of The University of Georgia in Partial Fulfillment of the Requirements of the Degree

DOCTOR OF PHILOSOPHY

AHTENS, GA

2003

THE KINETICS AND MECHANISM OF SUPEROXIDE REDUCTION BY TWO-IRON SUPEROXIDE REDUCTASE FROM *DESULFOVIBRIO VULGARIS*

by

JOSEPH PATRICK EMERSON

Approved:

Major Professor: Donald M. Kurtz, Jr.

Committee: Michael W. Adams
I. Jonathan Amster
Michael K. Johnson
Robert J. Maier

Electronic Version Approved:

Maureen Grasso
Dean of the Graduate School
The University of Georgia
May 2003

DEDICATION

I dedicate this work to my son, Griffin Emerson. I am truly amazed everyday at the little things that a son *teaches* a father.

ACKNOWLEDGEMENTS

I would like to thank my mentor, Dr. Donald Kurtz, Jr., for his support of my studies at the University of Georgia. I would also like to thank several individuals who have dramatically influenced my development as a scientist: Drs. Eric Coulter, Zanna Beharry, and Radu Silaghi-Dumitrescu have each in their own way shaped my development as a scientist.

I would also like to thank my wife, Melissa Emerson, for her patience and sacrifice in allowing me to pursue my educational goals. Without her support, little of the research reported within this work would have been possible.

TABLE OF CONTENTS

CHAPTER 1

INTRODUCTION TO OXIDATIVE STRESS AND OXIDATIVE STRESS DEFENSE

1.A. Oxidative Stress and the Univalent Pathway

Dioxygen, O_2, has the ability to systematically acquire electrons. The electronic properties of O_2 define a reductive pathway by which O_2 is reduced ultimately to two molecules of H_2O.[1] This pathway and the reduction-oxidation (redox) potentials of the reduced oxygen species, both at pH 7, are shown in Figure 1.1. Because of the high-positive reduction potential of the O_2/H_2O redox couple (c.f. Figure 1.1), aerobic organisms use dioxygen as a terminal electron acceptor to obtain energy via the metabolic process called "respiration."[2] Typically, biological systems which respire are designed to minimize un-coupling that would release the highly reactive intermediate reduction products of dioxygen within organisms. Occasionally, however, one-, two-, or three-electron reduced dioxygen species are adventitiously released and cause significant damage to intracellular bio-molecules. The biological damage caused by dioxygen and its reduced oxygen species is collectively referred to as oxidative stress.

The electronic structure of molecular oxygen favors a step-wise single-electron reduction process. Dioxygen is a paramagnetic molecule with two valence-unpaired π-

type electrons, i.e. a ground triplet state (c.f. Figure 1.2). Paired electrons in other molecules cannot interact with the unpaired electrons of dioxygen due to energy barriers arising from pairing electrons with the same spin, which would violate the Pauli exclusion principle.[3] Most organic molecules are, therefore, spin forbidden from reacting with O_2. However, single unpaired electrons from other sources, including transition metals, can be relatively easily paired with one of the unpaired electrons in the HOMOs of dioxygen, resulting in a reduced dioxygen species.[2, 3, 4] This pairing process, however, is slow compared to the lifetime of collision complexes between O_2 and its reductant. Therefore, the probability of spin pairing during a collision between O_2 and its reductant is low. During simple electron transfer reactions, bonds are not formed between dioxygen and reductant; an electron is transferred via an "outer-sphere pathway," reducing dioxygen by one-electron to superoxide. This one-electron reduction process continues, and is called the univalent electron transfer pathway, as shown in Figure 1.1. This univalent pathway requires a total of 4 e^- and 4 protons, to reach water via superoxide, O_2^-, hydrogen peroxide, H_2O_2, and hydroxyl radical, •OH.

Oxidative stress on biological systems can derive from reactions of any of these intermediate reactive oxygen species (ROS) with cellular components. Reaction products of reduced oxygen species with biological molecules are proposed to further propagate oxidative stress. For example hydrogen peroxide is rapidly reduced, via the Fenton reaction, to a hydroxide ion and a hydroxyl radical by a adventitious Fe^{2+}. Hydroxyl radical is a powerful oxidant that reacts with most proteins and nucleic acids. DNA oxidative damage is caused by ROS. Experimental evidences suggest the three

intermediate products resulting from dioxygen reduction, namely O_2^-, H_2O_2, and •OH, all play a significant part in the oxidation of DNA; approximately 150,000 oxidative adducts of DNA are estimated to occur per mammalian cell at any given time.[5] ROS also oxidize iron-sulfur clusters,[6] lipids,[7] and polypeptides[8] within cells. Oxidative stress and the resulting damage to of bio-molecules have been recently surveyed.[9]

Aerobic organisms have evolved systems to deal with the low steady-state flux of ROS within their cells, and to repair the resulting oxidative damage. Over the past 50 years, many ROS protection enzymes have been characterized. Superoxide dismutases, catalalases, and peroxidases are specifically expressed to help cells minimize ROS. This work focuses on the ROS, superoxide, and specifically on enzymes that are proposed to detoxify superoxide, O_2^-.

1.B. Superoxide and Aqueous Solutions

The production and properties of aqueous solutions of superoxide have been thoroughly investigated in order to better understand its role within oxidative stress.[10, 11] Due to the instability of superoxide ion in aqueous solution, pulse radiolysis is the most convenient way to rapidly generate superoxide in the presence of a reactant. A schematic representation of the production of superoxide via pulse radiolysis is shown in Figure 1.3. The Van de Graaff accelerator builds a static charge, which is discharged as a burst of radiation, releasing a flow of electrons into the sample. The electrons in solution react to produce radicals and/or solvated electrons. Radicals then react directly and/or indirectly with dioxygen in solution to form both superoxide and perhydroxyl (HO_2, the

conjugate acid of superoxide), via reactions 1.1 and 1.2.[10] Sodium formate is often added to facilitate other radical reactions 1.3 – 1.5, thereby increasing the yield of superoxide. At biologically relevant pHs, perhydroxyl will tend to dissociate into superoxide due to its pK_a of 4.8 (reaction 1.5).[10] A rapidly responding spectrophotometer oriented perpendicularly to the discharge path of the Van de Graaff accelerator, is used to record absorption changes of the sample, following a pulse. The accelerator at the Brookhaven National Laboratory uses a computer-controlled monochromator and photomultiplier to amplify the signal.

$$e^-_{(aq)} + O_2 \rightarrow O_2^- \quad (1.1)$$

$$H + O_2 \rightarrow HO_2 \quad (1.2)$$

$$OH + HCO_2^- \rightarrow H_2O + CO_2^- \quad (1.3)$$

$$CO_2^- + O_2 \rightarrow CO_2 + O_2^- \quad (1.4)$$

$$HO_2 \rightarrow H^+ + O_2^- \quad (1.5)$$

The instability of superoxide in water is due to its rapid disproportionation, reaction 1.6. The decay of superoxide can be directly monitored by the decrease in absorption in the ultraviolet region due to HO_2 and O_2^- (c.f. Table 1.1).[10] The actual pathway of superoxide disproportionation at pH 7 is better described as reactions 1.7 – 1.9.[10, 11] Disproportionation occurs with a second order rate constant of approximately 5×10^5 $M^{-1}sec^{-1}$ at pH 7.0 and 25 °C.[11]

$$2O_2^- + 2H^+ \rightarrow O_2 + H_2O_2 \quad (1.6)$$

$$2HO_2 \rightarrow H_2O_2 + O_2 \quad (1.7)$$

$$HO_2 + O_2^- + H_2O \rightarrow H_2O_2 + O_2 + OH^- \quad (1.8)$$

$$O_2^- + O_2^- \rightarrow \text{No Reaction} \quad (1.9)$$

The rate of disproportionation of superoxide decreases ~10-fold for every increased pH unit from 5 to 13, as shown in Figure 1.4. The kinetics of superoxide disproportionation must be taken into account in reactions of superoxide with other molecules. The lifetime of a species, which like superoxide, decays in a second order process, can be calculated from equation 1.10, where $[A]_o$ represents initial superoxide concentration, [A] is the superoxide concentration at time t, and *k* is the second order rate constant for disproportionation. For example, in aqueous solution at pH 7 and 25 °C, the half-life, $t_{½}$ of a 1 x 10^{-3} M superoxide solution is 1.8 milliseconds, while, for a 1 x 10^{-9} M superoxide solution, $t_{½}$ is 67 minutes.

$$[A] = [A]_o/(1+ kt[A]_o) \quad (1.10)$$

Since pulse radiolysis facilities are expensive, limited in number and also require dioxygen for superoxide production via reactions 1.1 – 1.5, alternative techniques have been developed to introduce superoxide into a reaction mixture.

Potassium superoxide has some limited ability to dissolve in organic solvents. This solubility can be increased using crown ethers; 18-crown-6 is the most commonly

used crown ether for this purpose.[12, 13] The superoxide anion is stable in completely dry non-aqueous solvents, such as acetonitrile and dimethyl sulfoxide (DMSO). However, most biologically relevant molecules are not stable in non-aqueous solvents. Due to the rapid disproportionation of superoxide in aqueous solutions at pH 7 (reactions 1.6 – 1.8), rapid mixing, and detection techniques must be used to monitor reactions with superoxide ion in water. Rapid mixing can be achieved using a stopped-flow mixing device equipped with a detector to monitor reaction progress. A schematic block diagram stopped-flow spectrophotometer is shown in Figure 1.5. Samples are loaded into the drive syringes, via the reservoir syringes. This loading can be done anaerobically, if necessary. The plunger block places equal pressure on the two drive syringes, forcing portions of their contents into the mixing chamber. Turbulent flow is the most common mixing technique. Under the pressure of the plunger block, the mixed solution is forced into the cell, and through to the stop-syringe. Modern stopped-flow mixing systems are computer-controlled, and an electronic trigger is used to initiate mixing and spectrophotometric monitoring. Spectrophotometric devices for monitoring reactions after rapid stopped-flow mixing can range from a single-wavelength monochromator to complex scanning systems. Most stopped-flow mixing devices are limited to low millisecond dead times. Further information on currently available commercially produced stopped-flow mixing systems can be found at www.kintek-corp.com, www.photophysics.com, www.stoppedflow.com, and www.olisweb.com. Images of the U. S. A. stopped flow mixer, used throughout this work, are shown in Figure 1.5.

Several problems can arise when mixing non-aqueous with aqueous solutions. First, many organic solvents are not miscible with water, and phase separation is not acceptable for spectrophotometric monitoring. Many organic solvents that are water miscible, such as DMSO, have densities different from that of water, which alter the refractive indices of the mixed solutions and inhibit efficient mixing. Mixing organic and aqueous solvents can also generate heat, which may affect the rates of reactions. Finally, high concentrations of organic solvents tend to denature proteins.

Several water-miscible solvent systems, such as acetonitrile and DMSO, have been investigated that stabilize superoxide.[13] Alternatively, the method of mixing can be changed. Several types of mixing chambers for stopped-flow experiments have been used to increase the effectiveness of the stopped-flow mixing of aqueous with non-aqueous solvents.[14] Another successful strategy has been to mix a smaller volume of the superoxide/non-aqueous solvent solution with a much larger volume of the aqueous protein solution. Such unequal volume mixing results in less heat produced, and less opportunity for protein damage. Mixing of aqueous solutions with DMSO in a 25:1 aqueous:DMSO (v/v) ratio using turbulent stopped-flow mixing has proven successful for studies of superoxide with several superoxide dismutases.[13, 14] Such variations in mixing ratio can be achieved by varying the relative volumes of the two drive syringes (c.f. Figure 1.5). A pre-mix system has also been used successfully for aqueous/non-aqueous stopped-flow mixing of superoxide with iron superoxide dismutase.[15] Superoxide can also be produced photolytically on the way to the mixing chamber via reactions 1.2 to 1.6, using a high energy light source.[16]

A newly proposed approach would be to use basic aqueous solutions of superoxide.[17] Using the stability of superoxide at basic pH, and mixing with a much larger volume of a well-buffered protein solution could allow stopped-flow monitoring of reactions with superoxide. The second order rate constant is ~ 0.8 $M^{-1}sec^{-1}$ for disproportionation at pH 13 (c.f. Figure 1.4). Using this rate constant and equation 1.7, a 1 mM solution of superoxide would disproportionate at a rate of 8 x 10^{-4} sec^{-1}; giving a half-life of approximately 20 minutes, at pH 13. Disadvantages are that pH 13 solutions are more viscous than neutral pH solutions, caustic solutions tend to etch the glass syringes of stopped-flow mixers, and heat is released upon mixing basic with neutral-pH solutions.

1.C. Superoxide Defense and Superoxide Dismutase

Superoxide dismutases, SODs, catalyze the disproportionation reaction, 1.6, at near diffusion-controlled rates. SODs are commonly found in organisms and keep the steady-state level of superoxide low; e.g., approximately 10^{-10} M in aerobically growing *E. coli* cells.[18] SODs use transition metal centers to react with O_2^-. Iron- (Fe-SOD), copper-zinc- (Cu/Zn-SOD), manganese- (Mn-SOD), and nickel- (Ni-SOD) superoxide dismutases have all been isolated and characterized in the past 50 years, and crystal structures are available for all but the nickel enzyme.[19 - 21]

The catalytic behavior of SODs has been thoroughly studied. The catalysis of reaction 1.6 by all SODs can be written as the sum of two reactions: oxidation of superoxide, reaction 1.11, and reduction of superoxide, reaction 1.12. Superoxide reduces

the metal center of oxidized SOD_{ox}, releasing molecular oxygen as the product. Superoxide can also oxidize the metal center of reduced SOD, SOD_{red}, thereby regenerating SOD_{ox} and producing hydrogen peroxide.

$$O_2^- + SOD_{ox} \xrightarrow{k_{ox}} O_2 + SOD_{red} \quad \text{(oxidation of } O_2^-\text{)} \quad (1.11)$$

$$2H^+ + O_2^- + SOD_{red} \xrightarrow{k_{red}} H_2O_2 + SOD_{ox} \quad \text{(reduction of } O_2^-\text{)} \quad (1.12)$$

The mechanism of SOD chemistry is still unclear. All SODs contain a transition metal center, which undergoes one-electron redox some type of reduction/oxidation chemistry. Both inner- and outer-sphere reactions for oxidation of superoxide to dioxygen have been proposed for Fe- and Cu/Zn-SODs. The reduction mechanism of superoxide to hydrogen peroxide has also been proposed as both inner- and outer-sphere. However, the reaction of SOD with superoxide is nearly diffusion controlled. Ligand exchange of iron ions is slower than ~ 10^{-7} sec^{-1} in aqueous solution, which indicates outer-sphere electron transfer may be very important in the mechanism of Fe-SOD, while ligand exchange is much faster for copper ions, therefore, inner-sphere electron transfer processes are more likely in Cu/Zn-SOD.[22]

The observed rate constant for catalysis, k_{obs}, of superoxide dismutation by an SOD is therefore a combination of the rate constants for reactions 1.8 and 1.9, k_{ox} and k_{red} respectively. The rates of SOD-catalyzed superoxide dismutation and the turn over number, TN, are listed for Fe- and Cu/Zn-SODs in Table 1.2. These parameters have been measured using stopped-flow and pulse radiolysis techniques,[11] which are

dependent on rapidly either producing superoxide or mixing solutions of superoxide with aqueous SOD solutions, as described above in section 1.B. Steady state kinetic data has also been obtained by monitoring the decrease of superoxide concentration directly between 230 and 260 nm (c.f. Table 1.1).

For lower concentrations of superoxide suitable for enzyme assays, superoxide is often produced enzymatically. Enzymatic production of a flux of superoxide better mimicks *in vivo* production, as well as steady-state concentrations. The most widely used SOD assay was developed by Fridovich and co-workers,[23 - 25] which uses xanthine plus xanthine oxidase (X.O.) to generate a flux of superoxide. Xanthine is oxidized to uric acid by dioxygen, which is reduced to hydrogen peroxide, reaction 1.12. The uni-valent side reaction 1.13, generates superoxide.[24] This method is limited by the range of pH at which the xanthine/xanthine oxidase system is active in producing superoxide. Generally SOD assays are conducted using xanthine/X.O. in phosphate buffer near pH 8.0 and room temperature.[24]

$$\text{Xanthine-}H_2 + O_2 \xrightarrow{\text{X.O.}} \text{uric acid} + H_2O_2 \qquad (1.12)$$

$$\text{Xanthine-}H_2 + 2O_2 \xrightarrow{\text{X.O.}} \text{uric acid} + 2H^+ + 2O_2^- \qquad (1.13)$$

As diagrammed in Figure 1.6, this assay indirectly measures the rate of superoxide consumption as an inhibition of the rate of reduction of cytochrome c by superoxide produced by xanthine/X.O. (reaction 1.13). The superoxide flux is adjusted by manipulating the amount of X.O. in the system, and can be quantitated using the strong

heme absorption of reduced cytochrome c ($\varepsilon_{550} \sim 21{,}500\ M^{-1}cm^{-1}$). Under standard assay conditions, the superoxide flux is adjusted so that absorption at 550 nm increases at a rate of 0.025/min, which corresponds to a flux of close to 1.2 μM superoxide/minute. Aliquots of the candidate SOD are then added to this precalibrated assay mixture. One unit of SOD activity is defined as the concentration of candidate that produces 50% inhibition of the pre-calibrated change in absorption at 550 nm, i.e., that reduces ΔA_{550}/min to 0.0125. Through a simple calculation, the units of SOD activity per milligram (U/mg) can be derived. Kinetic characteristics of two commercially available SODs are listed in Table 1.2.

1.D. Oxidative Stress in Microaerophilic and Anaerobic Organisms

Anaerobic bacteria and archaea are classified as those that cannot use O_2 as a respiratory electron acceptor. Furthermore, O_2 is toxic to anaerobic bacteria and archaea to varying degrees. Nevertheless, most known anaerobes can survive exposure to either low steady-state levels of molecular oxygen or transient exposure to high (aerobic) levels of dioxygen. Therefore, anaerobic bacteria and archaea are at least occasionally exposed to ROS, and therefore, also need a ROS protection system. One of the first classes of anaerobic bacteria to be characterized was the sulfate-reducers, which use sulfate rather than dioxygen as the terminal electron acceptor.[26] At least one sulfate-reducing bacteria, *Desulfovibrio vulgaris,* has been shown to survive and congregate at a region near the aerobic/anaerobic interface of a water column in which a dioxygen gradient has been established.[26] Evidence for aerobic respiration was even reported for *D. vulgaris*;

this respiration however, did not support growth.[26] ROS protection enzymes have been reported from many species of anaerobic bacteria and archaea, including several sulfate-reducers.[27 - 30] Unlike the well studied aerobic ROS defense, which functions by disproportionation systems, these anaerobic ROS defense systems are proposed to catalyze a reductive pathway for removal of ROS. Such a reduction ROS protection system has been proposed for *D. vulgaris* (c.f. Figure 1.7).[30]

1.E. Superoxide Reductase

History. Superoxide reductases (SORs) are part of the reductive paradigm by which anaerobic microorganisms minimize the toxic effects of adventitious superoxide production resulting from dioxygen exposure. The first described protein that turned out to be a SOR was originally named rubredoxin oxidoreductase, abbreviated Rbo. This name originated from the co-transcription of the genes encoding rubredoxin and Rbo in *Desulfovibrio vulgaris*.[31] A different research group isolated and purified what turned out to be the protein encoded by the Rbo gene, and gave it the trivial name, desulfoferrodoxin, Dfx, based on its spectroscopic properties and iron content. Characterization of Dfx using UV/visible, Mössbauer, EPR and resonance Raman spectroscopies[29, 32] showed two mono-nuclear iron sites, one of which was an iron-sulfur center similar to that in rubredoxin [$Fe(SCys)_4$], and a second novel center with both iron-cysteine and iron-histidine ligation. An enzyme named neelaredoxin, Nlr, subsequently isolated from another sulfate-reducer, *Desulfovibrio gigas*, was proposed to have the same cysteine/histidine mononuclear iron site, based on amino-acid sequence

homology and spectroscopic resemblance to Dfx; but Nlr lacked the [$Fe(SCys)_4$] center.[33, 34] Both the *D. desulfuricans* Dfx and the *D. gigas* Nlr were initially isolated with no known function, but were later implicated as SODs.[35, 36]

A breakthrough in understanding the true function of the Dfx/Nlr class of enzymes was the report by Touati and co-workers, who showed that expression of the *Deulfoarculus baarsii* Rbo gene could restore aerobic growth to a Δ*sod* strain of *E. coli*.[37] This mutated *E. coli* strain lacks both Mn- and Fe-SODs and is unable to grow aerobically in minimal media without added nutrients. Expression of the Rbo gene in the Δ*sod* strain, had, therefore protected the cell against oxidative stress, apparently by functioning as an SOD. Touati *et al.* also showed, however, that the isolated Rbo did not catalyze superoxide disproportionation using the standard SOD assay described in Section 1.C. Following Touati's report, Liochev and Fridovich[38] confirmed that expression of this same Rbo gene in the Δ*sod E. coli* strain lowered the intracellular superoxide concentration. They also proposed that Rbo was oxidized by superoxide, then re-reduced by unknown cellular reductants, possibly NADPH, i.e., that Rbo catalyzed the reduction rather than disproportionation of superoxide. Finally, Adams and co-workers conducted several simple experiments on a homolog of Nlr purified from the hyperthermophilic anaerobic archaeon, *Pyrococcus furiosus*.[27] The *P. furiosus* Nlr homolog was reported to have a high SOD activity, using the traditional SOD assay. However, when acetylated cytochrome c was substituted in the assay, the apparent SOD activity was drastically reduced. The lower positive charge on acetylated cytochrome c inhibits electron transfer, with negatively charged proteins. The Adams group, therefore,

proposed that their Nlr homolog, which they called SOR, was indeed reacting rapidly with superoxide, but that the SOR accepted electrons from reduced cytochrome c in order to catalytically turnover in the SOD assay. The *P. furiosus* SOR, thus, catalyzed reduction, not disproportionation of superoxide, reaction 1.14.

$$e^- + O_2^- + SOR_{red} + 2\,H^+ \rightarrow H_2O_2 + SOR_{ox} \qquad (1.14)$$

Touati and co-workers used a competition method to estimate the rate constant of the reaction of superoxide with the *D. baarsii* 2Fe-SOR.[39] The rate of oxidation of the ferrous $[Fe(NHis)_4(SCys)]$ site by superoxide, was inhibited using an SOD to compete for the flux of oxidant. At 50% inhibition, the velocities of the SOD-catalyzed reaction was set to equal the velocity of the reaction of superoxide with SOR. Using known concentrations and rate constants for commercially available SODs, they estimated the second-order rate constant for the reaction of superoxide and the SOR_{red} active center to be 6 - 7 x 10^8 $M^{-1}sec^{-1}$.[39]

Active site structure of superoxide reductases. A common iron-binding amino-acid sequence motif in all known SORs is shown by the sequence alignment in Figure 1.8. This unique motif H-X_n-H-X_5-H-X_n-C-N-X-H, provides five conserved ligands to the iron site: four histidines and a cysteine. The iron site structure associated with this sequence motif was elucidated from the crystal structures of the *Desulfovibrio desulfuricans* Dfx[40] and the *Pyrococcus furiosus* SOR.[41] Structures of the iron centers and proteins are shown in Figure 1.9. The crystallographic structures suggest the

5-coordinate, square pyramidal ferrous [$Fe^{II}(NHis)_4(SCys)$] site takes on a sixth ligand from a glutamate residue in the resting oxidized (ferric) form. This conserved glutamate resides on a flexible solvent exposed polypeptide loop that moves ~ 10 Å upon interconversion betwween the ferrous and ferric states. A side chain of a conserved lysine residue that is sequentially adjacent to the conserved glutamate residue near the ferrous [$Fe(NHis)_4(SCys)$] site. SORs containing only this iron site are referred to as 1Fe-SORs. Those SORs containing an additional [$Fe(SCys)_4$] site are referred to as 2Fe-SORs. This "rubredoxin-like" center is formed from an N-terminal C-X_2-C-X_n-C-C motif, Figures 1.8 and 1.9.[42] The *T. pallidum* 1Fe-SOR is unique in containing an N-terminal domain homologous to those of 2Fe-SORs,[43] but lacking three of the four cysteines that ligate the [$Fe(SCys)_4$] site in 2Fe-SORs (c.f. Figure 1.8).

Due to the similarity of the [$Fe(SCys)_4$] site in 2Fe-SOR to those of rubredoxins, proteins known to transfer electrons, the [$Fe(SCys)_4$] center in 2Fe-SOR has been proposed to be involved in an electron transfer pathway to the [$Fe(NHis)_4(SCys)$] site.[31] However, the intramolecular distances between the [$Fe(SCys)_4$] and [$Fe(NHis)_4(SCys)$] sites are 21.6 Å within the same monomer, and 31.9 Å between monomers (c.f. Figure 1.9).[40] These distances are long for rapid electron transfer reactions.[45] However, intermolecular electron transfer or independent reactivity of the [$Fe(SCys)_4$] center has not been ruled out. The [$Fe(SCys)_4$] site (~ 0 mV) has a lower potential than that of the [$Fe(NHis)_4(SCys)$] site (+90 — 290 mV vs. NHE).[33, 44]

An examination of the ferric and ferrous electronic structure of the [$Fe(NHis)_4(SCys)$] center of 1Fe-SOR from *P. furiosus* by magnetic circular dichroism

(MCD) and resonance Raman spectroscopy has recently been published.[46,47] The $[Fe^{II}(NHis)_4(SCys)]$ center has virtually no electronic absorption between 350 and 800 nm. A high-energy absorption at 320 nm was assigned as primarily a cysteine sulfur → ferrous ligand-to-metal charge transfer transition. The $[Fe^{III}(NHis)_4(SCys)]$ center shows significant absorption features centered at approximately 650 nm ($\varepsilon_{650} \sim 2{,}000\ M^{-1}cm^{-1}$) and 340 nm ($\varepsilon_{340} \sim 6{,}000\ M^{-1}cm^{-1}$). The absorption feature at 650 nm was assigned as a cysteine sulfur → ferric charge transfer transition.[46] The vibrational modes in the $[Fe^{III}(NHis)_4(SCys)]$ site of *P. furiosus* 1Fe-SOR have also been described.[47]

Three oxidation states are attainable for 2Fe-SORs, and their visible absorption spectra are shown in Figure 1.10. 2Fe-SOR_{clear} which has both ferrous sites shows little absorption in the visible region. However, a high-energy absorption at 320 nm is present. This absorption has a higher molar absorptivity than its 1Fe-SOR counterpart, which is likely due to the presence of the additional sulfur → ferrous charge transfer transitions of the $[Fe(SCys)_4]$ site in 2Fe-SOR. 2Fe-SOR_{pink} is the aerobically isolated oxidation state of this enzyme, having ferric $[Fe(SCys)_4]$ and ferrous $[Fe(NHis)_4(SCys)]$ sites. This mixed valent enzyme has strong absorption features at 380 and 500 nm. These absorptions are due to sulfur → ferric charge transfer transitions of $[Fe(SCys)_4]$ site, and are similar to those of the prototypical $[Fe(SCys)_4]$ protein, rubredoxin.[48, 49] The absorption feature of the 2Fe-SOR_{pink} at 320 nm is assigned to the sulfur → ferrous charge transfer transitions of the $[Fe(NHis)_4(SCys)]$ site. 2Fe-SOR_{gray} has both iron sites in the ferric oxidation state. The visible absorption spectrum of 2Fe-SOR_{gray} has an additional feature at approximately 650 nm. The difference absorption spectrum, 2Fe-

SOR_{gray} – 2Fe-SOR_{pink}, is very similar to the absolute absorption spectrum of oxidized *P. furiosus* 1Fe-SOR.[36] The 2Fe-SOR_{gray} absorption at 650 nm has been therefore, assigned to a sulfur → ferric charge transfer transition of ferric $[Fe(NHis)_4(SCys)]$ site, based on assignments for the *P. furiosus* 1Fe-SOR.[32, 44, 46] The form of 2Fe-SOR having ferrous $[Fe(SCys)_4]$ and ferric $[Fe(NHis)_4(SCys)]$ has never been reported, and given the redox potentials cited above, would not be expected to be stable. Table 1.2 lists the absorption wavelengths and intensities associated with each iron center for all three known forms of *D. vulgaris* 2Fe-SOR.

Rubredoxin has been shown to donate electrons to 2Fe-SOR.[50] Both iron centers of 2Fe-SOR can receive electrons from reduced rubredoxin, although the mechanisms of these reductions are still unclear. Based on this observation, an assay for SOR activity was developed using catalytic amounts of rubredoxin and SOR. A "bucket-brigade" of electrons, diagrammed in Figure 1.11, was used to supply electrons, from NADPH, to SOR. NADPH consumption can be conveniently monitored by the decrease in absorbance at 340 nm (ε_{340} ~ 6,220 $M^{-1}cm^{-1}$). Using a xanthine/xanthine oxidase system, NADPH consumption was correlated with the pre-calibrated superoxide flux, as described in Section 1.C, and catalase was added to remove any hydrogen peroxide. This assay required all components for superoxide-dependent turnover of NADPH. This SOR assay could be useful in understanding the full catalytic cycle of SORs.

1.F. Research Objectives

The aim of the research described herein is to investigate the superoxide chemistry of *D. vulgaris* 2Fe-SOR. Chapter 2 describes the initial spectroscopic detection of a transient species, formed during the reaction of pulse radiolytically produced superoxide with 2Fe-SOR_{pink}.[51] Chapter 3 is a detailed report of the kinetics of superoxide reduction by 2Fe-SOR_{pink} at varying pHs, temperatures, and ionic strengths, also using pulse radiolytically generated superoxide. The kinetics of two variants, E47A and K48A 2Fe-SOR, which substituted alanine for the conserved glutamate and adjacent lysine residues were studied. A refinement of the superoxide reductase mechanism is proposed from the more detailed and extensive kinetic data.[41]

Chapter 4 describes construction and characterization of a variant of *D. vulgaris* 2Fe-SOR, devoid of the [$Fe(SCys)_4$] center. The reactivity of this variant, C13S 2Fe-SOR, with O_2^- both *in vivo* and *in vitro* is reported.

The fifth chapter describes reactions of 2Fe-SOR with superoxide, hydrogen peroxide and dioxygen. Stopped-flow experiments using aqueous basic superoxide solutions for monitoring the reaction of superoxide with SOR are described and analyzed. The oxidation of the [$Fe(SCys)_4$] center of 2Fe-SOR with dioxygen is investigated, over short and long time scales. This autoxidation reaction of the [$Fe(SCys)_4$] center leads to oxidation of the [$Fe(NHis)_4(SCys)$] center. Finally, the interactions of 2Fe-SOR in several oxidation states with hydrogen peroxide are examined. Stopped-flow mixing of hydrogen peroxide solutions with 2Fe-SOR are conducted in order to characterize this reaction and address the recent report of a ferric-peroxo transient from mixing excess

hydrogen peroxide and 2Fe-SOR.[52] Possible physiological relevance of these reactions are discussed.

1.G. Reference

1. Fridovich, I. (1999) *Ann. N.Y. Acad. Sci. 893*, 13-18.
2. Ferguson-Miller, S., Babcock., G. (1996) *J. Chem. Rev. 96*, 2889-2907.
3. Fridovich, I. (1998) *J. Exp. Biol. 201*, 1203-1209.
4. Kurtz, D. M., Jr., (1999) *Essays in Biochemistry*, Ballou, D. P., Ed., Portland Press Ltd., 85-100.
5. Beckman, K. B., Ames, B. N. (1997) *J. Biol. Chem. 272*, 19633-19636.
6. Flint, D. H., Allen, R. M. (1996) *J. Chem. Rev. 96*, 2315 -2334.
7. Steinberg, D. (1997) *J. Biol. Chem. 272*, 20963-20966.
8. Stadtman, E. R., Berlett, B. S. (1997) *Chem. Res. Toxicol. 10*, 485-494.
9. Valentine, J., Wertz, D., Lyons, T., Liou, L., Goto, J., Gralla, E. (1998) *Curr. Opin. Chem. Biol. 2*, 253-262.
10. Bielski, B. H. J., Cabelli, D. E., Arudi, R. L., Ross, A. B. (1985) *J. Phys. Chem. Ref. Data 14*, 1041 - 1100.
11. Bielski, B., Cabelli D. E. (1991) *Int. J. Rad. Biol. 59*, 291-319.
12. Marklund, S. (1976) *J. Biol. Chem. 251*, 7504-7504.
13. Valentine, J. S., Curtis, A. B. (1975) *J. Am. Chem. Soc. 97*, 224-226.
14. McClune, G., J., Fee, J., A. (1978) *Biophys. J. 24*, 65-69.
15. Greenleaf, W. B., Silverman, D. N. (2002) *J. Biol. Chem.* 277, 49282-49286.
16. Baxendal, J. H., Wilson, J. A. (1957) *Trans. Faraday Soc. 53*, 344-356.
17. Bradic, Z., Wilkins, R. G. (1984) *J. Am. Chem. Soc. 106*, 2236-2239.
18. Imlay, J., Fridovich, I. (1991) *J. Biol. Chem. 266*, 6957-6965.

19. Tainer, J. A., Getzoff, E. D., Been, K. M., Richardson, J. S., Richardson, D. C. (1982) *J. Molec. Biol. 160*, 181-217.

20. Cooper, J. B., Driessen, H. P., Wood, S. P., Zhang, Y., Young, D. (1994) *J. Mol. Biol. 235*, 1156-1158.

21. Wagner, U. G., Pattridge, K. A., Ludwig, M. L., Stallings, W. C., Werber, M. W., Oefner, C., Frolow, F., Sussman, J. L. (1993) *Protein Sci. 2*, 814-825.

22. Cabelli, D. E., Riley, D., Rodriquez, J. A., Valentine, J. S., Zhu, H. (2000) Models of Superoxide Dismutase, in Biomimetic Oixdations Catalyzed by Transition Metal Complexes, Meunier, B. Ed., Imperial College Press, London

23. McCord, J., Fridovich, I. (1969) *J. Biol. Chem. 244*, 6049-6055.

24. Yost, F. J., Jr., Fridovich, I. (1973) *J. Biol. Chem. 248*, 4905-4908.

25. Bull, C., Fee, J. A. (1985) *J. Am. Chem. Soc. 107*, 3295-3304.

26. Cypionka, H. (2000) *Annu. Rev. Microbiol. 54*, 827-848.

27. Jenney, F., Jr., Verhagen, M., Cui, X., Adams, M. W. (1999) *Science 286*, 306-308.

28. Lombard, M., Touati, D., Fontecave, M., Niviere, V. (2000) *J. Biol. Chem. 275*, 27021-27026.

29. Moura, I., Tavares, P., Moura, J., Ravi, N., Huynh, B., Liu, M., LeGall, J. (1990) *J. Biol. Chem. 265*, 21596-21602.

30. Lumppio, H., Shenvi, N., Summers, A., Voordouw, G., Kurtz, D., Jr. (2001) *J. Bacteriol. 183*, 101-108.

31. Brumlik, M., Voordouw, G. (1989) *J. Bacteriol. 9*, 4996-5004.

32. Tavares, P., Ravi, N., Moura, J. J. G., Le Gall, J., Huang, Y., Crouse, B. G., Johnson, M. K., Huynh, B. H., Moura, I. (1994) *J. Biol. Chem. 269*, 10504-10510.

33. Chen, L. S. P., Le Gall, J., Mariano, A., Teixeira, M., Xavier, A. (1994) *Eur. J. Biochem. 226*, 613-618.

34. Silva, G., Oliveira, S., Gomes, C., Pacheco, I., Liu, M., Xavier, A., Teixeira, M., Le Gall, J., Rodrigues-Pousada, C. (1999) *Eur. J. Biochem. 259*, 235-243.

35. Pianzzola, M., Soubes, M., Touati, D. (1996) *J. Bacteriol. 178*, 6736-6742.

36. Romaõ, C. V., Liu, M. Y., Le Gall, J., Gomes, C. M., Braga, V., Pacheco, I., Xavier, A. V., Teixeira, M. (1999) *Eur. J. Biochem*. *261*, 438-443.

37. Silva, G., Olivelira, S., Gomes, C. M., Pacheco, I., Liu, M. Y., Xavier, A., Teixeira, M., LeGall, J., Rodrigues-Poseda, C., (1999) *Eur. J. Biochem. 259*, 235-243.

38. Liochev, S., Fridovich, I. (1997) *J. Biol. Chem. 272*, 25573-25575.

39. Lumbard, M., Fontecave, M., Touati, D., Niviere, V. (2000) *J. Biol. Chem. 275*, 115-121.

40. Coelho, A., Matias, P., Fulop, V., Thompson, A., Gonzalez, A., Carrondo, M. (1997) *J. Biol. Inorg. Chem. 2*, 680-689.

41. Yeh, A., Hu, Y., Jenney, F., Jr., Adams, M., Rees, D. (2000) *Biochemistry 39*, 2499-2508.

42. Emerson, J. P., Coulter, E. D., Cabelli, D. E., Phillips, R. S., Kurtz, D. M., Jr. (2002) *Biochemistry 41*, 4348-4357.

43. Jovanovic, T., Ascenso, C., Hazlett, K., Sikkink, R., Krebs, C., Litwiller, R., Benson, L., Moura, I., Moura, J., Radolf, J., Huynh, B., Naylor, S., Rusnak, F. (2000) *J. Biol. Chem. 275*, 28439-28448.

44. Verhagen, M., Voorhorst, W., Kolkman, J., Wolbert, R., Hagen, W. (1993) *FEBS Letters 336*, 13-18.

45. Page, C. C., Moser, C. C., Chen, X., Dutton, P. L., (1999) *Nature 402*, 47-52.

46. Clay, M., Jenney, F., Jr., Noh, H., Hagedoorn, P., Adams, M. W., Johnson, M. K. (2002) *J. Am. Chem. Soc. 124*, 788-805.

47. Clay, M., Jenney, F., Jr., Noh, H., Hagedoorn, P., Adams, M., Johnson, M. (2002) *Biochemistry 41*, 9833-9841.

48. Lovenberg, W. *Iron-Sulfur Proteins*; Academic Press: New York, 1973.

49. Ascenso, C., Rusnak, F., Cabrito, I., Lima, M. J., Naylor, S., Moura, I., Moura, J. J. (2000) *J. Biol. Inorg. Chem. 5*, 720-729.

50. Coulter, E. D, Kurtz, D. M., Jr. (2001) *Arch. Biochem. Biophys. 394*, 76-86.

51. Coulter, E. D., Emerson, J. P., Cabelli, D. E., Kurtz, D. M., Jr. (2000) *J. Am. Chem. Soc. 122*, 11555-11557

52. Mathe, C., Mattioli, T. A., Horner, O., Lombard, M., Latour, J. M., Fontecave, M., Niviere, V. (2002) *J. Am. Chem. Soc. 124*, 4966-2967.

Table 1.1. Effective extinction coefficients, ε_x ($M^{-1}cm^{-1}$) for [HO_2^- and O_2^-] in aqueous solutions.[10]

pH	ε_{230}	ε_{240}	ε_{250}	ε_{260}
0.15-1.5	1368	1241	904	534
2.0	1369	1242	906	536
3.0	1381	1248	925	556
4.0	1482	1391	1090	727
5.0	1879	1909	1734	1396
6.0	2149	2262	2170	1852
7.0	2193	2319	2241	1925
8.0-9.0	2198	2326	2248	1933
10.0	2188	2319	2244	1929
11.0	2150	2287	2219	1913
12.0	2053	2205	2156	1869
13.0	2015	2173	2134	1850

Table 1.2. Kinetic properties of commercially available SODs.

Enzyme	SOD activity (U/mg)	k_{SOD}[d] ($M^{-1}sec^{-1}$)	K_m[d] (μM)	TN[d] (sec^{-1})
Cu/Zn SOD[a]	3200[b]	2×10^9	~ 5	~ 5×10^6
Fe-SOD[a]	2300[c]	3.25×10^8	~ 80	~ 2.6×10^4

[a]Bovine Cu/Zn SOD and *E. coli* Fe-SOD are commercially available from Sigma Chemical Co. [b]McCord and Fridovich.[23] [c]Yost and Fridovich.[24] [d]Observed reaction rates, measured K_m for Cu/Zn SOD, estimated K_m for Fe-SOD, and turnover numbers (TN) are taken from Bull and Fee.[25]

Table 1.3 Iron centers of 2Fe-SOR and their absorption features and intensities at various oxidation states.

SOR Species	Iron oxidation states	Wavelength (nm)	Molar Absorptivity ($M^{-1}cm^{-1}$)
2Fe-SOR_{pink}	$[Fe^{III}(SCys)_4]$	370 502	7,100 4,300[§]
	$[Fe^{II}(NHis)_4(SCys)]$	-	-
2Fe-SOR_{gray}	$[Fe^{III}(SCys)_4]$	360 502	10,100 4,680
	$[Fe^{III}(NHis)_4(SCys)(OGlu)]$	650	2,300
2Fe-SOR_{clear}	$[Fe^{III}(SCys)_4]$	-	-
	$[Fe^{II}(NHis)_4(SCys)]$	-	-
2Fe-SOR_{gray} - 2Fe-SOR_{pink}	$[Fe^{III}(NHis)_4(SCys)(OGlu)]$[#]	645	1,900[§]

[#]The oxidation state of the $[Fe(SCys)_4]$ center does not change, therefore its absorbance is subtracted out, leaving only the absorbance due to the $[Fe^{III}(NHis)_4(SCys)(OGlu)]$ site.
[§]data from Emerson *et al*.[42] and Verhagen *et al*.[44]

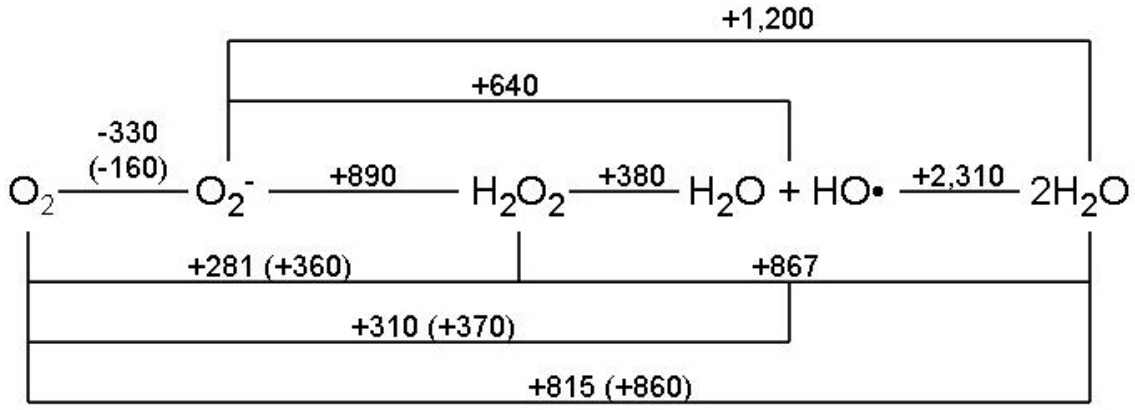

Figure 1.1. Standard reduction potentials, in milli-volts (mV), for dioxygen and its reduced species, in water at 1 atm or at unit activity of O_2 in parentheses, both at pH 7. Adapted from Sawyer, D. T. (1991) Oxygen chemistry, Oxford University Press, Inc., New York, NY.

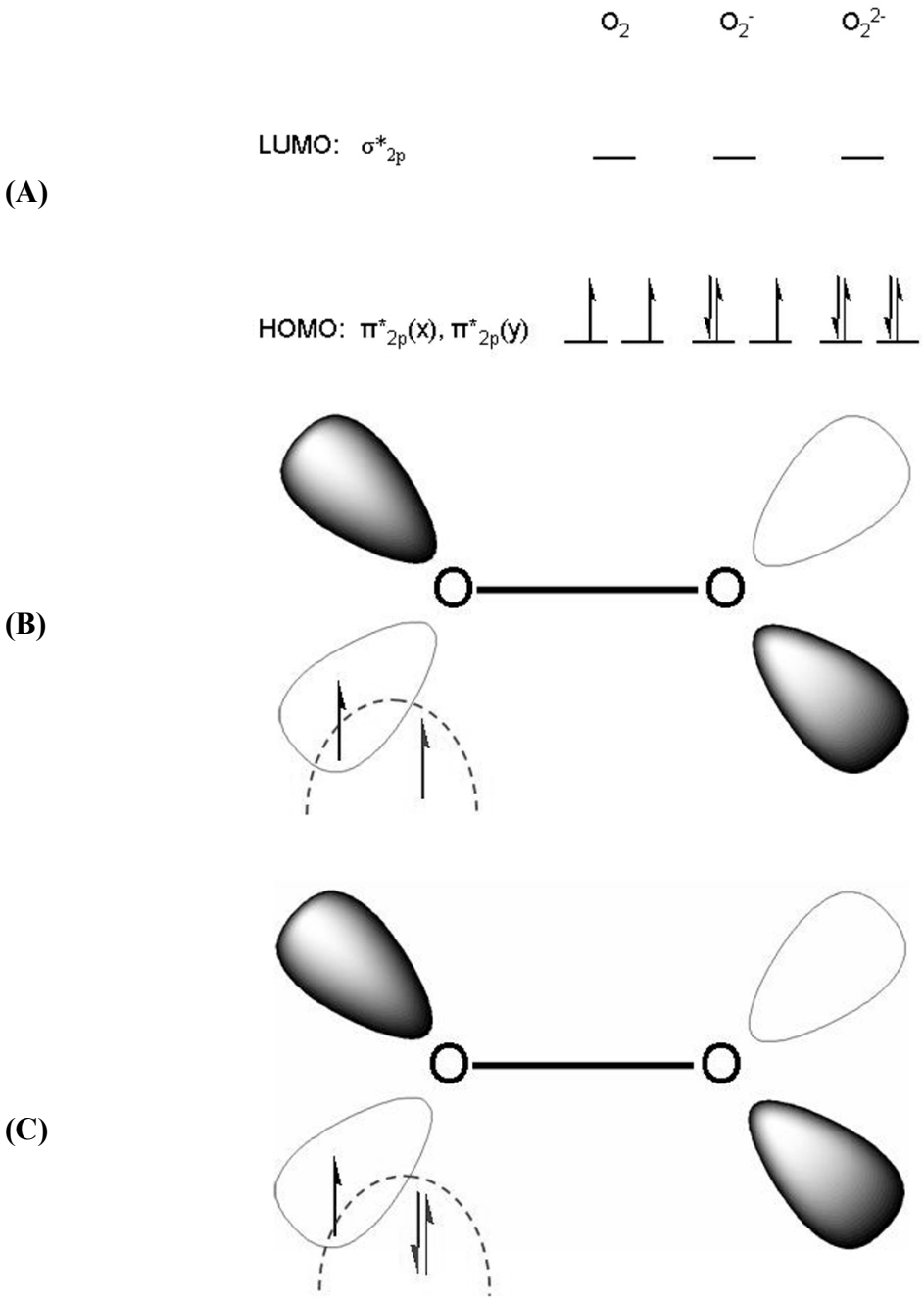

Figure 1.2. HOMOs and LUMOs of dioxygen, superoxide, and hydrogen peroxide. (A) Energy level diagram (B) shows one of the π^*_{2p} orbitals, the other HOMO is oriented perpendicular to the plane of the page. A single unpaired electron of another atom or molecule in an overlapping orbital (dashed) can effectively reduce dioxygen by pairing electrons. (C) A pair of electrons in this overlapping orbital cannot reduce dioxygen, due to spin restrictions.[4]

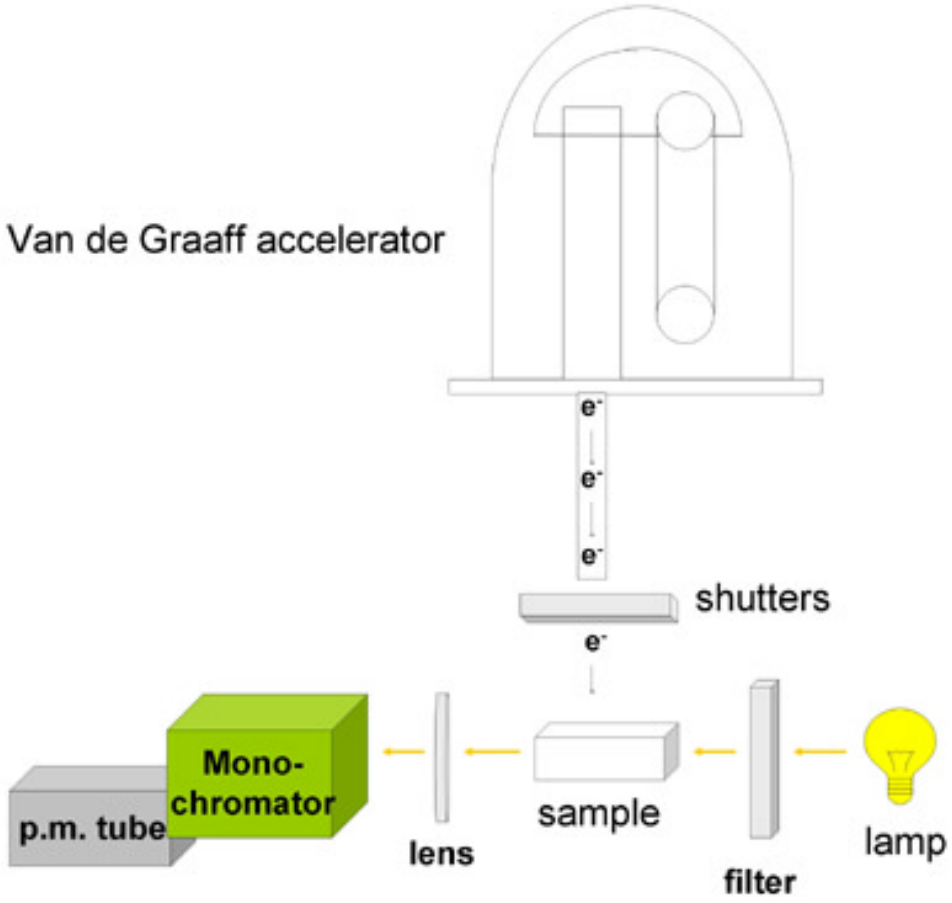

Figure 1.3. Schematic diagram of the pulse radiolysis apparatus used in the production of superoxide.

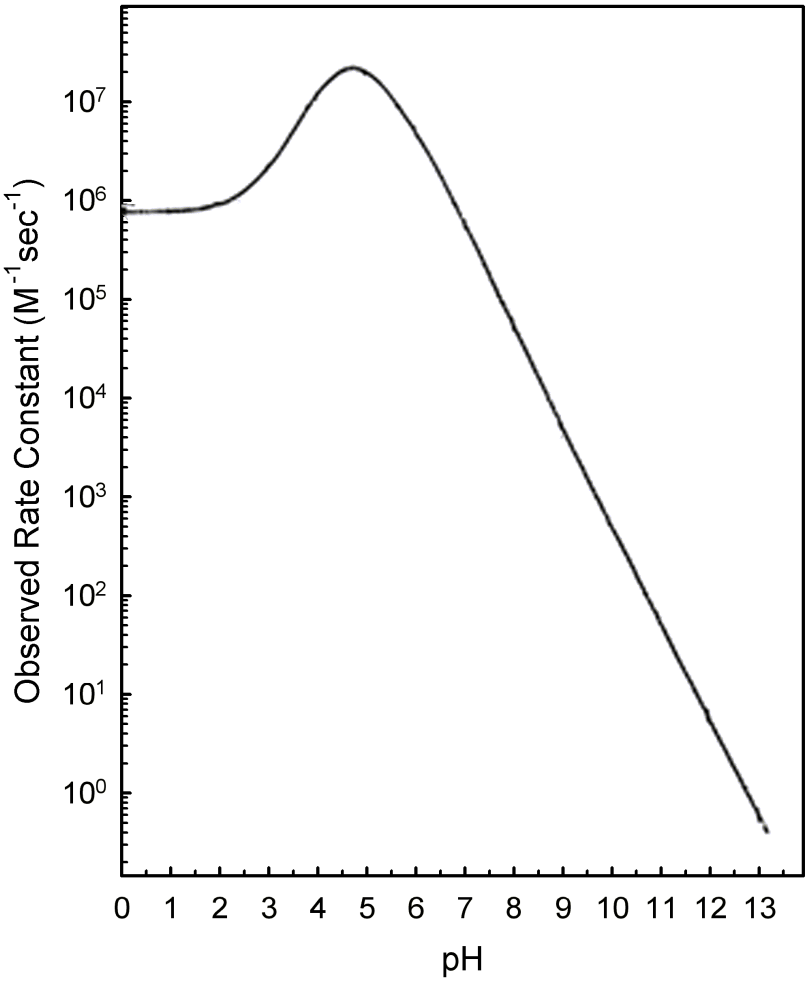

Figure 1.4. Plot of the second order rate constant for disproportionation of superoxide (corrected for the absorption of hydrogen peroxide) vs. pH, at 25 °C. Adapted from Bielski and Cabelli.[11]

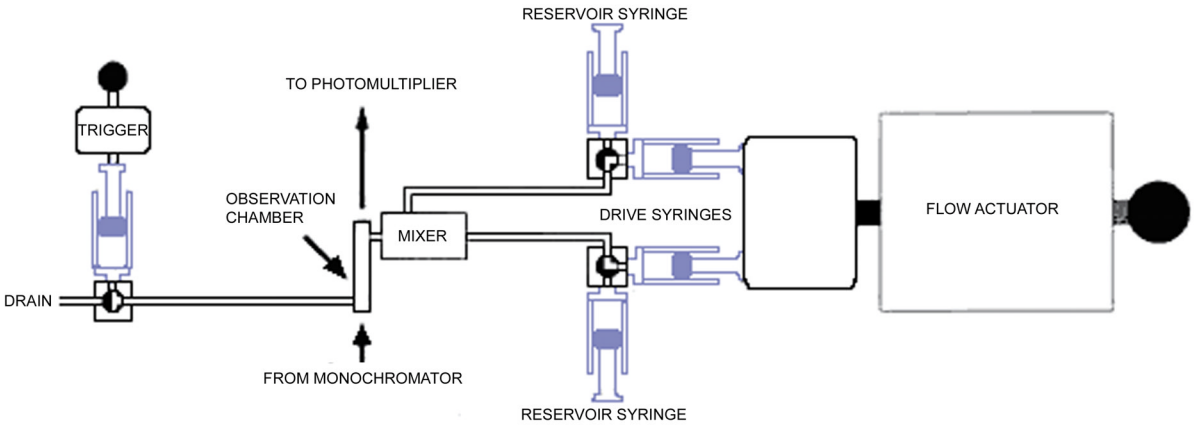

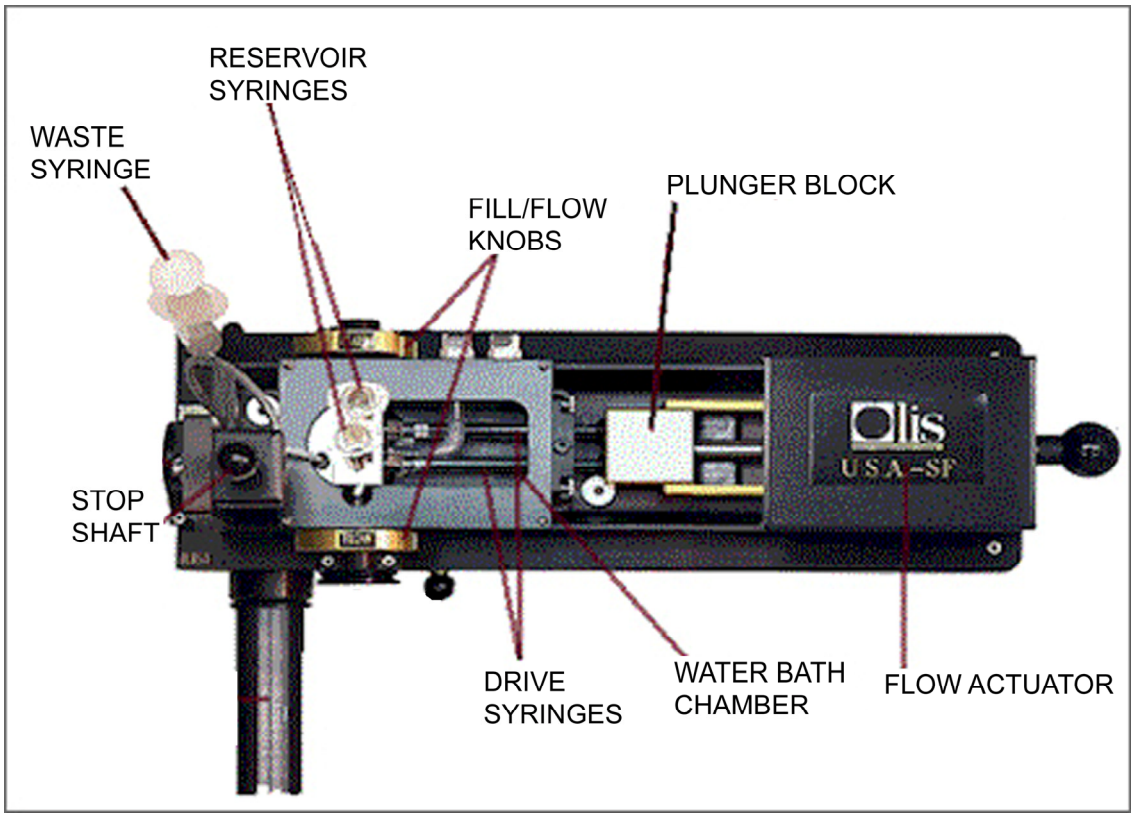

Figure 1.5. Block diagram and Top-view Photograph of the U.S.A. Stopped-flow mixer. Top represents a schematic representation of the working of a stopped-flow mixer, while the photos shows the actual location and names of important components described in the text. Adapted from the website of Olis, Inc. (www.olisweb.com), Bogart, GA, with permission.

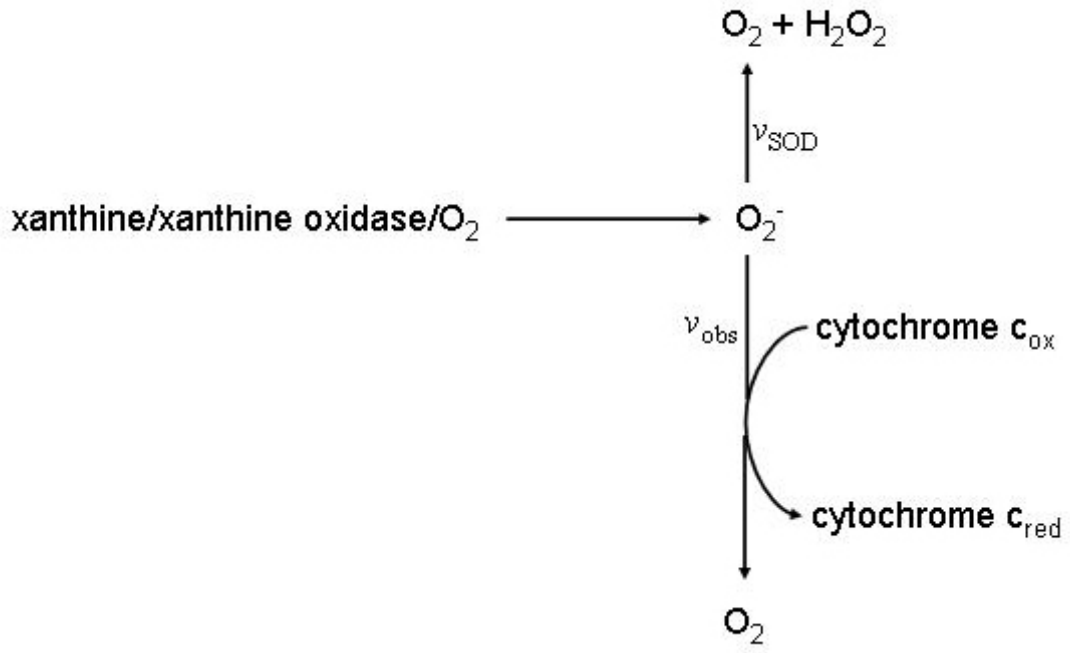

Figure 1.6. Schematic diagram of the reduction of cytochrome c by xanthine/xanthine oxidase/dioxygen in the SOD assay, where v_{SOD} is the velocity of disproportionation of superoxide catalyzed by candidate SOD, and v_{obs} is the velocity of reduction of cytochrome c by superoxide.

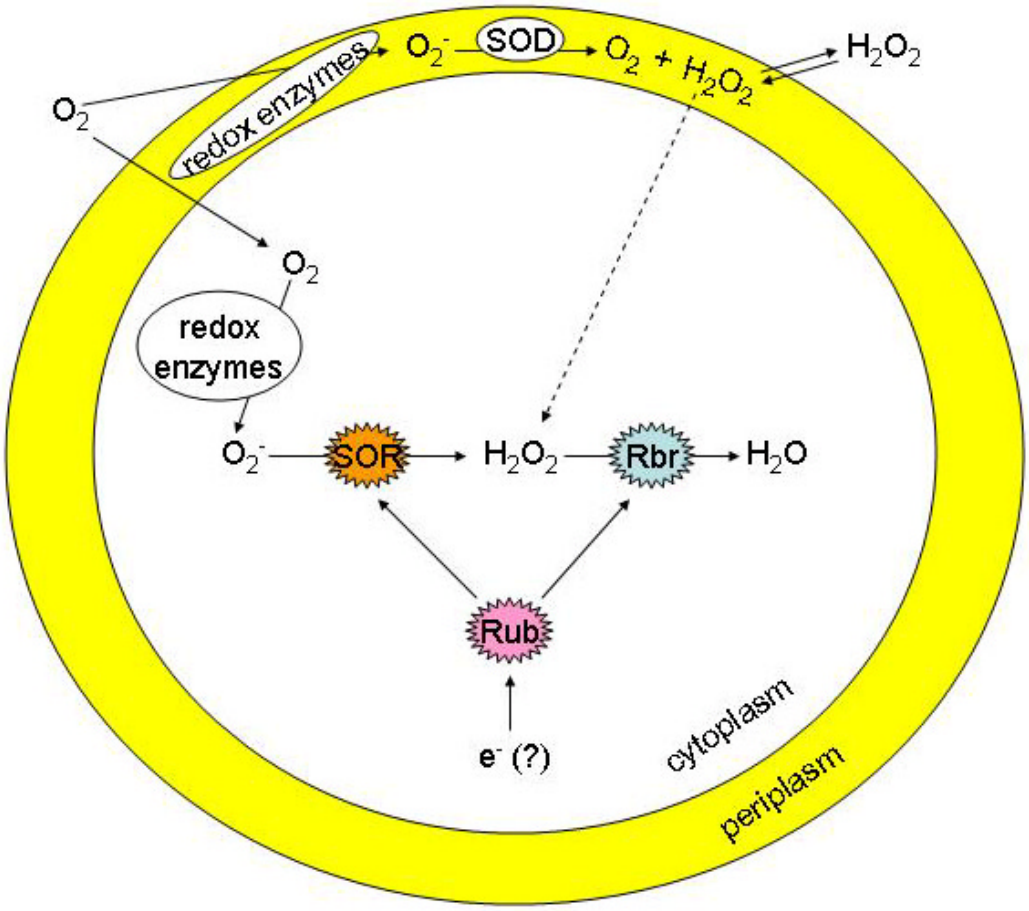

Figure 1.7. Schematic representation of the oxidative stress defense system of *D. vulgaris*, adapted from Lumppio *et al.*[30]

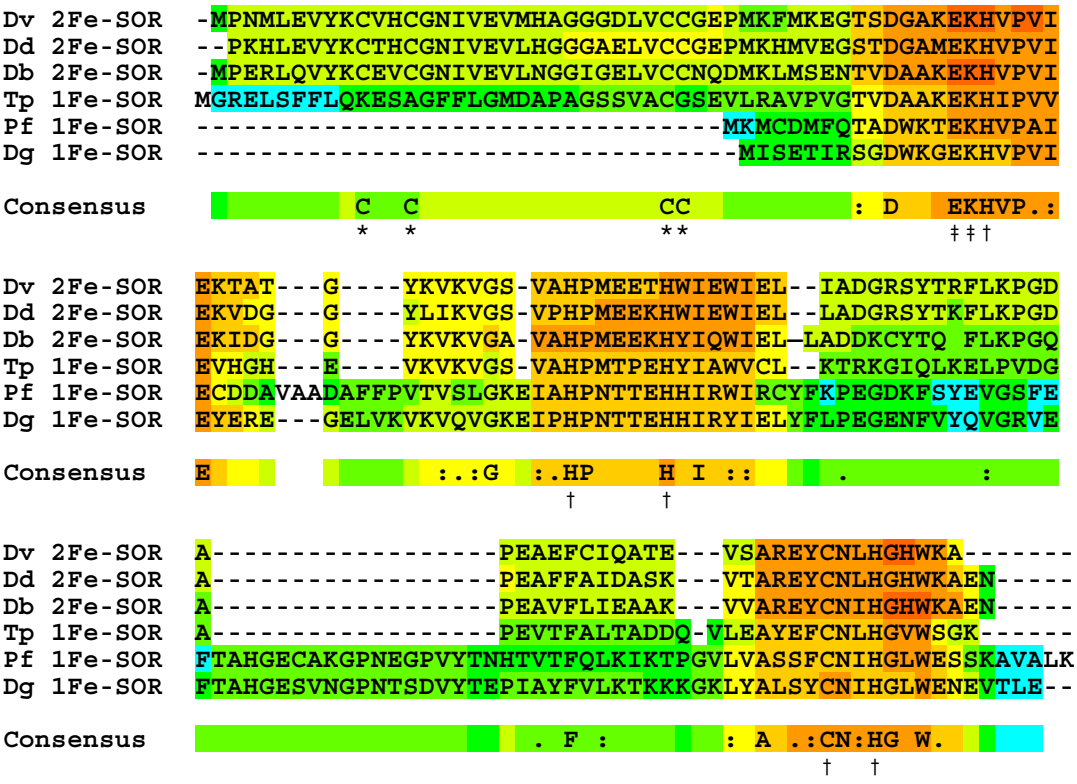

Figure 1.8. Amino-acid sequence alignment of SORs, from *Desulfovibrio vulgaris* (*Dv*) *Desulfovibrio desulfuricans* (*Dd*), *Desulfoarculus baarsii* (*Db*), *Treponema pallidum* (*Tp*), *Pyrococcus furiosus* (*Pf*), and *Desulfovibrio gigas* (*Dg*), and their respective gene accession numbers BAA11174, P22076, Q46495, A71276, AAD13200.1, P82385 respectively. Individual residues providing ligands to the [Fe(SCys)$_4$] or [Fe(NHis)$_4$(SCys)] sites are indicated by "*" and "†", respectively. The axially coordinating glutamate in the resting ferric [Fe(NHis)$_4$(SCys)(OGlu)] site is labeled with a "ǂ", as well as its neighboring lysine. The consensus sequence lists strictly conserved residues by letter. ":" and "." indicate decreasing similarity of aligned residues. A coloring system indicates conservation of sequence regions, highly conserved areas are colored red, while non-conserved areas are colored blue. The alignment software T-COFFEE, publicly available on the ExPASy molecular biology server (http://us.expasy.org/) was used to align sequences found on the National Center for Biotechnical Information, NCBI, homepage (http://www.ncbi.nlm.nih.gov/)

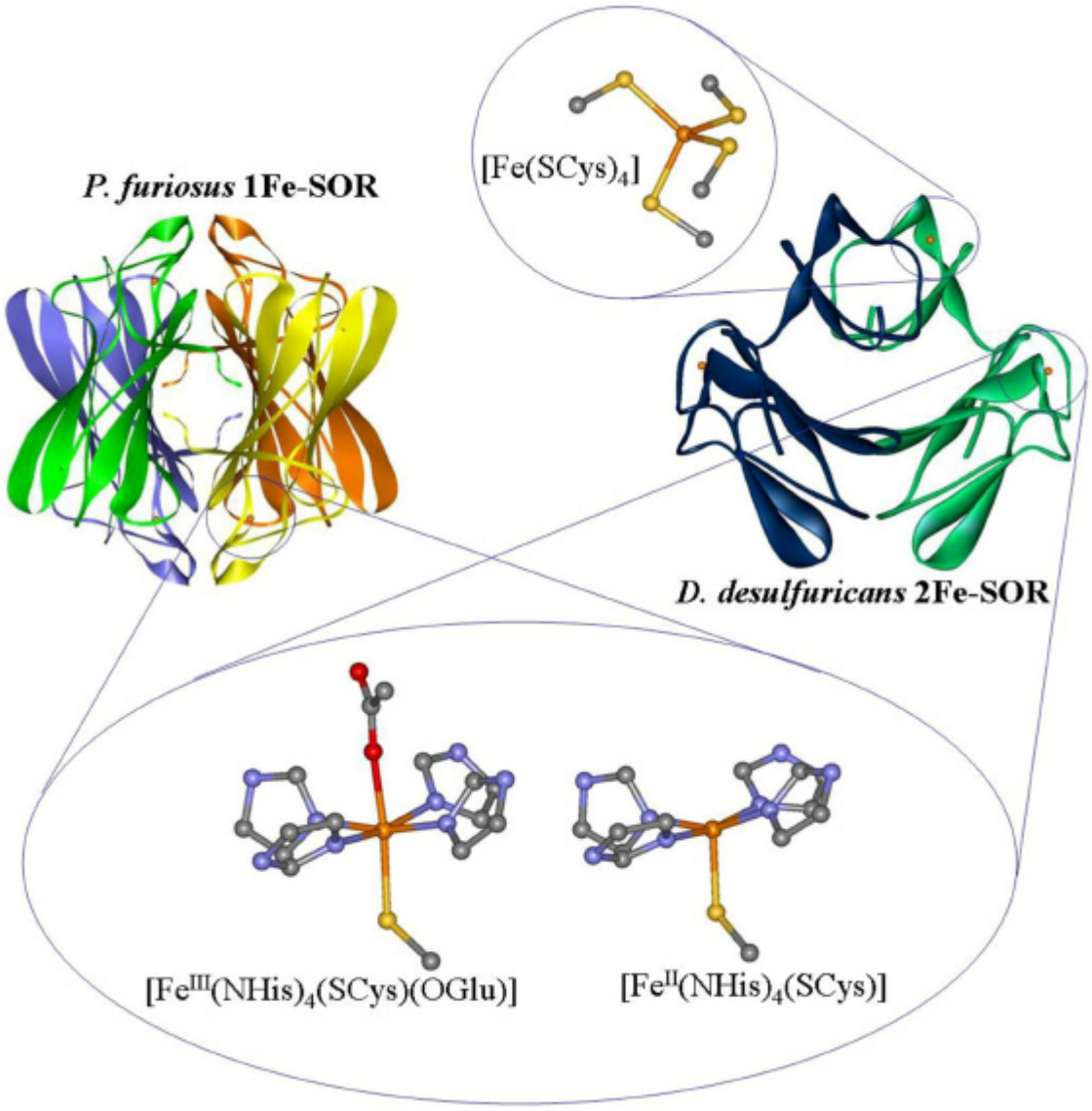

Figure 1.9. Drawings of the X-ray crystal structures of 1Fe- and 2Fe-SORs, and their metal binding domains. The structure of the tetrameric 1Fe-SOR from *P. furiosus* (1DQI) is shown on the left, and that of the dimeric 2Fe-SOR from *D. desulfuricans* (1DFX) on the right. Different colored ribbons within a structure indicate different subunits. Irons are shown as orange spheres. The reduced $[Fe(NHis)_4(SCys)]$ center of *D. desulfuricans* 2Fe-SOR and the oxidized $[Fe(NHis)_4(SCys)(OGlu)]$ center from *P. furiosus* 1Fe-SOR, along with the $[Fe(SCys)_4]$ center of the *D. desulfuricans* 2Fe-SOR have been expanded and rotated for clarity. All drawings were created using the ViewerLite software package using coordinates from the Brookhaven Protein DataBank.

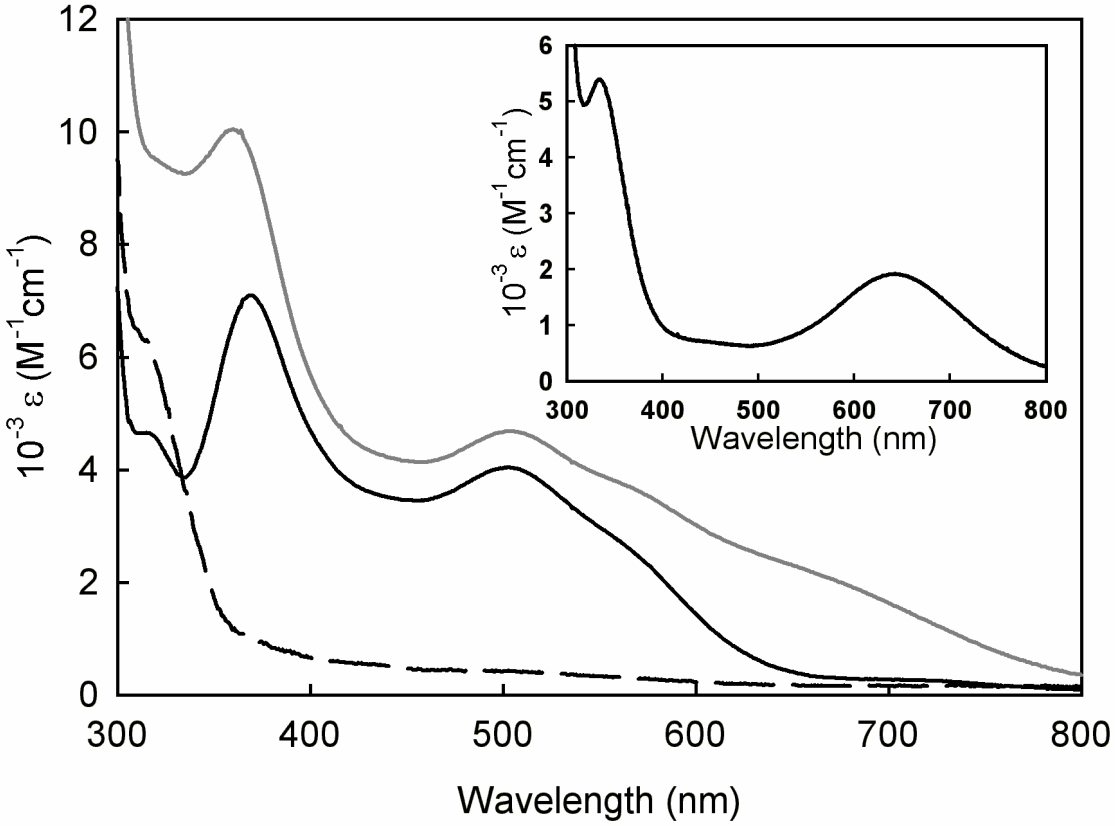

Figure 1.10. Optical absorption spectra of *D. vulgaris* 2Fe-SOR in its three stable oxidation states; As-isolated 2Fe-SOR_{pink} (black trace); fully oxidized 2Fe-SOR_{gray} (solid gray trace), oxidized with O_2^- from a xanthine/xanthine oxidase system; fully reduced 2Fe-SOR_{clear} (dashed black trace) reduced by titration with sodium dithionite). All molar absorptivities of 2Fe-SORs are in monomers (protein in solution is dimeric). Inset: Difference absorption spectrum, 2Fe-SOR_{gray} – 2Fe-SOR_{pink}, due to the ferric [$Fe(NHis)_4(SCys)(OGlu)$] center.

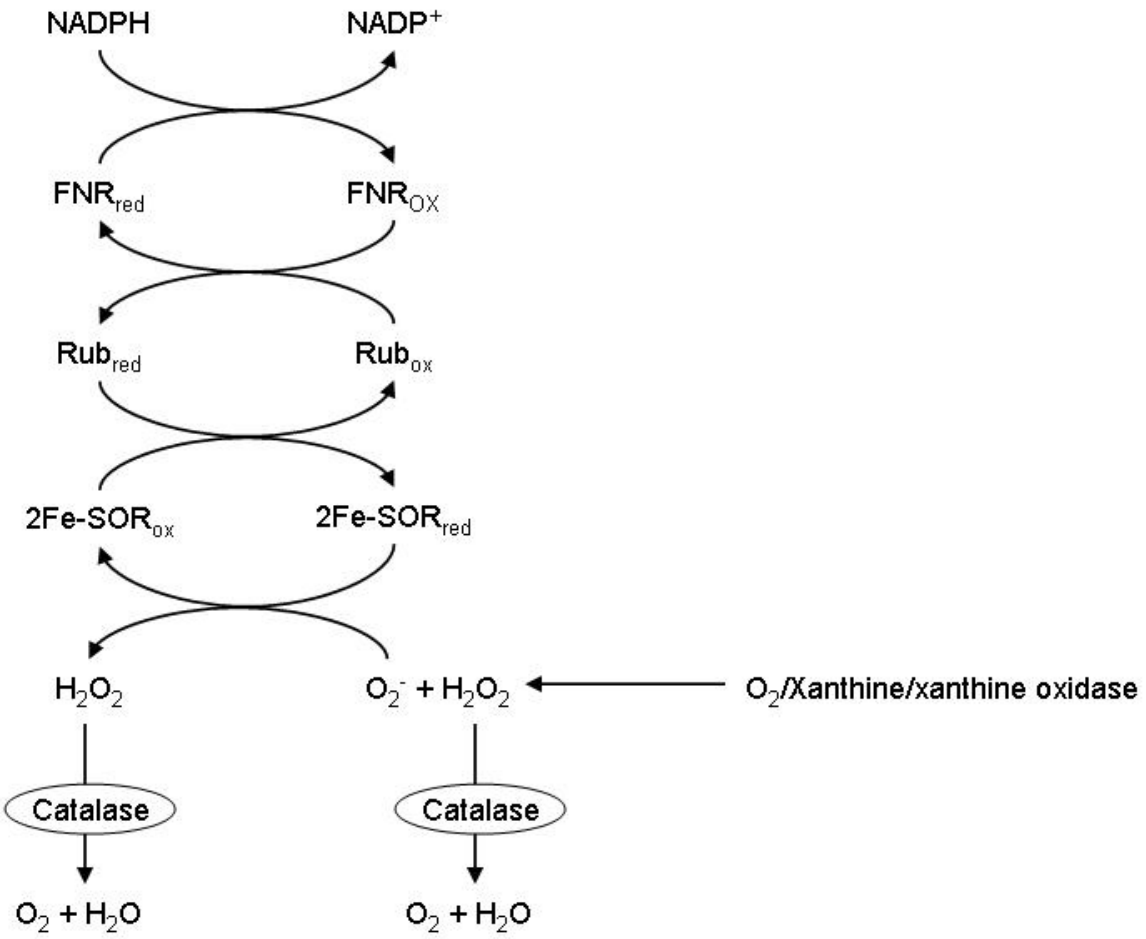

Figure 1.11. Diagram of the SOR assay as described in the text and by Coulter and Kurtz.[50] FNR refers to spinach ferrodoxin:NADPH reductase, and Rub refers to the *D. vulgaris* rubredoxin.

CHAPTER 2

INITIAL EXPERIMENTAL EVIDENCE FOR THE MECHANISM OF SUPEROXIDE REDUCTION BY THE *DESULFOVIBRIO VULGARIS* TWO-IRON SUPEROXIDE REDUCTASE: A PULSE RADIOLYSIS STUDY

2.A. Introduction

At the time of the experiments described in this chapter, a newly proposed pathway for resistance to superoxide, consisting of superoxide reduction, reaction 2.1, instead of the more accepted SOD type disproportionation reaction, reaction 2.2, was still highly speculative. SORs had been implicated as both superoxide dismutases[1] and superoxide reductases.[2, 3]

$$2O_2^- + 2H^+ \rightarrow O_2 + H_2O_2 \qquad (2.1)$$

$$e^- + O_2^- + 2H^+ \rightarrow H_2O_2 \qquad (2.2)$$

This chapter describes experiments, employing pulse radiolysis to rapidly produce superoxide, to measure catalytic disproportionation rates, i.e. SOD activity, as well as probing the superoxide/SOR reaction for transient reactive species found between the

starting ferrous center, $[Fe^{II}(NHis)_4(SCys)]$, to the resting ferric center, $[Fe^{III}(NHis)_4(SCys)(OGlu)]$ in *D. vulgaris* 2Fe-SOR. An engineered variant, E47A 2Fe-SOR, which replaced the coordinating glutamate with alanine, was also examined.

2.B. Materials and Methods

General molecular biological procedures followed as described in the *Current Protocols in Molecular Biology* series.[4]

Preparation of the recombinant D. vulgaris 2Fe-SOR and E47A 2Fe-SOR. Expression plasmid, pRbo, containing the *D. vulgaris* 2Fe-SOR gene (Genbank accession number M28848) was generated by insertion of the PCR-amplified gene into the *NdeI*/*SapI* restriction sites of pCYB1 (New England BioLabs, Inc.).[5] The plasmid pE47ARbo, containing the E47A-mutated 2Fe-SOR gene, was generated using pRbo as template, two complimentary oligonucleotide primers containing the desired mutation (underlined): 5′-GGGGCCAAGGAAGCGCACGTGCCGGTC-3′ and 5′-GACGGC-ACGTGCGCTTTCTTGGCCCC-3′ and the QuikChange mutagenesis kit (Stratagene, Inc.) following procedures described in the product manual. Oligonucleotide sequencing of these plasmids at the University of Georgia Molecular Genetics Instrumentation Facility confirmed the correctness of the 2Fe-SOR and E47A 2Fe-SOR gene sequences. pRbo or pE47ARbo were transformed separately into *E. coli* strain QC774 (*sodA*, *sodB*), originally obtained from Touati and co-workers.[6]

All *E. coli* cultures were aerobically grown with shaking at 37 °C in M9 minimal media, with 100 mg/L ampicillin. Fifty-milliliter overnight cultures of *E. coli*

QC774[pRbo] or -[pE47ARbo] were used to inoculate 1-L volumes of media. The 1-L cultures were grown with shaking to an $O.D._{600}$ of ~ 0.6 at which point isopropyl-β-D-thiogalactoside (100 mg/L) was added to induce 2Fe-SOR expression. The cultures were also supplemented with 25 mg/L $Fe(II)SO_4$, and incubated a further 3 hrs, after which the cells were harvested by centrifugation. The buffer used throughout protein purification was 50 mM 3-(*N*-morpholino)ethanesulfonate (MOPS), pH 7.3. After a freeze-thaw cycle the harvested cells from up to 10 L of culture were resuspended in 50 mL of buffer/L culture and sonicated for 20 x 10 second pulses using a 550 Sonic Dismembraner (Fisher Scientific). The supernatant was loaded onto a 2.5 x 5 cm DEAE Sepharose fast flow column (Amersham Pharmacia BioTek (APBT)) equilibrated with buffer, and the flow-through was collected and concentrated to ~ 2 mL/L culture. This concentrated sample was loaded onto a 1.6 x 2.5 HiTrap anion-exchange column (APBT) equilibrated with buffer and eluted at a flow rate of 2 mL/min. A pink fraction that eluted when the column was washed with buffer (no added salt) was collected, concentrated to ~ 2 mL/L culture and loaded onto a HiPrep 16/60 Sephacryl S-100 column (APBT) equilibrated with buffer with 250 mM NaCl and eluted at 0.5 mL/min. A pink eluting fraction was adjudged to be pure 2Fe-SOR by sodium dodecyl sulfate polyacrylamide gel electrophoresis. The pure wild type $2Fe\text{-}SOR_{pink}$ had an absorbance ratio, A_{280}/A_{502} = 5.8. The literature reports this absorbance ratio be 6.7 for the protein isolated directly from *D. vulgaris*;[7] our lower ratio presumably indicates purer protein. E47A 2Fe-SOR was isolated and purified analogously to the procedure described for the wild type protein.

Inductively coupled plasma atomic emission metal analyses of the 2Fe-SORs were performed at the Chemical Analysis Laboratory of the University of Georgia. Protein concentrations were determined using the Bio-Rad protein assay with BSA as standard for wild type 2Fe-SOR and wild type 2Fe-SOR as standard for E47A 2Fe-SOR. An extinction coefficient, ε_{502} = 4,300 $M^{-1}cm^{-1}$,[7] was used to determine 2Fe-SOR_{pink} concentrations for pulse radiolysis.

Spectroscopy of wild type and E47A 2Fe-SOR. [$Fe(NHis)_4(SCys)$] centers in both wild type and E47A 2Fe-SOR_{pink} were oxidized to form 2Fe-SOR_{gray} and E47A 2Fe-SOR_{gray} respectively by reaction with a xanthine/xanthine oxidase superoxide-generating system[1, 3] at room temperature in 50 mM MOPS, pH 7.3. Absorption spectra were collect on a Shimadzu UV-2401 PC spectrophotometer. Thirty-four micromolar (in [$Fe(NHis)_4(SCys)$] sites) 2Fe-SOR_{pink} and E47A 2Fe-SOR_{pink} were oxidized to completion in approximately 5 minutes by reaction of 500 mM xanthine (Sigma) with catalytic amounts of xanthine oxidase (Sigma).

Pulse Radiolysis. The rates of reactions of *D. vulgaris* 2Fe-SOR_{pink} and its E47A variant with superoxide were measured by pulse radiolysis using the 2-MeV Van de Graaff accelerator at Brookhaven National Laboratory, as described else where.[8] Dosimetry was calibrated using the KSCN dosimeter.[9] Superoxide radicals were generated at radiation doses of 150-200 rads,[10, 11] yielding 1 - 20 μM superoxide per pulse in either air- or dioxygen-saturated solutions containing 1 - 100 μM 2Fe-SOR_{pink} [$Fe(NHis)_4(SCys)$] sites, 10 mM sodium formate, 0.12 mM tris(hydroxymethyl)aminomethane (Tris) and, where stated, either 5 or 100 μM EDTA to

minimize the effects of free metal ions in water that had been purified by passage through a Millipore Ultrapurification system to achieve a resistivity of ~ 18 MΩ. Following addition of all other reagents, the pH was adjusted by addition of either sodium hydroxide or sulfuric acid. 2Fe-SOR_{pink} oxidation by superoxide was monitored at 500 - 700 nm via absorbance changes as a function of time from microseconds to second time scales. The sample cell path lengths were either 2 or 6.1 cm, and all experiments were conducted at 25 °C. The data was analyzed using the BNL Pulse Radiolysis Program.

2.C. Results and Discussion

Iron and protein analyses by inductively coupled plasma atomic emission (ICP-AE) confirmed the presence of ~ 4 Fe/2Fe-SOR homodimer for both wild type and E47A 2Fe-SOR, as expected for full occupancy of both iron centers, $[Fe(SCys)_4]$ and $[Fe(NHis)_4(SCys)]$.

Absorption spectra of 2Fe-SOR_{pink} and 2Fe-SOR_{gray} are shown in Figure 2.1.A and the corresponding spectra of E47A 2Fe-SOR in Figure 2.1.B. The wild-type 2Fe-SOR_{gray} - 2Fe-SOR_{pink} difference absorption spectrum in Figure 2.2 shows the previously reported feature at 647 nm (ε_{647} ~ 1,900 $M^{-1}cm^{-1}$) due to the ferric $[Fe(NHis)_4(SCys)(OGlu)]$ site.[1, 3, 7, 11] The corresponding feature in the difference spectrum of E47A 2Fe-SOR is blue shifted to approximately 590 nm and is much less intense (ε_{590} ~ 500 $M^{-1}cm^{-1}$). These results suggest that E47 interacts with the iron atom of the ferric $[Fe(NHis)_4(SCys)]$ site, most likely by carboxylate ligation. The published 2Fe-SOR crystal structure,[13] professedly of 2Fe-SOR_{gray}, is more likely to be that of

2Fe-SOR$_{pink}$, i.e., the form containing ferrous rather than ferric [Fe(NHis)$_4$(SCys)] sites, possibly resulting from exposure of 2Fe-SOR$_{gray}$ to the X-ray source. In our hands, *D. vulgaris* 2Fe-SOR$_{gray}$ slowly autoreduces to 2Fe-SOR$_{pink}$ at ambient temperature even in aerobic solutions. The polypeptide loop containing E47 was reported to be highly mobile in the 2Fe-SOR crystal structure. During oxidation to 2Fe-SOR$_{gray}$, movement of this loop would allow coordination of the E47 carboxylate to the [Fe(NHis)$_4$(SCys)] center, as occurs in *P. furiosus* 1Fe-SOR.[14]

SOD activity of 2Fe-SOR was monitored by the rate of disappearance of superoxide absorbance at 260 nm.[15] As shown in Figure 2.3, no enhancement of the spontaneous disproportionation rate was observed in the presence of 1 μM 2Fe-SOR$_{pink}$. At pH 7.8, typical SODs enhance the superoxide disproportionation rate constant by four orders of magnitude.[16] The measurements in Figure 2.3 indicate a limiting catalytic rate constant for 2Fe-SOR below that for spontaneous superoxide disproportionation (~ 10^5 $M^{-1}sec^{-1}$ at ambient temperature and pH 7.8 [8]), thus, establishing that 2Fe-SOR does not function as a "classical" SOD. In the same fashion, E47A 2Fe-SOR was also shown to be devoid of SOD activity. The iron-coordinated glutamate residue in *P. furiosus* SOR was proposed to obstruct the reaction of the ferric center with superoxide, thereby disfavoring SOD activity.[13] The lack of SOD activity for E47A 2Fe-SOR does not support such a role for the analogous glutamate residue in 2Fe-SOR.

Figure 2.4 shows absorbance time courses obtained on microsecond and millisecond time scales during reactions of 2Fe-SOR$_{pink}$ with sub-stoichiometric levels of superoxide generated by pulse radiolysis and optical absorption spectra constructed from

the time courses obtained between 440 - 710 nm at 10-nm intervals. An intermediate exhibiting an absorption centered at ~ 600 nm (ε_{600} ~ 3,500 $M^{-1}cm^{-1}$) is fully formed by ~ 60 μsec after the superoxide pulse (Figure 2.4.B.). This intermediate accumulates at a nearly diffusion-controlled rate (1.5 x 10^9 $M^{-1}sec^{-1}$) that is first order in both superoxide and 2Fe-SOR concentrations (0.5-5 μM superoxide and 25-100 μM $[Fe(NHis)_4(SCys)]$ sites, respectively). The 600-nm intermediate then decays in a first-order process (40 sec^{-1}) (Figure 2.4.C.) that is independent of superoxide concentration to yield a final spectrum (λ_{max} ~ 650 nm, ε_{650} ~ 2,300 $M^{-1}cm^{-1}$) closely resembling that of the $[Fe(NHis)_4(SCys)(OGlu)]$ site in $2Fe\text{-}SOR_{gray}$ (Figure 2.2). The second-order rate constant for the $[Fe(NHis)_4(SCys)]$ center oxidation by superoxide obtained in our studies agrees well with the value of (6 - 7) x 10^8 $M^{-1}sec^{-1}$ previously estimated via competition experiments between Cu/Zn- or Fe-SOD and *Desulfoarculus baarsii* 2Fe-SOR.[3]

The extinction coefficients listed for the 600-nm intermediate and final product are based on the initial concentration of sub-stoichiometric superoxide generated by pulse radiolysis and assumes that all such superoxide reacts with ferrous $[Fe(NHis)_4(SCys)]$ site of $2Fe\text{-}SOR_{pink}$. It can also be reasonably assumed that the absorption spectrum of the final pulse radiolysis product (filled squares in Figure 2.4.A) is that of the $[Fe(NHis)_4(SCys)]$ center in $2Fe\text{-}SOR_{gray}$. If so, then the close agreement between the corresponding extinction coefficients indicates a 1:1 molar stoichiometry between superoxide generated and $[Fe(NHis)_4(SCys)]$ centers reacted, i.e., a one-electron process, as expected formed the SOR-catalyzed reaction 2.2. An essentially identical 600-nm intermediate forms at approximately the same diffusion-controlled rate upon reaction of

E47A 2Fe-SOR with superoxide (Figure 2.4.A). The E47A 600-nm intermediate decays on the same time scale as for wild type, but in a more complicated fashion (not shown). Nevertheless, the final spectrum obtained via pulse radiolysis closely resembles the E47A difference absorption spectrum (Figure 2.2). A SOR reaction cycle consistent with these pulse radiolysis results is shown in Scheme 2.1. The increased absorption intensity of the transient species over that of the "resting" carboxylate-ligated ferric $[Fe(NHis)_4(SCys)(OGlu)]$ site implies an axial ligand other than carboxylate and is consistent with an inner-sphere electron transfer from the iron center to superoxide. The one electron reduction product of superoxide along with two protons is hydrogen peroxide, presumably the product of this reaction. Therefore, a likely formulation for the transient species is a ferric-peroxo or a ferric-hydroperoxo, as shown in Scheme 2.1.

Synthetic ferric-peroxo or ferric-hydroperoxo complexes have been well characterized.[17 - 19] Both ferric-peroxo and -hydroperoxo complexes typically exhibit peroxo $\rightarrow Fe^{III}$ charge transfer (CT) transitions between 500 and 750 nm (500 – 2,000 $M^{-1}cm^{-1}$). This range of wavelengths encompasses the 600-nm absorbing transient species resulting from reaction of superoxide with the ferrous $[Fe(NHis)_4(SCys)]$ center of 2Fe-SOR. However, the absorption spectrum associated with the resting ferric $[Fe(NHis)_4(SCys)(OGlu)]$ center with $\lambda_{max} \sim 650$ nm (c.f. Figure 2.2), is due to primarily to Cys-S $\rightarrow Fe^{III}$ CT bands.[20] The absorption of the transient species could, therefore, be a combination of Cys-S $\rightarrow Fe^{III}$ and peroxo $\rightarrow Fe^{III}$ CT bands. Kovacs and co-workers reported a 5-coordinate trigonal bypyramidal ferrous complex, with four nitrogen and one thiolate ligands.[21] At low temperatures (-90 °C) this complex reacted

with superoxide in a "wet" acetonitrile solution, yielding a short-lived transient species proposed to be a ferric-hydroperoxo (with peroxide coordinating *cis* to the thiolate) with λ_{max} ~ 452 nm (2,780 $M^{-1}cm^{-1}$). IR spectroscopy of this complex showed a Fermi doublet at 788 and 781 cm^{-1} for the O—O stretch,[22] which is similar to O—O stretching frequencies of other ferric-(hydro)peroxo complexes.[18] This transient species decayed to a 6-coordinate octahedral ferric-thiolate species, with methanol occupying the putative peroxo coordination site.[21] This ferric complex had λ_{max} 511 nm (1,765 $M^{-1}cm^{-1}$). These CT transitions remain to be assigned, but are likely to contain some thiolate → Fe^{III} CT character.[22]

Silaghi-Dumitrescu *et al.* used computational methods to model the transient species formed at the active center of 2Fe-SOR, as a ferric-peroxo or -hydroperoxo.[23] The DFT optimization of the SOR active center geometry suggested the formation of an end-on ferric-(hydro)peroxo species from the reaction of the ferrous $[Fe(NHis)_4(SCys)]$ center with superoxide, as shown in Figure 2.5.[23] The side-on ferric-peroxo models (c.f. Figure 2.5) were calculated to be higher in energy than those of the end-on models. This higher energy of the side-on peroxo model was attributed to steric interactions of the equatorial histidines ligands with the peroxo ligand leading to elongation of two of the His-N—Fe bonds and in some cases to breaking of a His-N—Fe bond. A side-on ferric peroxo complex was calculated to convert to an end-on hydroperoxo in the presence of an amine proton donor.[23] A calculated visible absorption spectrum for the end-on ferric-hydroperoxo model was found to consist primarily of Cys-S → Fe^{III} CT with some His-N → Fe^{III} CT character, and very little peroxo → Fe^{III} CT character.[23]

The only side-on ferric-peroxo species characterized in aqueous solution is a ferric-EDTA complex.[24, 25] However, this side-on ferric-peroxo complex is stable only under basic conditions (pH $\geq$ 10). Interconversion between side-on ferric-peroxo and end-on ferric-hydroperoxo has also been shown to be directly dependent on available protons.[19] Side-on ferric-peroxo complexes in organic solvents immediately coverted to end-on ferric-hydroperoxo when a proton source was added. Therefore, in aqueous solution at neutral pH, it is very unlikely that a side-on ferric-peroxo would be stable, especially a solvent exposed ferric-peroxo, such as that proposed for the transient intermediate of 2Fe-SOR. Therefore, the absorption intensity of the 600-nm intermediate is likely due to Cys-S $\rightarrow$ Fe^{III} LMCT transitions of an end-on ferric-hydroperoxo species. Protonation of the coordinated hydroperoxo by an amino acid side chain, would lead to release of hydrogen peroxide and 2Fe-SOR_{gray}, which we propose has a six-coordinate ferric [$Fe(NHis)_4(SCys)(OGlu)$] site. Re-insertion of an electron from the proposed reductant, rubredoxin,[26] would then lower the affinity of Glu47 for iron, leading to regeneration of the five-coordinate ferrous [$Fe(NHis)_4(SCys)$] site. The nearly diffusion-controlled initial reduction of superoxide by the ferrous [$Fe(NHis)_4(SCys)$] site is consistent with the presumed superoxide scavenging function of 2Fe-SOR. SOR-type enzymatic turnover of 2Fe-SOR, however, may be critically dependent on subsequent steps of the cycle, such as protonation of the ferric-(hydro)peroxo complex,[27] or the reduction process.

The results in this chapter clearly show that any mechanism for the SOR reaction must include a diffusion-controlled formation of an intermediate and intramolecular

decay of this intermediate. This intermediate is reasonably formulated as a ferric-(hydro)peroxo species (c.f. Scheme 2.1).

2.D. References

1. Romaõ, C. V., Liu, M. Y., Le Gall, J., Gomes, C. M., Braga, V., Pacheco, I., Xavier, A. V., Teixeira, M. (1999) *Eur. J. Biochem*. *261*, 438-443.
2. Liochev, S. I., Fridovich, I. (1997) *J. Biol. Chem*. 272, 25573-25575.
3. Lombard, M., Fontecave, M., Touati, D., Niviere, V. (2000*) J. Biol. Chem*. *275*, 115-121.
4. Current Protocols in Molecular Biology; (1996) Ausubel, F. M., Brent, R., Kingston, R. E., Moore, D. D., Seidman, J. G., Smith, J. A., Struhl, K., Ed., John Wiley & Sons, Inc. USA, vol. 1-3.
5. Lumppio, H., Shenvi, N., Summers, A., Voordouw, G., Kurtz, D. M., Jr. (2001) *J. Bacteriol. 183*, 101-108.
6. Carlioz, A., Touati, D. (1986) *EMBO J. 5*, 623-630.
7. Verhagen, M. F., Voorhorst, W. G., Kolkman, J. A., Wolbert, R. B., Hagen, W. R. (1993) *FEBS Lett*. *336*, 13-18.
8. Coulter, E. D., Emerson, J. P., Cabelli, D. E., Kurtz, D. M., Jr. (2000) *J. Am. Chem. Soc. 122*, 11555-11556.
9. Goto, J. J., Gralla, E. B., Valentine, J. S., Cabelli, D. E. (1998) *J. Biol. Chem. 273*, 30104-30109.
10. Schwarz, H. A. (1981) *J. Chem. Ed. 58*, 101-105.
11. Abreu, I. A., Saraiva, L. M., Carita, J., Huber, H., Stetter, K. O., Cabelli, D., Teixeira, M. (2000) *Mol. Microbiol. 38*, 322-334.

12. Tavares, P., Ravi, N., Moura, J. J., LeGall, J., Huang, Y. H., Crouse, B. R., Johnson, M. K., Huynh, B. H., Moura, I. (1994) *J. Biol. Chem*. *269*, 10504-10510.

13. Coehlo, A. V., Matias, P., Fülöp, V., Thompson, A., Gonzalez, A., Carrondo, M. A. (1997) *J. Bio. Inorg. Chem*. *2*, 680-689.

14. Yeh, A. P., Hu, Y., Jenney, F. E., Jr., Adams, M. W., Rees, D. C. (2000) *Biochemistry 39*, 2499-2508.

15. Bielski, B. H. J., Cabelli, D. E. (1991*) Int. J. Radiat. Biol*. *59*, 291-319.

16. Fee, J. A., McClune, G. J., O'Neill, P., Fielden, E. M. (1981) *Biochem. Biophys*. *Res. Commun*. *100*, 377-384.

17. Solomon, I., Brunold, T. C., Davis, M. I., Kemsley, J. N., Lee, S.-K., Lehnert, N.; Neese, F., Skulan, A. J., Yang, Y.-S., Zhou, (2000) *J. Chem. Rev. 100*, 235-350.

18. Girerd, J.-J. Banse, F., Simaan, A. J., (2000) Characterization and Properties of Non-Heme Iron Peroxo Complexes, in Metal-Oxo and Metal-Peroxo Species in Catalytic Oxidations, Meunier, B., ed., Springer-Verlag Berlin Heidelberg.

19. Roelfes, G., Vrajmasu, V., Chen, K., Ho, R. Y. N., Rohde, J.-U., Zondervan, C., la Crois, R. M., Schudde, E. P., Lutz, M., Spek, A. L., Hage, R., Feringa, B. L., Munck, E., Que, L., Jr., (2003) *Inorg. Chem. 42,* 2639-2653

21. Clay, M. D., Jenney, F. E., Hagedoorn, P. L., George, G. N., Adams, M. W. W., Johnson, M. K. (2002) *J. Am. Chem. Soc. 124*, 788-805.

21. Shearer, J., Nehring, J., Lovell, S., Kaminsky, W., Kovacs, J. A. (2001) *Inorg. Chem. 40*, 5483-5484.

22. Shearer, J., Scarrow, R. C., Kovacs, J. A., (2002) *J. Am. Chem. Soc. 124*, 11709-11717.

23. Silaghi-Dumitrescu, R., Silaghi-Dumitrescu, I., Coulter, E. D., Kurtz, D. M., Jr., (2003) *Inorg. Chem. 42,* 446-456.

24. Ahmad, S., McCallum, J. D., Shiemke, A. K., Appelman, E. H., Loehr, T. M., Sanders-Loehr, J., (1988) *Inorg. Chem. 27,* 2230-2233.

25. Neese, F., Solomon, E. I., (1998) *J. Am. Chem. Soc. 120*, 12829-12848.

26. Coulter, E. D., Kurtz, D. M., Jr., (2001) *Arch. Bioch. Biophys. 394*, 76-86.

27. Cabelli, D. E., Riley, D., Rodriguez, J. A., Valentine, J. S., Zhu, H. In Biomimetic Oxidations Catalyzed by Transition Metal Complexes; (2000) Meunier, B., Ed., Imperial College Press/World Scientific: London, 461-508.

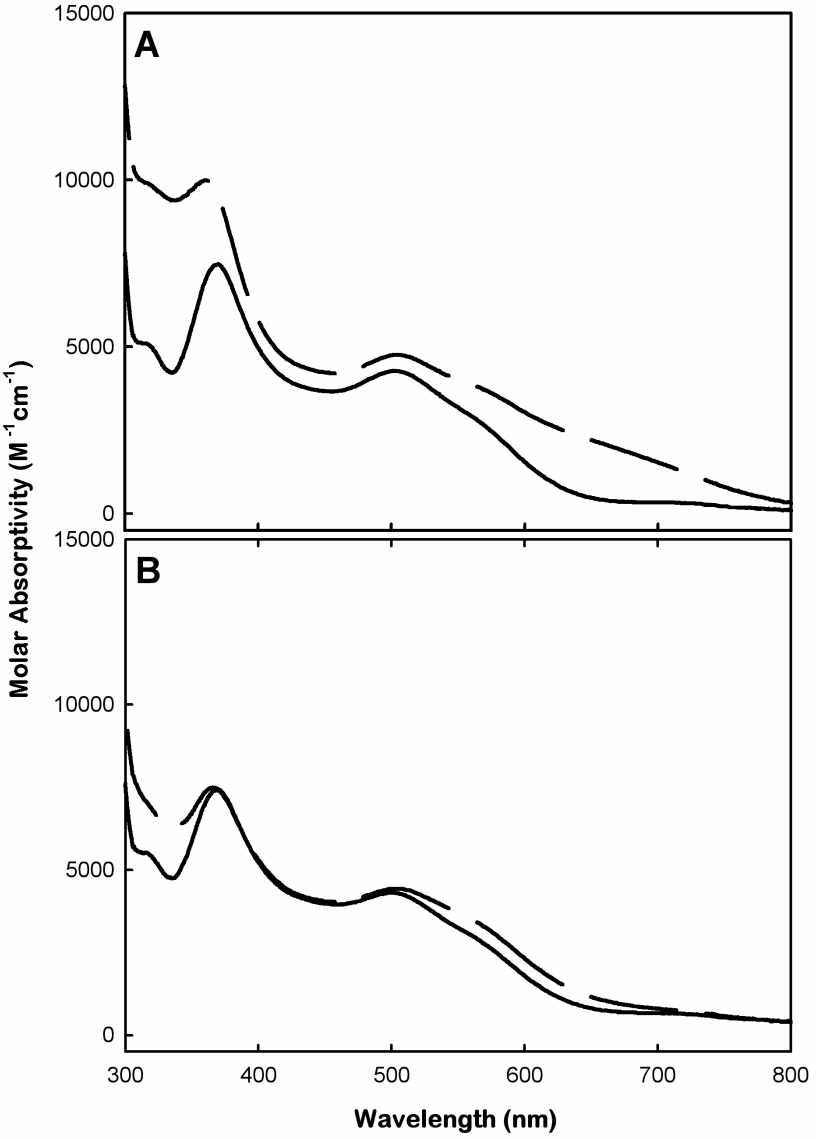

Figure 2.1. Optical absorption spectra of pink (solid trace) and gray (dashed trace) *D. vulgaris* 2Fe-SOR (~ 34 μM [$Fe(NHis)_4(SCys)$] sites) of wild type (A) or E47A (B) 2Fe-SOR (~ 23 °C) in 50 mM MOPS at pH 7.3. 2Fe-SOR_{gray} spectra were generated by superoxide oxidation using a superoxide flux from 500 mM xanthine and a catalytic amount of xanthine oxidase. Extinction coefficients of the absorption spectra are reported in 2Fe-SOR monomers (2Fe-SOR in solution is a homodimer).

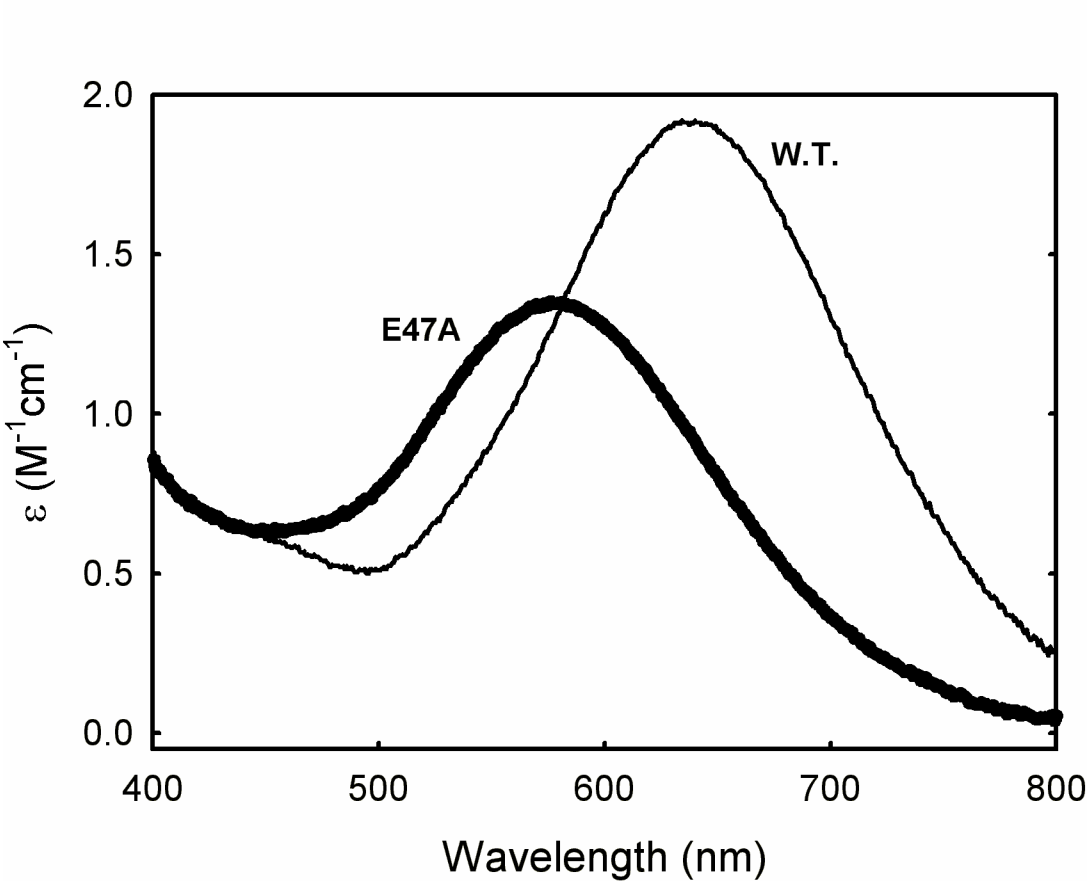

Figure 2.2. Difference absorption spectra (~ 23 °C) of wild type (W.T.) or E47A (bold trace) [2Fe-SOR_{gray} - 2Fe-SOR_{pink}], in which 2Fe-SOR_{gray} was generated by aerobic reaction of ~ 34 μM 2Fe-SOR_{pink} [$Fe(NHis)_4(SCys)$] sites with xanthine (0.4 mM)/xanthine oxidase (10 μg) in 50 MOPS at pH 7.3.

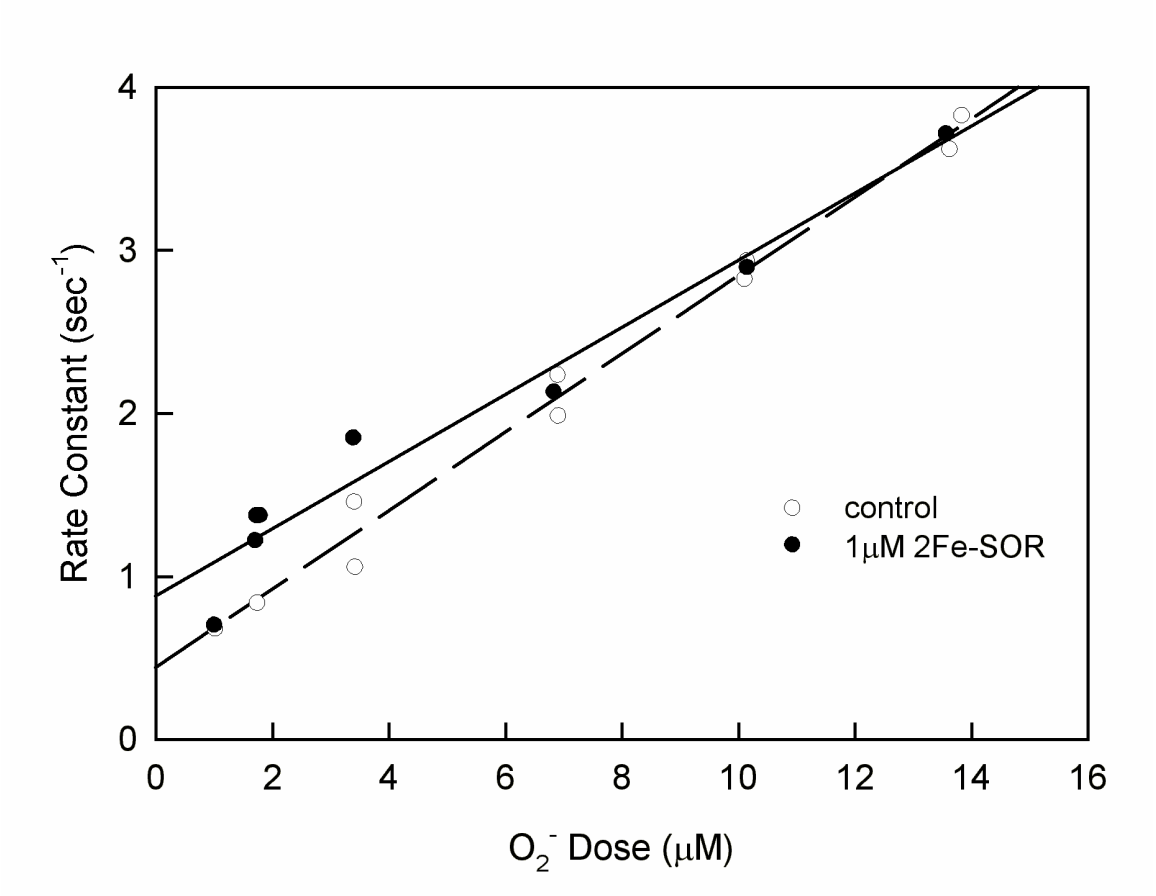

Figure 2.3. *D. vulgaris* 2Fe-SOR does not catalyze dismutation of superoxide. Rates of superoxide disappearance were measured spectrophotometrically as the decrease in absorbance at 260 nm (ε_{260} = 2,100 $M^{-1}cm^{-1}$[15]) following pulse radiolysis to generate superoxide in either the absence (control) or presence of 1 μM 2Fe-SOR_{pink} [$Fe(NHis)_4(SCys)$] sites in 10 mM Tris, 10 mM formate pH 7.76 at 25 °C. Lines indicate the least squares fits for the control (dashed) and the 1 μM SOR (solid) solutions.

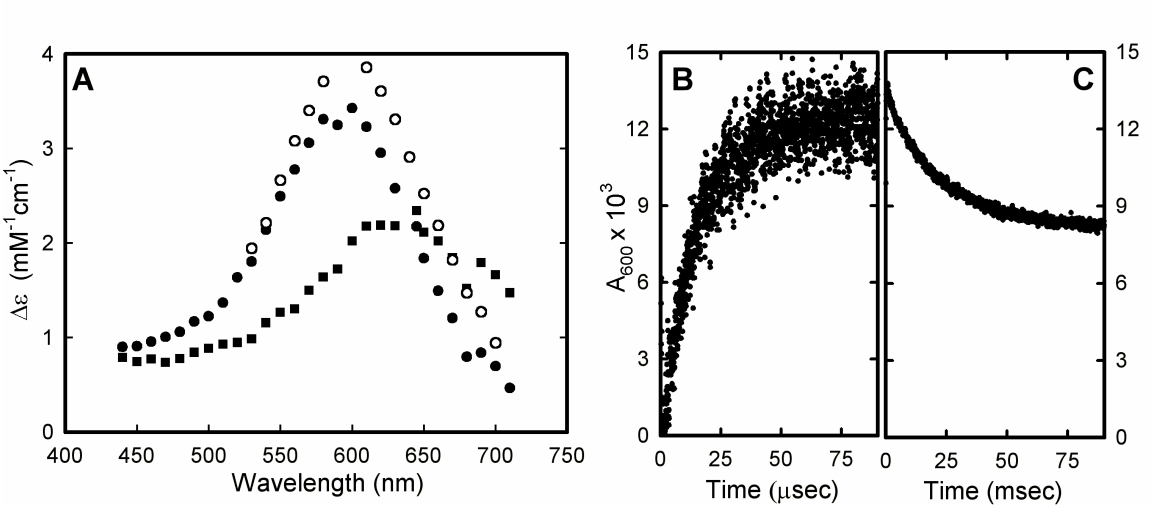

Figure 2.4. (A) Optical absorption spectra of the 600-nm intermediate (~ 75 μsec after pulse) (●) and final product (■) obtained ~ 100 msec after pulse radiolysis of *D. vulgaris* 2Fe-SOR$_{pink}$ (100 μM [Fe(NHis)$_4$(SCys) sites) solution to generate 1.7 μM superoxide. (○) E47A 2Fe-SOR 600-intermediate (~ 75 μsec after pulse). (B and C) Time courses for the formation (B) and decay (C) of the 600-nm intermediate following pulse radiolysis of 2Fe-SOR$_{pink}$ (50 and 25 μM [Fe(NHis)$_4$(SCys)] sites, respectively) solutions to generate 1.7 μM superoxide. Conditions: 0.12 mM Tris, 10 mM formate, 5 μM EDTA at pH 7.78, 25 °C, 2.0-cm optical path.

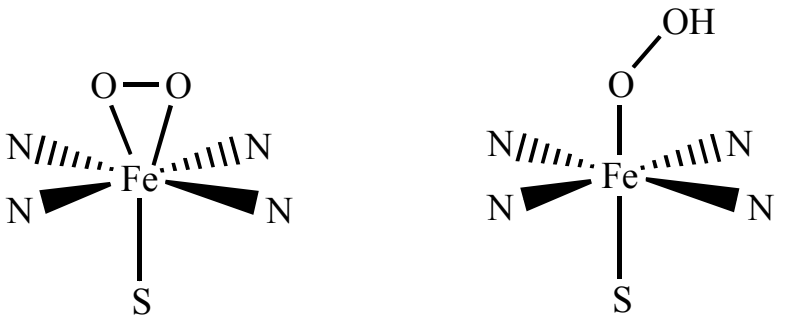

side-on ferric-peroxo end-on ferric-hydroperoxo

Figure 2.5 Possible coordination geometries of side-on ferric-peroxo and end-on ferric-hydroperoxo complexes formed at the $[Fe(NHis)_4(SCys)]$ site of 2Fe-SOR, based on models in [23].

Scheme 2.1.

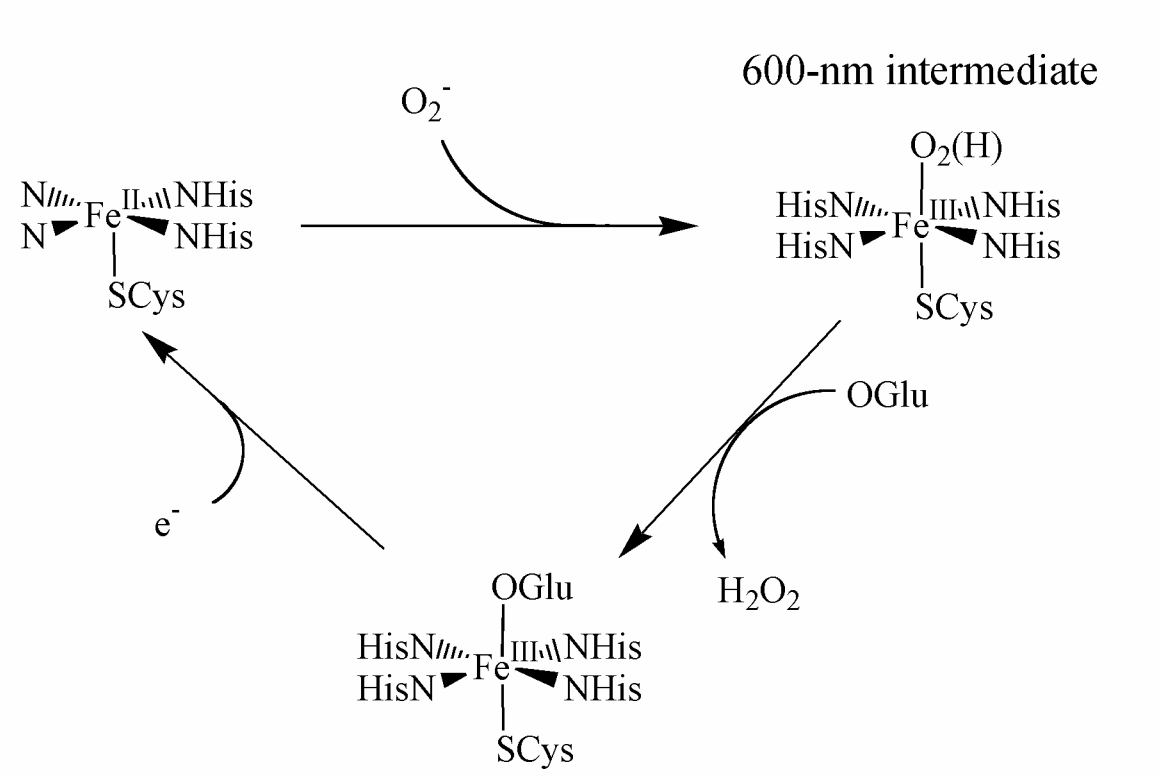
600-nm intermediate
O_2^-
$O_2(H)$
N
N
Fe II
NHis
NHis
SCys
HisN
HisN
Fe III
NHis
NHis
SCys
OGlu
e^-
H_2O_2
OGlu
HisN
HisN
Fe III
NHis
NHis
SCys

CHAPTER 3

KINETICS AND MECHANISM OF SUPEROXIDE REDUCTION BY THE TWO-IRON SUPEROXIDE REDUCTASE FROM *DESULFOVIBRIO VULGARIS*

3.A. Introduction

A newly emerging paradigm for protecting air-sensitive bacteria and archaea from the toxic reduction products of dioxygen involves reduction rather than disproportionation of superoxide, as described in Chapter 1 Section 1.D.[1 - 14]

This chapter reports a systematic and extensive investigation of the kinetics of superoxide reduction by *D. vulgaris* 2Fe-SOR and its E47A and K48A variants. The results of these studies allow a more complete and precise description of the mechanism shown in Scheme 3.1, which was based on the preliminary pulse radiolysis studies, described in Chapter 2. Other laboratories have conducted pulse radiolysis studies on other SORs,[15 - 17] and the results from these other studies are compared to those described in this chapter.

3.B. Material and Methods

Preparation of 2Fe-SOR and Variants. Expression and purification of recombinant *D. vulgaris* 2Fe-SOR and its E47A variant have been described previously

in Chapter 2 Section 2.B, as well as in the literature.[7] Plasmid pK48ARbo, containing the K48A-mutated *D. vulgaris* 2Fe-SOR gene, was generated using pRbo as template,[7] two complimentary oligonucleotide primers containing the desired mutation (underlined): 5′-GGGGCCAAGGAAGCGCACGTGCCGGTC-3′ and 5′-GACGGCACGTGCGC-TTCTTGGCCCC -3′ and the QuikChange mutagenesis kit (Stratagene, Inc.) following procedures described in the product manual. Oligonucleotide sequencing of these plasmids at the University of Georgia Molecular Genetics Instrumentation Facility confirmed the correctness of the K48A 2Fe-SOR gene sequence in pK48ARbo. This plasmid was then transformed into *E. coli* strain QC774 (*sodA, sodB*)[18] for overexpression of the K48A variant. The expression and purification protocol described in Chapter 2 [7] for recombinant *D. vulgaris* wild type 2Fe-SOR was used for the K48A variant. All 2Fe-SORs were judged to be pure by sodium dodecyl sulfate-polyacrylamide gel electophoresis.[19]

Metal and Protein Determinations. Metal analyses on 2Fe-SOR samples were conducted by inductively coupled plasma-atomic emission at the University of Georgia Chemical Analysis Laboratory. Protein concentrations were determined using the Bio-Rad protein assay with BSA as standard for wild type 2Fe-SOR and wild type 2Fe-SOR as standard for the E47A and K48A variants. 2Fe-SOR concentrations for all experiments were then determined using ε_{502} = 4,300 $M^{-1}cm^{-1}$, which is due to the ferric [$Fe(SCys)_4$] site in $2Fe\text{-}SOR_{pink}$.[13] Both wild type and variant 2Fe-SORs were isolated with ferric [$Fe(SCys)_4$] and predominantly ferrous [$Fe(NHis)_4(SCys)$] sites.

SOD Assays. Using the standard assay for SOD activity,[20] wild-type, E47A, and K48A 2Fe-SORs gave activites of 30, 160, and 40 units/mg, respectively. These activities may be compared with 4000 units/mg for bovine Cu/Zn SOD and 2000 units/mg for FeSOD.[21] Thus, the somewhat higher "SOD activity" of the E47A variant is still an order of magnitude below that of classical SODs. As described in Chapter 2 [7] neither the wild type nor E47A 2Fe-SORs possess SOD activities that could out-compete spontaneous disproportionation of micromolar levels of superoxide at pH 7.8.

Pulse Radiolysis Experiments. The rates of reactions of *D. vulgaris* 2Fe-SOR_{pink} and its E47A and K48A variants with superoxide were measured by pulse radiolysis using the 2-MeV Van de Graaff accelerator at Brookhaven National Laboratory, as described previously.[7] Dosimetry was calibrated using the KSCN dosimeter.[22] Superoxide radicals were generated at radiation doses of 150-200 rads,[23, 24] yielding 1-20 μM superoxide per pulse in either air- or dioxygen-saturated solutions containing 20-100 μM 2Fe-SOR_{pink} [$Fe(NHis)_4(SCys)$] sites, 10 mM sodium formate, 0.12 mM Tris, tris(hydroxymethyl)aminomethane (Tris) and, where stated, either 5 or 100 μM EDTA to minimize the effects of free metal ions, in water that had been purified by passage through a Millipore Ultrapurification system to achieve a resistivity of ~ 18 MΩ. (No significant differences in the kinetics were found for solutions containing vs. omitting EDTA.) For experiments in which formate concentration was varied, formate was added from a concentrated stock solution. Ionic strength was adjusted by addition of sodium chloride. Following addition of all other reagents, the pH was re-checked and adjusted by addition of either sodium hydroxide or sulfuric acid. Except for pH studies (where pH

is explicitly reported,) all experiments were conducted at pH 7.7. A set of experiments was also conducted using 0.5 M ethanol in place of formate; using ethanol to produce •OH radicals which rapidly produce superoxide.[25] For solvent deuterium isotope studies, solutions were prepared identically to that described above in 99.9 atom % D_2O (Isotek, Inc.). 2Fe-SOR_{pink} oxidation by superoxide was monitored at 500-700 nm via absorbance changes as a function of time from microseconds to second time scales. The sample cell path lengths were either 2 or 6.1 cm. The data were analyzed using the BNL Pulse Radiolysis Program. Except for temperature-dependent studies, all rates were measured at 25 ºC. Appropriate monitoring wavelengths and concentrations of oxidized $[Fe(NHis)_4(SCys)]$ sites were determined from the absorption difference spectra of superoxide-oxidized minus as-isolated wild-type or variant 2Fe-SOR_{pink}, and the following molar absorptivities (expressed on a $[Fe(NHis)_4(SCys)]$ site basis): ε_{645} = 1,900 $M^{-1}cm^{-1}$ for wild type, ε_{580} = 1,400 $M^{-1}cm^{-1}$ for E47A, and ε_{640}= 1,600 $M^{-1}cm^{-1}$ for K48A. The superoxide-oxidized 2Fe-SORs were prepared by incubation of 40-60 μM (in protein monomer determined using ε_{502} = 4,300 $M^{-1}cm^{-1}$ (c.f. Chapter 3 Section 3.C)) 2Fe-SOR_{pink} with 0.2 mM xanthine and sufficient xanthine oxidase to generate 5-10 μM superoxide/min in 50 mM potassium phosphate, 0.1 mM EDTA, pH 7.8.[14] Complete oxidation of $[Fe(NHis)_4(SCys)]$ sites by the superoxide flux occurred within 5-10 minutes and was taken to be the point at which the visible absorbance stopped increasing.

Oxidations of 2Fe-SORs by H_2O_2. Since H_2O_2 is generated along with superoxide during pulse radiolysis,[23] the kinetics of oxidation of the wild-type and variant ferrous $[Fe(NHis)_4(SCys)]$ sites by H_2O_2 were measured. These reactions were found to be

sufficiently slow so that H_2O_2 (50 – 2,000 μM) could be manually added to 2Fe-SOR_{pink} solutions (50 – 2,000 μM in monomer) in a spectroscopic cuvette, after which absorbance increases at 645 nm (wild-type), 580 nm (E47A), or 640 nm (K48A) were monitored with time. Reactions were conducted aerobically at room temperature in 50 mM potassium phosphate, 0.1 mM EDTA, pH 7.8. Rate constants for oxidation of the ferrous [$Fe(NHis)_4$(SCys)] sites were calculated from the extinction coefficients listed above for the oxidized sites. At pH 7.8 and room temperature, wild-type 2Fe-SOR_{pink} was oxidized to 2Fe-SOR_{gray} by H_2O_2 with a second-order rate constant of 21 ± 2 $M^{-1}sec^{-1}$, which is similar to that determined for the analogous oxidation of *D. Baarsii* 2Fe-SOR.[11] The second-order rate constant for the analogous reactions of the E47A and K48A variants were determined to be 37 ± 2 $M^{-1}sec^{-1}$ and 11 ± 1 $M^{-1}sec^{-1}$, respectively. Some instability of the SORs were noted when larger excesses of hydrogen peroxide were used. No intermediates were detected during these H_2O_2 oxidations, using either rapid mixing stopped-flow or manual mixing spectrophotometries. Given these second-order rate constants, the micromolar concentrations of H_2O_2 generated during pulse radiolysis cannot interfere with the superoxide oxidation kinetics of the [$Fe(NHis)_4$(SCys)] site of 2Fe-SOR_{pink}, which occur on the microsecond to millisecond time scales.

Stopped-Flow Spectrophotometry. The kinetics of *D. vulgaris* 2Fe-SOR_{pink} oxidation by ferricyanide were monitored by stopped-flow spectrophotometry on an RSM-1000 stopped-flow spectrophotometer fitted with a rapid scanning monochromator (OLIS, Inc.). Both 2Fe-SOR and potassium ferricyanide solutions were prepared in 50 mM MOPS pH 7.74. Solutions of 2Fe-SOR_{pink} (100 μM in [$Fe(NHis)_4$(SCys)] sites)

were mixed 1:1 (v/v) with 800 μM potassium ferricyanide in the stopped-flow instrument, and the subsequent absorbance changes at wavelengths between 440 and 680 nm were monitored.

Visible Absorption Spectrophotometry. UV/vis absorption measurements (other than stopped-flow) were measured in 1-cm pathlength quartz cuvettes on a Shimadzu UV2101PC scanning spectrophotometer.

3.C. Results

Protein Characterization. The recombinant wild-type *D. vulgaris* 2Fe-SOR and the two variants, E47A and K48A, were determined to contain 2.1 ± 0.30 mol of iron/mol of 2Fe-SOR monomer. These values indicated full occupancy of both [$Fe(SCys)_4$] and [$Fe(NHis)_4(SCys)$] sites by iron in all three proteins. Zinc and other transition metal contents were negligible (<0.05 mol metal/mol monomer) for all three 2Fe-SORs. These metal analyses in combination with the Bio-Rad protein assay (using wild type 2Fe-SOR as a standard) yielded a molar extinction coefficient 4.2 $mM^{-1}cm^{-1}$/monomer at 502 nm for the K48A variant, which is identical within experimental error to the published wild type value of 4.3 $mM^{-1}cm^{-1}$.[13] Gel filtration was used to verify that all three 2Fe-SORs are dimeric at the protein concentrations used in this study.[26] Throughout the Results section (namely Section 3.C.), these three *D. vulgaris* 2Fe-SORs are referred to simply as either wild- type or variant SORs.

Wild Type SOR: Pulse Radiolysis Kinetics. Figures 3.1.A. and 3.1.B. depict representative 600-nm absorbance vs. time traces, for reactions of wild type SOR_{pink} with

superoxide generated by pulse radiolysis at pH 7.7 and 25 ºC. These experiments were conducted under pseudo-first-order conditions in which the concentration of SOR [$Fe(NHis)_4(SCys)$] sites (20-100 μM) was typically in 5-100-fold molar excess over the superoxide generated by each pulse. Verifying our previous results, the rate of formation of the 600-nm transient was found to be first order in both superoxide (1-5 μM O_2^-) and SOR (between 20-200 μM [$Fe(NHis)_4(SCys)$] sites), whereas the rate of decay of this transient was found to be independent of superoxide concentration. Table 3.1 lists the rate constants derived from fits of these and analogous time courses assuming that single exponential functions accurately describe the absorbance vs. time courses for both a second-order formation and first-order decay of the 600-nm intermediate. Because pulse radiolysis studies on other SORs have indicated formation of a second distinct chromophoric intermediate maximizing ~ 5 msec following the superoxide pulse,[16, 27] we closely examined our decay curves for such a chromophore. Figure 3.1.B. shows that a sum of two exponential functions with k_2 = 350 sec^{-1} and k_3 = 80 sec^{-1} (gray trace) visually appears to provide a marginally improved fit to the time course for decay of the 600-nm intermediate. The sum-of-two exponentials fit would imply a second transient, i.e., a reaction sequence such as that in reaction 3.1.

$$SOR_{pink} + O_2^- \xrightarrow{k_1} \text{600-nm transient} \xrightarrow{k_2} 2^{nd}\text{-transient} \xrightarrow{k_3} SOR_{gray} \qquad (3.1)$$

However, the calculated goodness-of-fit parameters indicated that the sum-of-two-exponentials did not constitute a significant improvement over the one-exponential fit with k_{obs} = 80 sec^{-1}. Furthermore, the family of kinetic transients plotted in Figure

3.1.C and the absorption spectra constructed therefrom in Figure 3.1.D show no evidence for distinct chromophores other than those of the initial 600-nm intermediate and the final product.

The extinction coefficients for the intermediate and final product of pulse radiolysis on the *y*-axis of Figure 3.1.D were calculated assuming that each superoxide generated during a pulse oxidizes one [Fe(NHis)$_4$(SCys)] site in 2Fe-SOR$_{pink}$. The reasonably good agreement of the product spectrum in Figure 3.1.D obtained 100 msec following the superoxide pulse with the "resting" 2Fe-SOR$_{gray}$ spectrum, using the criteria of extinction coefficient (ε_{647} = 1,900 $M^{-1}cm^{-1}$ [7]), λ_{max}, and overall shape of the absorption curve confirms the one-electron nature of the reaction. This determination also means that the pulse radiolysis kinetics do not represent the sum of reaction rates of superoxide with the ferrous sites plus a portion of the newly formed ferric sites, as could in principle occur for SOD-type chemistry. Our pulse radiolysis kinetics are, thus, adequately described by formation of single 600-nm absorbing intermediate on the 100-μsec time scale and its decay to the "resting" 2Fe-SOR$_{gray}$ state on the 100-msec time scale.

As expected for a second order rate constant exceeding 10^9 $M^{-1}sec^{-1}$, the rate of formation of the 600-nm intermediate is only modestly temperature-dependent, showing an approximate 2.5-fold increase between 15 and 75 ºC. From the Erying plot in Figure 3.2, the activation parameters for formation of the 600-nm intermediate were estimated to be: $\Delta H^{\ddagger}_{formation}$ = +2 kcal/mol, $\Delta S^{\ddagger}_{formation}$ = -24 cal/molK and $\Delta G^{\ddagger}_{formation}$ = +11 kcal/mol. These values are reasonable for a second order associative mechanism involving

diffusion of a small molecule to an open coordination site in a metalloprotein.[28, 29] The rate constant for decay of the 600-nm intermediate appeared to exhibit a much larger temperature dependence, increasing approximately 800-fold between 15 and 75 ºC, with activation parameters: $\Delta H^{\ddagger}_{formation}$ = +12 kcal/mol, $\Delta S^{\ddagger}_{formation}$ = -2 cal/molK and $\Delta G^{\ddagger}_{formation}$ = +14 kcal/mol. Unfortunately, the pK_a of Tris, which was used to buffer these solutions, decreases significantly with increasing temperature (~ -0.03 ΔpK_a/ºC).[30] Since, as shown below, the decay rate constant, k_2, increases significantly at acidic pHs, the temperature dependence of k_2 is likely to be convoluted with its pH dependence in Tris-sulfate buffer.

The pH dependences for rates of formation and decay of the 600-nm intermediate are plotted in Figure 3.3 from the data listed in Table 3.2. The rate constant for formation of the 600-nm intermediate is nearly invariant over the pH range 5 to 9.5, indicating the lack of involvement of either protons or hydroxide in the rate-determining step. The pH/rate profile for the decay contains an "upward bend" below pH 7.5, which is typically analyzed in terms of separate pathways consisting of rate-determining protonation at low pH and either attack by water or unimolecular decomposition at high pH. The observed pH dependence of the decay can, thus, be analyzed according to $k_2 = k_2'[H^+] + k_2''$, where k_2' applies to a second order protonation of the 600-nm intermediate and k_2'' applies to a first order pH-independent decay of this intermediate. From a fit of this equation to the data plotted in Figure 3.3., k_2' is estimated to be 1.5 x 10^9 $M^{-1}sec^{-1}$, and k_2'' is estimated to be 50 sec^{-1}. This analysis, thus, suggests that the biphasic pH dependence arises from rapid, essentially diffusion-controlled, protonation of the 600-nm

intermediate at low pH that is out-competed at high pH by a first order pH-independent decay process.

Figure 3.4 plots the ionic strength dependences of the formation and decay rate constants for the 600-nm intermediate, and the corresponding data are listed in Table 3.2. At pH 7.7 the formation of the 600-nm intermediate shows an approximate 4-fold decrease in its rate of formation as ionic strength was increased from 0 to 0.4 M NaCl (0.1-0.7 $\mu^{1/2}$, including the 0.01 M formate), whereas the corresponding decay rate constant showed no more than a 1.3-fold decrease over the same ionic strength range. The formation and decay rate constants were found to be only modestly dependent on the concentration of formate (c.f. Table 3.3.), which was used to convert hydroxyl radicals to superoxide in the pulse radiolysis solutions.[22] Spectroscopic monitoring indicated that formate does not form a complex with the ferric [$Fe(NHis)_4(SCys)$] site of SOR_{gray} in the concentration range used for the pulse radiolysis. The same 600-nm intermediate was found to form in pulse radiolysis experiments using 0.5 M ethanol rather than formate to generate superoxide (c.f. Figure 3.5).

At pH 5.5, the formation rate constant, k_1, showed essentially the same ionic strength dependence as at pH 7.7, as expected if proton transfer is not rate-determining (the pK_a of HO_2, 4.8, would not be a significant factor in the pH range examined here). The decay rate constant, k_2, however showed a definite increase with increasing ionic strength at pH 5.5, as opposed to the relative invariance seen at pH 7.7. The ~ 5-fold increase in k_2 from 0 - 0.4 M NaCl at pH 5.5 is consistent with the decay consisting of rate-determining protonation of a positively charged intermediate by solvent at acidic pH.

Consistent with the ionic strength and pH dependences, the decay, but not the formation, rate constant shows a substantial solvent D_2O effect. For two consecutive sets of pulse radiolysis experiments carried out at pH 7.7 and 25 ºC in H_2O and D_2O, respectively, under identical conditions, $k_1[H_2O]/k_1[D_2O] = 1.2 (\pm 0.3)$, whereas $k_2[H_2O]/k_2[D_2O] = 2.0 (\pm 0.2)$. Thus, a proton transfer in the rate-determining step is evident in decay but not in formation of the 600-nm intermediate at pH 7.7.

Wild-Type 2Fe-SOR: Oxidation by Ferricyanide. To compare the kinetics of SOR_{pink} oxidation by superoxide with other one-electron oxidants, we examined the oxidation of SOR_{pink} with ferricyanide by stopped-flow spectrophotometry. Absorbance increases were monitored at fixed wavelengths of 600 nm and 650 nm and also by rapid scanning spectrophotometry between 440 and 680 nm up to ~ 2 sec following stopped-flow mixing. At 25 ºC in 50 mM MOPS pH 7.4, 50 μM $[Fe(NHis)_4(SCys)]$ site of 2Fe-SOR_{pink} was oxidized by 400 μM potassium ferricyanide to a species indistinguishable from 2Fe-SOR_{gray} with a rate constant of 30 ± 0.3 sec^{-1}, as determined from ΔA_{650} vs. time data, Figure 3.6. No faster-forming intermediate absorbing within the range of 440 to 680 nm was detected to have accumulated prior to the mixing dead time (~ 2 msec). Fitting of the ΔA_{650} time courses with a sum of two exponentials did not improve the fit over the single 30 sec^{-1} exponential.

E47A and K48A SOR Pulse Radiolysis Kinetics. The data presented in Figure 3.7 and in Table 3.1. indicate the intermediate formed upon pulse radiolysis of the E47A SOR_{pink} variant has kinetics and absorption spectral characteristics closely resembling those of the wild type at pH 7.8, i.e., second order, nearly diffusion-controlled formation

of a 600-nm absorbing intermediate on the 100-μsec time scale and its first order, single-exponential decay on the 100-msec time scale. The decay time course for E47A SOR in Figure 3.7.B was also fit to a sum of two exponentials according to reaction sequence 3.1 with k_2 = 350 sec^{-1} and k_3 = 70 sec^{-1}. As for wild-type, while visually appearing to provide a slightly better fit to the early stages of the decay kinetics, the sum-of-two-exponentials does not constitute a statistically significantly improvement over the one-exponential fit with k_2 = 65 sec^{-1}. Furthermore the 3-dimentional plot in Figure 3.7.C shows no evidence for a second distinct chromophore between the 600-nm intermediate and the final product. The final product spectrum, constructed from data obtained at 100 msec (Figure 3.7.D), is once again in reasonably good agreement with the "resting" E47A SOR_{gray} absorption spectrum at pH 7.8.[7] Removal of the E47 carboxylate ligand could in principle allow solvent coordination to the $[Fe(NHis)_4(SCys)]$ site. The absorption spectrum of the E47A intermediate (c.f. Figure 3.7.D), however, closely resembles that of the wild type (compare Figure 3.1.D), and is essentially pH-independent between 5.6 and 9.1. These results show that the E47 carboxylate does not affect either the rate of formation or the nature of the intermediate, nor does it affect the decay kinetics of the intermediate at pH 7.8. The decay rate for the E47A 2Fe-SOR intermediate is significantly lower than for wild type 2Fe-SOR, at pH 5.5 (c.f. Figure 3.8). The E47A intermediate does not have a pK_a near pH 5.5 (c.f. Figure 3.7.D), so the slower rate is consisted with some involvement of the E47 in decay of the intermediate at pH 5.5.

The first detectable intermediate upon pulse radiolysis of K48A SOR_{pink} formed with a second-order rate constant (c.f. Table 3.1 and Figure 3.9.A) that was 6-7-times

slower than that for formation of the wild-type SOR intermediate under the same conditions (pH 7.7). The ionic strength dependence of the K48A formation rate constant was also much smaller than for wild type (Table 3.4). The first-order decay of the K48A intermediate was 3-4-fold slower than for wild type under the same conditions (c.f. Table 3.1 and Figure 3.9.B and 3.9.C). The initial portion of the K48A decay trace in Figure 3.9.B shows evidence of a second intermediate, i.e., that the reaction 3.1 sequence may apply. Fits of the K48A decay curve with a sum of two exponentials yielded k_2 = 275 sec^{-1} and k_3 = 20 sec^{-1}. However, once again, the family of decay transients in the 3-D plot of Figure 3.9.C showed no clear evidence for a distinct chromophore that could be associated with a second intermediate (which for k_2 = 275 sec^{-1} should accumulate maximally at ~ 8 msec reaction time). Furthermore, the absorption spectrum of the K48A intermediate obtained 800 μsec after pulse radiolysis (Figure 3.9.D) is very similar to that of wild type, with an absorption maximum at 590 nm (ε_{590} = 3,600 $M^{-1}sec^{-1}$).

3.D. Discussion

Scheme 3.2 is a refinement of Scheme 3.1 that follows directly from the results presented here. The key evidence for Scheme 3.2 can be summarized as follows:

1. The oxidation kinetics of the ferrous [Fe(NHis)$_4$(SCys)] site in *D. vulgaris* SOR_{pink} by superoxide consists of second-order formation of an intermediate absorbing at 600 nm and its first-order decay to a species indistinguishable from the ferric, carboxylate-ligated site of SOR_{gray}.

2. The lack of any detectable intermediate during oxidation of ferrous [Fe(NHis)$_4$(SCys)] site by the outer-sphere oxidant ferricyanide, despite the very similar overall time scales for oxidation by ferricyanide and superoxide, further supports the chemically reasonable formulation of the 600-nm intermediate as the product of an inner-sphere redox reaction, generating a ferric-(hydro)peroxo species.
3. The second-order rate constant exceeding 10^9 $M^{-1}sec^{-1}$, the low positive activation enthalpy, and the negative activation entropy for formation of the 600-nm intermediate are all consistent with rate-determining diffusion of superoxide to the ferrous [Fe(NHis)$_4$(SCys)] site.
4. The formation rate constant for the 600-nm intermediate decreases with increasing ionic strength, consistent with interaction of incoming superoxide anion with a positive charge at or near the ferrous [Fe(NHis)$_4$(SCys)] site.
5. The rate constant for the formation of the 600-nm intermediate is essentially pH-independent (pH 5-9.5) and shows no D_2O solvent isotope effect; i.e., its formation does not involve a rate-determining protonation.
6. The first-order rate constant for decay of the 600-nm intermediate follows the pH-dependent rate law: $k_2(\text{obs}) = k_2'[H^+] + k_2''$, and shows a significant D_2O solvent isotope effect at pH 7.7. The values of k_2' and k_2'' indicate that the 600-nm intermediate converts to SOR_{gray} via a diffusion-controlled protonation by either solvent or a protein residue at acidic pHs and a pH-independent first-order process involving water or a water-exchangeable proton on the protein at basic pHs.

7. The rate constant for decay of the 600-nm intermediate increases with increasing ionic strength at pH 5.5, which, together with the rate law in 6, suggests diffusion-controlled protonation of a positively charged intermediate at acidic pHs.

Assuming that the coordination sphere of the ferrous [$Fe(NHis)_4(SCys)$] site is retained, a ferric-peroxo adduct would be overall charge-neutral (i.e., four neutral imidazoles, cysteinate and peroxo ligated to Fe^{III}). Based on the structures of other SORs,[5, 6] the conserved Lys48--εNH_3^+ *in D. vulgaris* 2Fe-SOR appears to be the only positively charged center near the [$Fe(NHis)_4(SCys)$] site at neutral pH, and to be localized above what would be the peroxo coordination position. The Lys48--εNH_3^+ would, therefore, likely be attracted to both the negatively charged incoming superoxide and the resulting peroxo ligand. This role for K48 is supported by both the 6-to 7- fold slower rate constant for formation of the intermediate and the much smaller ionic strength dependence of this formation rate constant for the K48A variant. The absorption spectra in Figures 3.1.D and 3.4.D show that the 600-nm intermediate does not have a pK_a between pH 5.6 and 9.1. The apparently diffusion-controlled, acid-catalyzed decay pathway in Scheme 3.2 that dominates at acidic pHs could then consist of disruption of the K48-NH_3^+---O_2^{2-} salt bridge by protonation of the ferric-peroxo followed by rapid addition of a second proton and release of H_2O_2. The pH-independent, first order decay pathway in Scheme 3.2, which dominates at basic pHs, could involve rate-determining water attack on the ferric-peroxo or, as formulated in Scheme 3.2, proton transfer from the lysyl side chain to the ferric-peroxo oxygen. Either explanation is consistent with the solvent D_2O effect on k_2 at pH 7.7.

Our data do not rule out an alternative mechanism consisting of rapid protonation of an initially formed ferric-peroxo to generate a ferric-hydroperoxo 600-nm intermediate. If so, however, the rate constant for this rapid protonation of the ferric-peroxo would have to exceed 10^{10} $M^{-1}sec^{-1}$ in order to explain the pH and D_2O independence of a formation rate constant exceeding 10^9 $M^{-1}sec^{-1}$. A protein side chain might conceivably supply a proton sufficiently rapidly to form a ferric-hydroperoxo 600-nm intermediate. However, the only proximal side chain capable of proton donation at pH 7.8 appears to be the ε-amino group of K48, and the K48A variant forms a spectrally nearly identical 600-nm intermediate, albeit 6-7 times slower than does wild-type. A ferric-(hydro)peroxo 600-nm intermediate in the K48A variant would presumably have to acquire its proton directly from solvent.

The same 600-nm intermediate forms in the E47A variant (compare Figure 3.7.D and Figure 3.1.D). The lack of significant perturbation of the formation and decay rate constants from their wild-type values in the E47A variant (c.f. Table 3.1) suggests that Glu47 does not directly displace the (hydro)peroxo ligand of the 600-nm intermediate at basic pHs. Since we did not detect any other distinct species between the 600-nm intermediate and the final product, we can only infer the existence of a transient species, which is formulated as a hydroperoxo adduct within brackets in Scheme 3.2. At pH 5.5, on the other hand, k_2 for the E47A variant is significantly lower than for wild type (c.f. Figure 3.8), consistent with some involvement of E47 in decay of the 600-nm intermediate at acidic pHs. The minimal involvement in superoxide reduction kinetics at or above neutral pH of this strictly conserved glutamate, a result also reported for 1Fe-

SOR,[17] is somewhat surprising. One possible explanation is that *in vivo* this glutamate prevents coordination of small molecules to the "resting" ferric [Fe(NHis)$_4$(SCys)] site that would either inhibit SOR activity or result in adventitious side reactions, but that, during SOR turnover, this glutamate does not ligate iron. Another candidate for the inferred bracketed species in Scheme 3.2 is, thus, a five-coordinate ferric [Fe(NHis)$_4$(SCys)] site.

The fairly modest effect of K48A substitution on the decay kinetics (3- to 4-fold slower with some evidence for a second intermediate) may underemphasize an additional important role for K48. The interaction with K48 shown in Scheme 3.2 may affect how the ferric-peroxo intermediate is protonated during its decay. If the intermediate contains an end-on-coordinated peroxo, protonation of the iron-bound oxygen atom is likely to favor dissociation of hydrogen peroxide, whereas protonation of the terminal oxygen would more likely favor O—O bond cleavage. These alternative proton-directed decay pathways have, in fact, been proposed to occur in the structurally analogous heme-thiolate active site of cytochrome P450, with O—O bond cleavage leading to the highly oxidizing oxo-ferryl (Fe^{V}=O) species.[31] K48 in SOR could, thus, direct decay of the intermediate towards hydrogen peroxide formation and away from potentially toxic P450-type oxidative chemistry.

Following our initial report on pulse radiolysis of *D. vulgaris* 2Fe-SOR,[7] Lombard et al. reported a pulse radiolysis study on reaction of superoxide with a closely homologous (70% sequence-identical) 2Fe-SOR from *Desulfoarculus baarsii,*[15] which was interpreted as proceeding via two successive intermediates at pH 7.6 (the only pH

reported). The first of these intermediates formed on a time scale similar to that which we observed for formation of the 600-nm intermediate of *D. vulgaris* SOR and had similar absorption features. The second *D. baarsii* 2Fe-SOR intermediate was reported to maximize at ~ 5-msec reaction time and to show a red-shifted absorption maximum with a significant increase in absorption intensity relative to the first intermediate. The same study reported similar consecutive chromophoric intermediates for an E47A variant of *D. baarsii* 2Fe-SOR. The results presented above on the other hand provide no clear evidence for a second distinct chromophoric intermediate in the reactions of either wild-type or E47A *D. vulgaris* 2Fe-SORs with superoxide. If the bracketed species shown in Scheme 3.2 corresponds to the second intermediate seen in the *D. baarsii* 2Fe-SOR, it does not accumulate sufficiently to be detected in *D. vulgaris* 2Fe-SOR. Pulse radiolysis of a K48I variant of *D. baarsii* 2Fe-SOR[15] gave kinetics and spectral features of two consecutive intermediates that might be more similar to the intermediate and final product we observed for the K48A variant of *D. vulgaris* 2Fe-SOR, but with differing effects on rates. The K48I substitution was reported to slow the formation rate 20-30-fold (vs. the 6-7-fold slowing we observed for *D. vulgaris* K48A) but to have no effect on decay rate (vs. 3-4-fold slowing for the *D. vulgaris* K48A). A second pulse radiolysis study by the same group on a 1Fe-SOR from *T. pallidum* also reported two consecutive chromophoric intermediates, which were similar to those they reported for the *D. baarsii* 2Fe-SOR.[16] Pulse radiolysis kinetics of a 1Fe-SOR from *Archaeoglobus fulgidus*[17] which were measured in the same laboratory used for the studies, on *D. vulgaris* 2Fe-SOR reported in this chapter detected only a single intermediate. The rate of formation

and spectral properties of the *A. fulgidus* 1Fe-SOR intermediate closely resembled the 600-nm species observed for the *D. vulgaris* 2Fe-SOR, but decayed to the "resting" oxidized form ~ 250-times faster. Even if it were turnover-limiting, the much slower decay rate constant for the *D. vulgaris* 2Fe-SOR intermediate is likely to be orders of magnitude faster than spontaneous disproportionation of superoxide *in vivo*. At pH 7 and 25 °C, the 600-nm intermediate of the *D. vulgaris* 2Fe-SOR decays with a first-order rate constant of 270 sec^{-1} (c.f. Table 3.1.). Under the same conditions, superoxide disproportionates with a second-order rate constant of ~ 5 x 10^5 $M^{-1}sec^{-1}$.[25] Thus, in order for spontaneous disproportionation to compete with decay of the 600-nm intermediate, the intracellular steady-state superoxide concentration would have to be ~ 10^{-3} M, which is probably several orders of magnitude above the lethal level. While no estimates are available for sulfate-reducing bacteria, in aerobically growing *E. coli*, the steady-state intracellular superoxide concentration is estimated to be 10^{-10} M, and to be just below the threshold of lethality.[32]

In fact, none of the pulse radiolysis studies published to date directly address SOR turnover. The exogenous electron donor(s) that would return the ferric $[Fe(NHis)_4(SCys)]$ site to the ferrous form (and perhaps also reduce the $[Fe^{III}(SCys)_4]$ site) *in vivo* has (have) not been identified. Coulter and Kurtz [14] recently showed that *D. vulgaris* rubredoxin catalyzes reduction of both iron sites in *D. vulgaris* 2Fe-SOR and serves as a catalytically competent proximal electron donor to 2Fe-SOR in a newly developed SOR turnover assay.

3.E. References

1. Pianzzola, M. J., Soubes, M., Touati, D. (1996) *J. Bacteriol. 178*, 6736-6742.
2. Liochev, S. I., Fridovich, I. (1997) J. Biol. Chem. *272*, 25573-25575.
3. Jenney, F. E., Jr., Verhagen, M. F. J. M., Cui, X., Adams, M. W. W. (1999) *Science 286*, 306-309.
4. Lumppio, H. L., Shenvi, N. V., Summers, A. O., Voordouw, G., Kurtz, D. M., Jr. (2001) *J. Bacteriol. 183*, 101-108.
5. Yeh, A. P., Hu, Y., Jenney, F. E., Jr., Adams, M. W., Rees, D. C. (2000) *Biochemistry 39*, 2499-508.
6. Coehlo, A. V., Matias, P., Fülop, V., Thomson, A., Gonzalez, A., Carrondo, M. A. (1997) *J. Biol. Inorg. Chem. 2*, 680-689.
7. Coulter, E. D., Emerson, J. P., Kurtz, D. M., Jr., Cabelli, D. E. (2000) *J. Am. Chem. Soc. 122*, 11555-11556.
8. Brumlik, M. J., Voordouw, G. (1989) *J. Bacteriol. 171*, 4996-5004.
9. Moura, I., Tavares, P., Moura, J. J., Ravi, N., Huynh, B. H., Liu, M. Y., LeGall, J. (1990) *J. Biol. Chem. 265*, 21596-21602.
10. Tavares, P., Ravi, N., Moura, J. J. G., LeGall, J., Huang, Y.-H., Crouse, B. R., Johnson, M. K., Huynh, B. H., Moura, I. (1994) *J. Biol. Chem. 269*, 10504-10510.
11. Lombard, M., Fontecave, M., Touati, D., Niviere, V. (2000) *J. Biol. Chem. 275*, 115-21.
12. Clay, M. D., Jenney, F. E., Jr., Hagedoorn, P. L.,George, G. N., Adams, M. W. W., Johnson, M. K. (2002) *J. Am. Chem. Soc. 124,* 788-805.

13. Verhagen, M. F. J. M., Voorhorst, W. G., Kolkman, J. A., Wolbert, R. B., Hagen, W. R. (1993) *FEBS Lett. 336*, 13-18.

14. Coulter, E. D., Kurtz, D. M., Jr. (2001) *Arch. Biochem. Biophys. 394,* 76-86.

15. Lombard, M., Houee-Levin, C., Touati, D., Fontecave, M., Niviere, V. (2001) *Biochemistry 40*, 5032-5040.

16. Niviere, V., Lombard, M., Fontecave, M., Houee-Levin, C. (2001) *FEBS Lett. 497*, 171-3.

17. Abreu, I. A., Saraiva, L. M., Soares, C. M., Teixeria, M., Cabelli, D. E. (2001) *J. Biol. Chem. 276*, 38995-39001.

18. Carlioz, A., Touati, D. (1986) *EMBO J. 5*, 623-630.

19. Schagger, H., von Jagow, G. (1987) *Analyt. Biochem. 166*, 368-379.

20. McCord, J. M., Fridovich, I. (1969) *J. Biol. Chem. 244*, 6049-6055.

21. Coulter, E. D., Shenvi, N. V., Kurtz, D. M., Jr. (1999) *Biochem. Biophys. Res. Commun. 255*, 317-323.

22. Goto, J. J., Gralla, E. B., Valentine, J. S., Cabelli, D. E. (1998) *J. Biol. Chem. 273*, 30104-9.

23. Schwarz, H. A. (1981) *J. Chem. Ed. 58*, 101-105.

24. Abreu, I. A., Saraiva, L. M., Carita, J., Huber, H., Stetter, K. O., Cabelli, D., Teixeira, M. (2000) *Mol. Microbiol. 38*, 322-34.

25. Bielski, B. H. J., Cabelli, D. (1991) *Int. J. Radiat. Biol. 59*, 291-319.

26. Apiyo, D., Jones, K., Guidry, J., Wittung-Stafshede, P. (2001) *Biochemistry 40*, 4940-8.

27. Beyer, W. F., Fridovich, I. (1987) *Analyt. Biochem. 161*, 559-561.

28. Xiong, J., Phillips, R. S., Kurtz, D. M., Jr., Jin, S., Ai, J., Sanders-Loehr, J. (2000) *Biochemistry 39*, 8526-36.

29. Farmer, C. S., Kurtz, D. M., Jr., Phillips, R. S., Ai, J., Sanders-Loehr, J. (2000) *J. Biol. Chem. 275*, 17043-17050.

30. Williams, A., Frasca, V. (1999) in *Current Protocols in Protein Science* (Coligan, J. E., Dunn, B. M., Ploegh, H. L., Speicher, D. W., and Wingfield, P. T., Eds.) pp 8.2.1-8.2.30, John Wiley & Sons, Inc., New York.

31. Loew, G. H., Harris, D. L. (1998) *J. Am. Chem. Soc. 120*, 8941-8948.

32. Gort, A. S., Imlay, J. A. (1998) *J. Bacteriol. 180*, 1402-1410.

Table 3.1. Rate Constants for Formation, k_1, and Decay, k_2, of the Intermediate during Reaction of *D. vulgaris* Wild-Type and Variant 2Fe-SOR [$Fe^{II}(NHis)_4(SCys)$] Sites with Superoxide, as Measured by Pulse Radiolysis[a]

2Fe-SOR	$10^{-9}k_1$ ($M^{-1}sec^{-1}$)	k_2 (sec^{-1})
wild type	1.4 (±0.3)	84 (± 2)
E47A	2.2 (± 0.3)	65 (± 6)
K48A	0.21 (±0.01)	25 (± 10)

[a]Rates were determined from the time courses of absorbance changes at 600 nm following pulse radiolysis at 25 °C in solutions containing 100 μM SOR_{pink} [$Fe(NHis)_4(SCys)$] sites, 0.12 mM Tris-sulfate, 5 μM EDTA, 10 mM formate, pH 7.7, and pulsed with 1.1-1.7 μM O_2^-. Rate constants and ranges (listed in parentheses) are the averages of 3-5 determinations.

Table 3.2. Temperature, pH, and Ionic Strength Dependences of the Rate Constants for Formation, k_1, and Decay, k_2, of the Intermediate during Reaction of *D. vulgaris* 2Fe-SOR [$Fe^{II}(NHis)_4(SCys)$] Sites with Superoxide, As Measured by Pulse Radiolysis[a]

T (°C)	$10^{-9}k_1$ ($M^{-1}sec^{-1}$)	k_2 (sec^{-1})
15.5	1.0 (±0.2)	62 (±2)
25.0	1.1 (±0.1)	79 (±6)
34.2	1.5 (±0.1)	140 (±2)
44.2	1.6 (±0.1)	370 (±20)
53.9	2.1 (±0.1)	750 (±50)
59.4	2.4 (±0.1)	1140 (±80)
75.0	2.6 (±0.3)	4800 (±540)

pH	$10^{-9}k_1$ ($M^{-1}sec^{-1}$)	k_2 (sec^{-1})
5.5	2.0 (± 0.1)	5400 (± 300)
6.0	1.7 (±0.2)	1700 (±200)
6.5	1.7 (±0.1)	330 (±20)
7.0	1.6 (± 0.1)	270 (±45)
7.5	1.5 (± 0.3)	72 (±5)
8.0	1.5 (± 0.2)	55 (±4)
8.5	1.7 (± 0.1)	49 (±3)
9.0	1.7 (± 0.3)	56 (±1)
9.5	ND[b]	60 (± 4)

NaCl (mM)	$10^{-9}k_1$ ($M^{-1}sec^{-1}$)	k_2 (sec^{-1})
0	1.1 (± 0.2)	96 (±3)
31	0.75 (±0.1)	92 (±4)
62	0.66 (±0.04)	94 (±3)
125	0.53 (±0.02)	93 (±4)
250	0.34 (±0.03)	84 (±3)
400	0.26 (±0.05)	66 (±3)

[a]Rates were determined from the time courses of absorbance changes at 600 nm following pulse radiolysis, as described in section 2.C. Materials and Methods. Unless otherwise indicated, all reactions were carried out at 25 °C in solutions containing 100 μM SOR_{pink} [$Fe(NHis)_4(SCys)$] sites, 0.12 mM Tris-sulfate, 5 μM EDTA, 10 mM formate, pH 7.7, and pulsed with 1.1-1.7 μM O_2^-. Rate constants and ranges (listed in parentheses) are for the averages of 3-5 determinations. [b]Not determined.

Table 3.3. Tris and formate concentration dependences of the formation and decay rates of *D. vulgaris* 2Fe-SOR_{pink} reaction with superoxide, as measured by pulse radiolysis.[c]

Tris (mM)	$10^{-9}k_1$ ($M^{-1}sec^{-1}$)	k_2 (sec^{-1})
10	0.40 (± 0.4)	140 (± 6)
5.0	0.56 (± 0.4)	120 (± 3)
2.5	0.73 (± 0.2)	100 (± 1)
1.2	1.1 (± 0.03)	82 (± 3)
Formate (mM)	**$10^{-9}k_1$ ($M^{-1}sec^{-1}$)**	**k_2 (sec^{-1})**
5	1.1 (± 0.1)	78 (± 2)
10	1.5 (± 0.1)	100 (± 5)
20	1.5 (± 0.1)	150 (± 10)
40	1.5 (± 0.1)	240 (± 8)
80	1.1 (± 0.1)	370 (± 10)

[c]Solutions contained 100 μM SOR_{pink} [$Fe(NHis)_4(SCys)$] sites, 10 mM formate (except where listed otherwise), 5 μM EDTA, 0.12 mM Tris-sulfate (except where listed otherwise) pH 7.7.

Table 3.4. Ionic strength dependences of formation and decay rate constants of the 600-nm intermediate following pulse radiolysis of *D. vulgaris* K48A 2Fe-SOR$_{pink}$.[a]

NaCl (M)	$10^{-9}k_1$ ($M^{-1}sec^{-1}$)	k_2 (sec^{-1})
0.4	0.18 (± 0.02)	15 (± 3)
0.2	0.21 (± 0.03)	13 (± 1)
0.15	0.23 (± 0.03)	15 (± 1)
0	0.27 (± 0.02)	18 (± 2)

[a]Solutions contained 100 μM K48A SOR [Fe(NHis)$_4$(SCys)] sites, 0.12 mM Tris, 5 μM EDTA, and 0.5 M ethanol pH 7.7, 25 ºC. Rate constants and ranges (in parentheses) are for the average of 3 – 5 determinations.

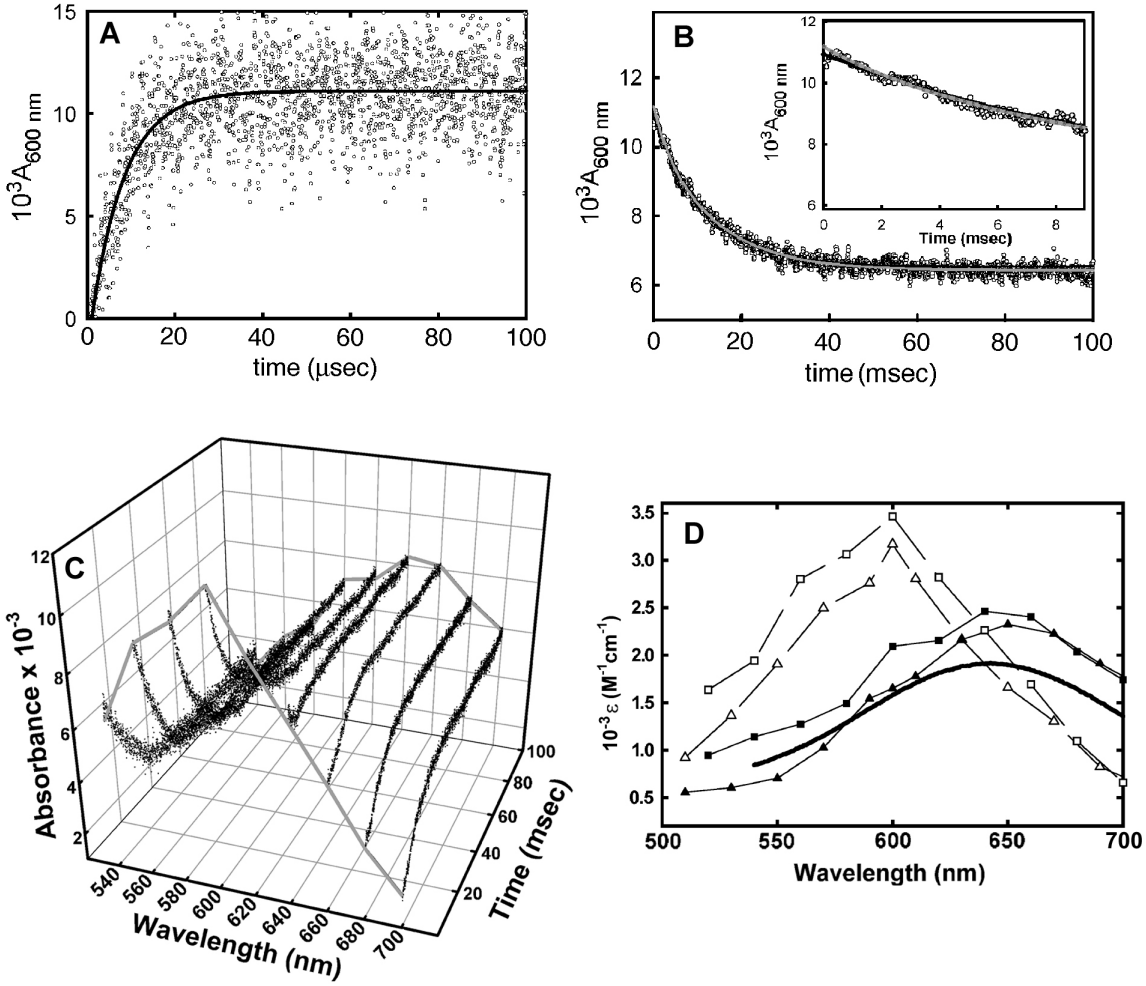

Figure 3.1. Absorbance vs. time courses at 25 °C for formation (A) and decay (B and C) of the 600-nm intermediate following pulse radiolysis of 100 μM wild-type *D. vulgaris* 2Fe-SOR_{pink} [$Fe(NHis)_4(SCys)$] sites with 1.7 μM O_2^-. In panel B, both one exponential (black curve) and sum of two exponential fits (gray curve) using the values listed in the text and tables are shown as solid traces through the data points. Panel D shows spectra of the intermediate (open symbols) 75 μsec and product (closed symbols) 100 msec after the superoxide pulse constructed from molar absorptivities of kinetic traces from reactions of wild-type SOR_{pink} (25-100 μM in [$Fe(NHis)_4(SCys)$] sites) with 1.1-1.7 μM O_2^-. Molar absorptivities were calculated assuming a quantitative 1:1 mol/mol reaction of superoxide with ferrous [$Fe(NHis)_4(SCys)$] sites. All solutions were aerobic in 0.12 mM Tris-sulfate and 10 mM formate, pH 7.8. Solutions in panels A and B also contained 5 μM EDTA. The spectra in panel D are plotted for reactions at both pH 7.8 (squares) and pH 5.5 triangles). The "resting" absorption difference spectrum of [SOR_{gray} - SOR_{pink}] (smooth thick trace) at pH 7.8 is included for comparison.

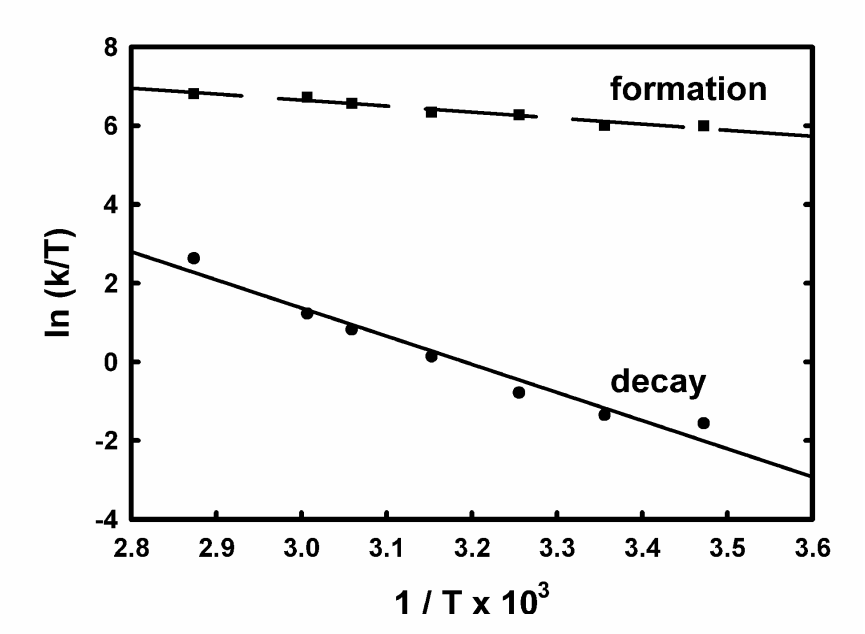

Figure 3.2. Eyring plot of temperature dependences of formation and decay rate constants for the 600-nm intermediate in the reaction of wild type *D. vulgaris* 2Fe-SOR_{pink} with superoxide according to Scheme 2.1 (c.f. text). Kinetic data were collected from A_{600} vs. time traces following, pulse radiolysis to generate 1.6 - 2.0 μM superoxide in solutions containing 100 μM (in $[Fe(NHis)_4(SCys)]$ sites) SOR_{pink} in aerobic 10 mM formate, 0.12 mM Tris-sulfate and 5 μM EDTA.

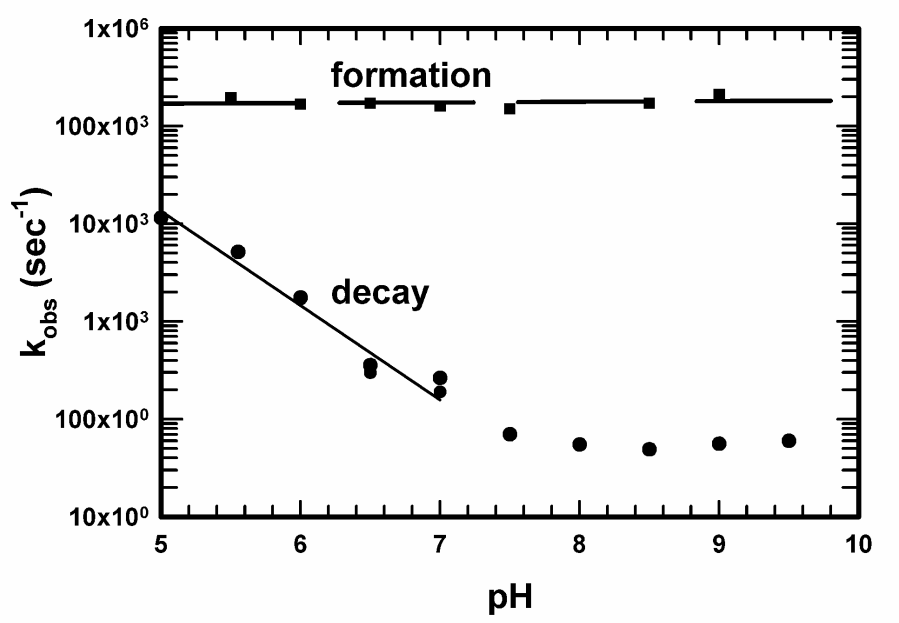

Figure 3.3. pH dependence of the formation and decay rate constants of the 600-nm intermediate in the pulse radiolysis reaction of wild-type *D. vulgaris* 2Fe-SOR_{pink} with O_2^-. Kinetics data were collected 25 °C from A_{600} vs. time traces following pulse radiolysis to generate 1.6-2.0 μM superoxide in solutions containing 100 μM (in $[Fe(NHis)_4(SCys)]$ sites) SOR_{pink} in aerobic 10 mM formate, 0.12 mM Tris-sulfate.

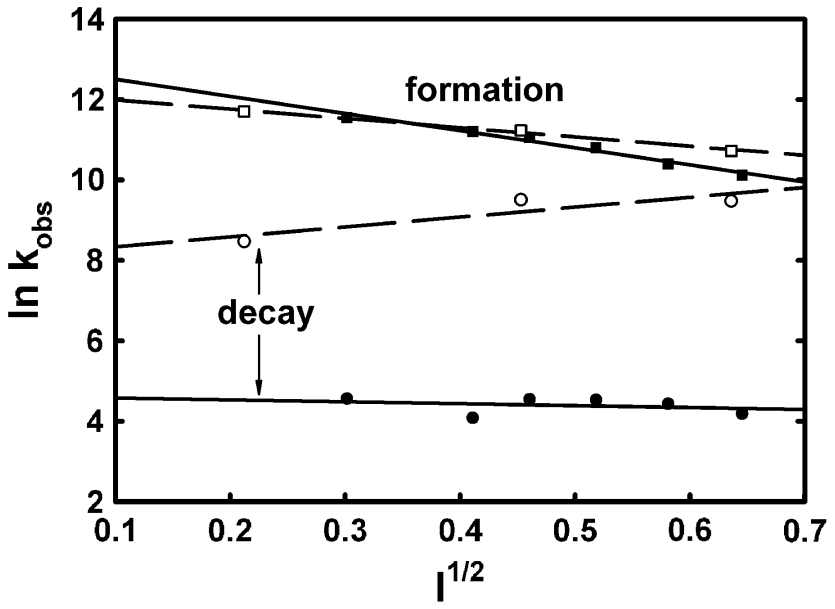

Figure 3.4. Ionic strength dependences of formation (squares) and decay (circles) rate constants for the 600-nm intermediate in the pulse radiolysis reaction of *D. vulgaris* 2Fe-SOR_{pink} with superoxide. Closed symbols are at pH 7.7, and open symbols are at pH 5.5. Data were collected under the conditions listed in the Figure 3.3 legend except that the solutions contained 5 μM EDTA. Ionic strength was adjusted by addition of NaCl.

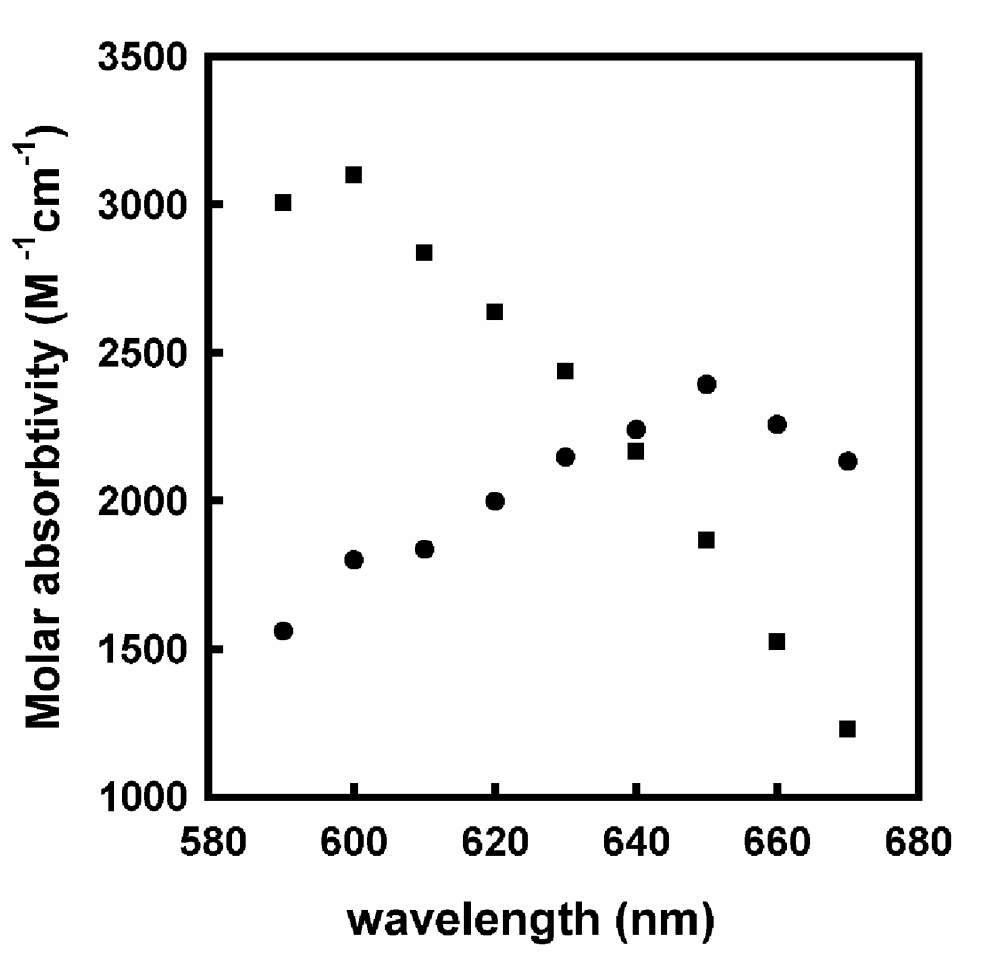

Figure 3.5. Spectra of the intermediate 100 μsec (squares) and final product 100 msec (circles) after the superoxide pulse constructed from molar absorptivities of kinetic traces for the reaction of wild type *D. vulgaris* 2Fe-SOR_{pink}, 125 μM in $[Fe(NHis)_4(SCys)]$ sites pulsed with 1.6 μM O_2^- in 0.5 M ethanol, 0.1 mM Tris-sulfate, pH 7.7.

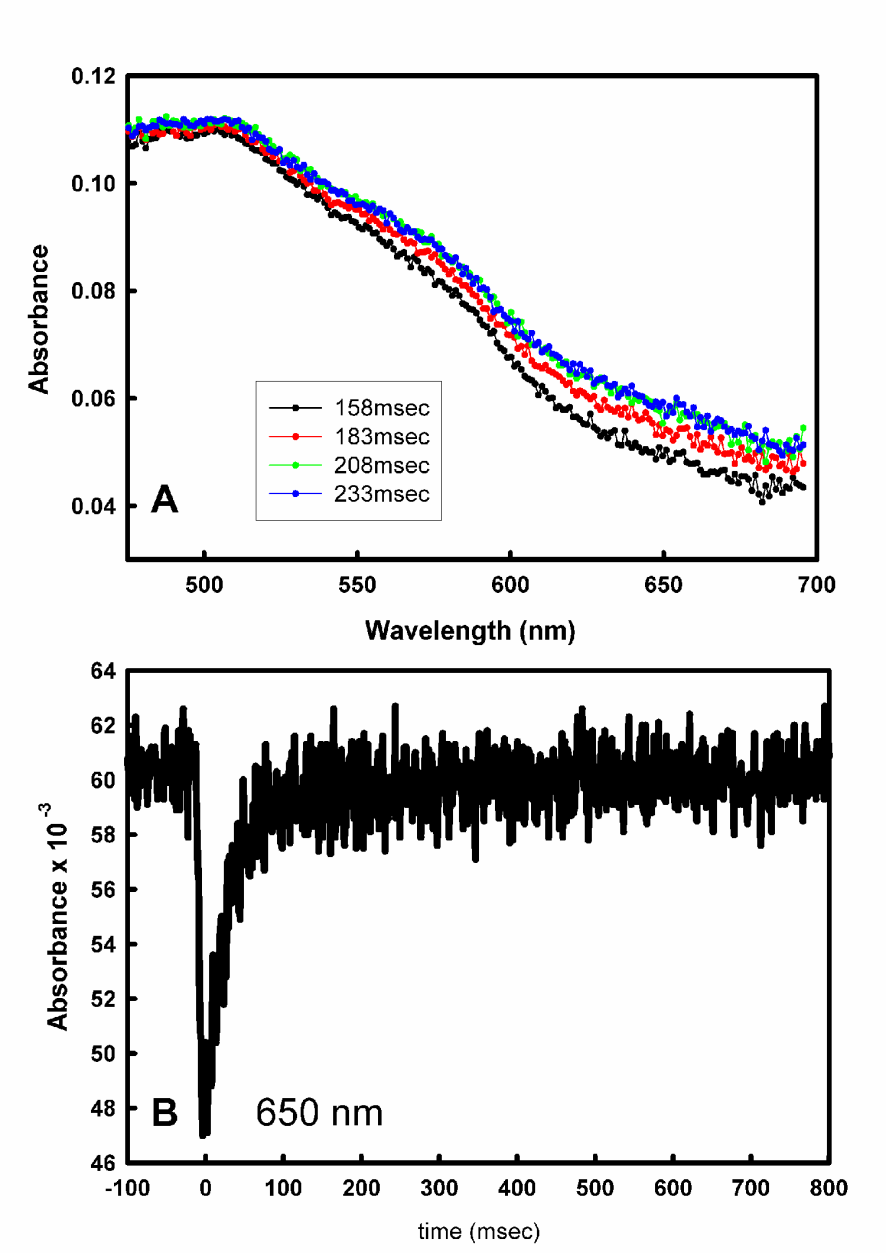

Figure 3.6. Time-dependence of absorbance changes following stopped-flow mixing of *D. vulgaris* 2Fe-SOR$_{pink}$ with potassium ferricyanide. **(A)** Scanning-spectrophotometry of a solution containing 2Fe-SOR$_{pink}$, 50 µM in [Fe(NHis)$_4$(SCys)] sites and 400 µM ferricyanide immediately after mixing in 50 mM MOPS solution, at pH 7.4. **(B)** Absorbance vs. time trace at 650 nm for the reaction in **(A)**.

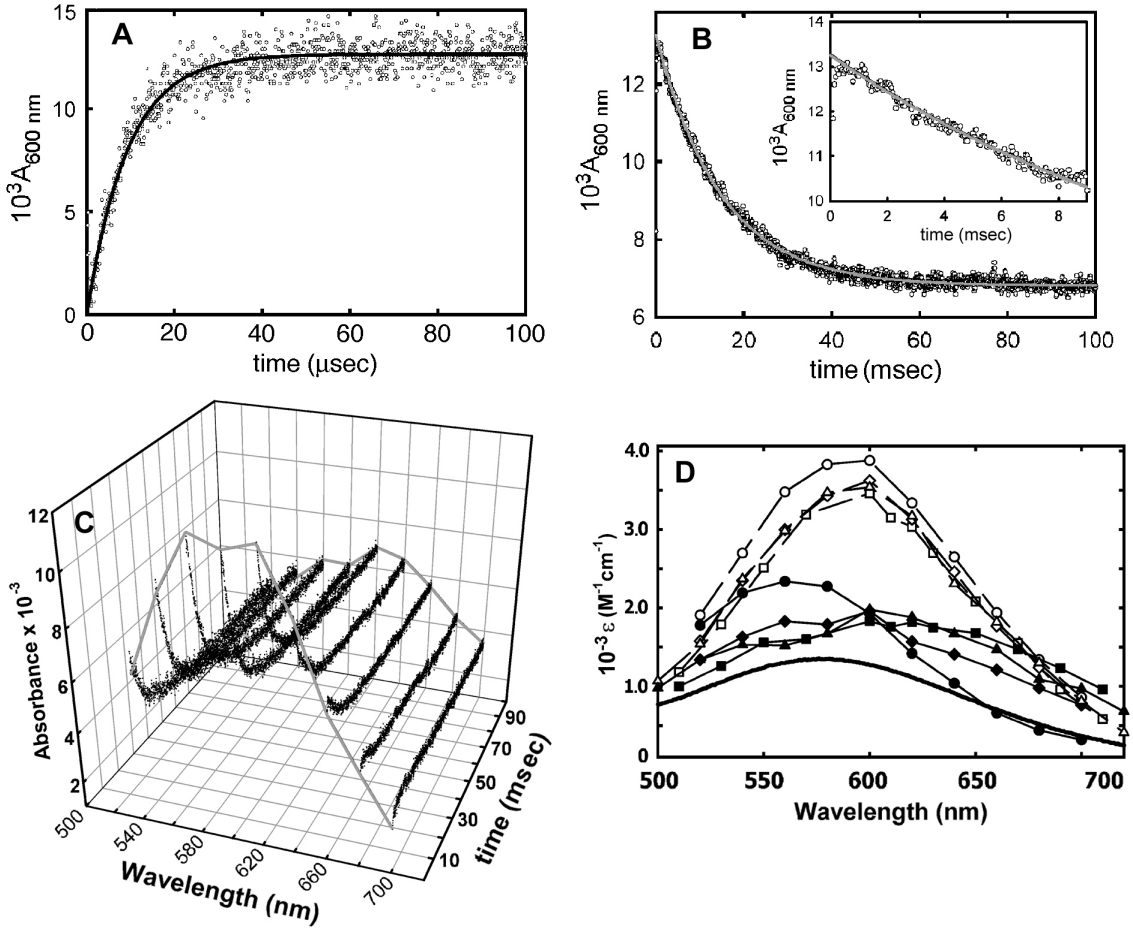

Figure 3.7. Absorbance vs. time courses at 25 °C for formation (A) and decay (B and C) of the 600-nm intermediate following pulse radiolysis of 50-100 μM E47A *D. vulgaris* 2Fe-SOR_{pink} [$Fe(NHis)_4(SCys)$] sites with 1.7 μM O_2^-. In panel B, both one exponential (black trace) and sum of two exponential fits (gray trace) using the values listed in the text and tables are shown as solid curves through the data points. Panel D plots spectra of the E47A intermediate (open symbols) 75 μsec and product (closed symbols) 100 msec after the superoxide pulse constructed from molar absorptivities calculated as described in the Figure 3.1 legend. All solutions were aerobic in 0.12 mM Tris-sulfate and 10 mM formate, pH 7.8, with 5 μM (panels A and B) or 100 μM (panel D) EDTA added. Spectra in panel D are plotted at pH 9.1 (circles), 7.8 (diamonds), 6.7 (triangles), and 5.6 (squares). The "resting" absorption difference spectrum of E47A [SOR_{gray} - SOR_{pink}] (smooth thick trace) at pH 7.8 is included for comparison.

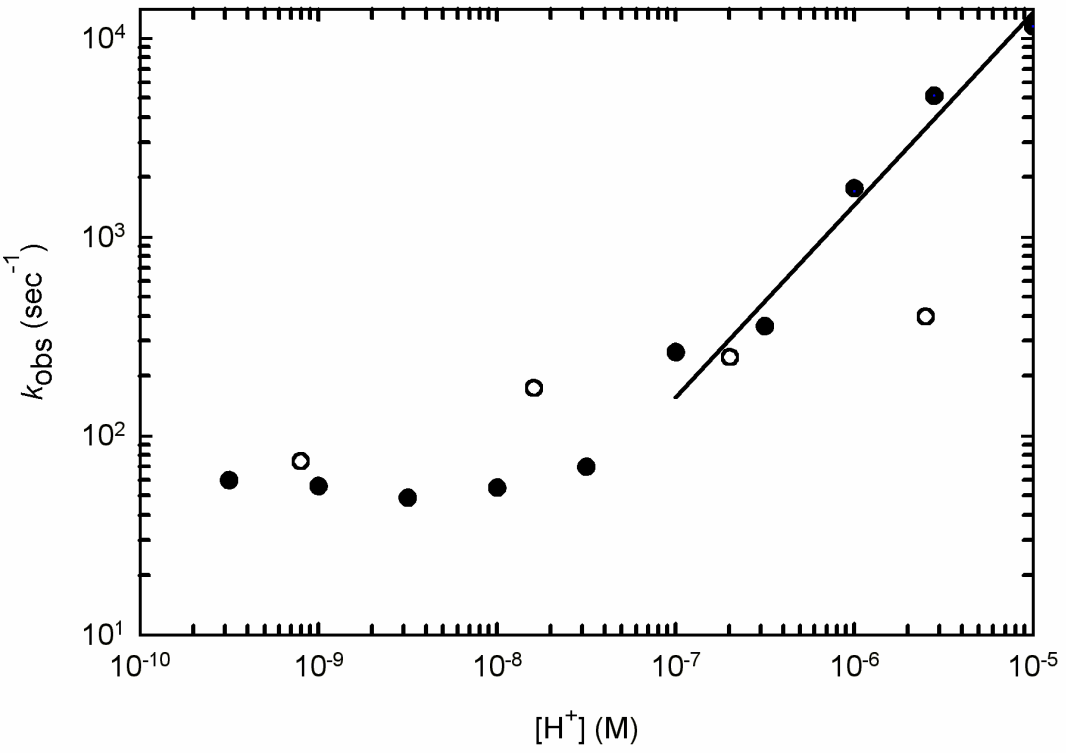

Figure 3.8. Comparison of the [H^+] dependence of decay rate constants of the intermediate for wild type and E47A 2Fe-SORs. The k_{obs} for the decay of the 600-nm intermediate produced by pulse radiolysis of 100 μM wild-type SOR_{pink} (●) or 100 μM E47A 2Fe-SOR_{pink} (○) with 1.7 μM superoxide are plotted. The reactions were carried out in 10 mM formate, 0.12 mM Tris-sulfate, 5 μM EDTA aerobically at the indicated pH.

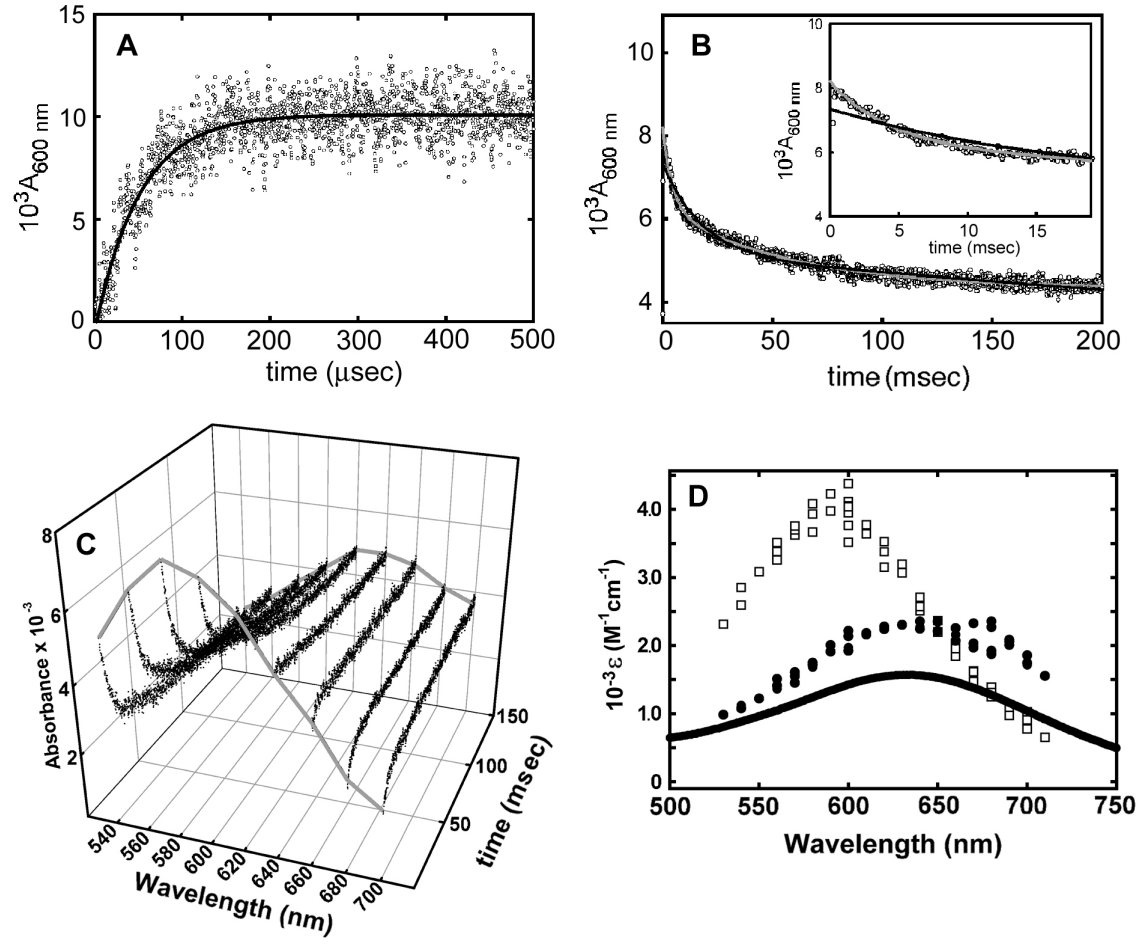

Figure 3.9. Absorbance vs. time courses at 25 °C for formation (A) and decay (B and C) of the 600-nm intermediate following pulse radiolysis of 100 μM K48A 2Fe-SOR_{pink} [$Fe(NHis)_4(SCys)$] sites with 1.2 μM (panels A and B) or 1.0 μM (panel C) O_2^-. In panel B, both one exponential (black trace) and sum of two exponential fits (gray trace) using the values listed in the text and tables are shown as solid curves through the data points. Panel D plots spectra constructed from three sets of experiments of the intermediate (open squares) 300 μsec and final product (closed symbols) 200 msec after the superoxide pulse for reactions of K48A SOR_{pink} (100 μM in [$Fe(NHis)_4(SCys)$] sites) with 1.3-1.7 μM O_2^- at 25 °C. Molar absorptivities were calculated as described in the Figure 3.1 legend. All solutions were aerobic in 0.12 mM Tris-sulfate and 10 mM formate, pH 7.8. The "resting" absorption difference spectrum of K48A [SOR_{gray} - SOR_{pink}] (smooth thick trace) at pH 7.8 is included for comparison.

Scheme 3.1.

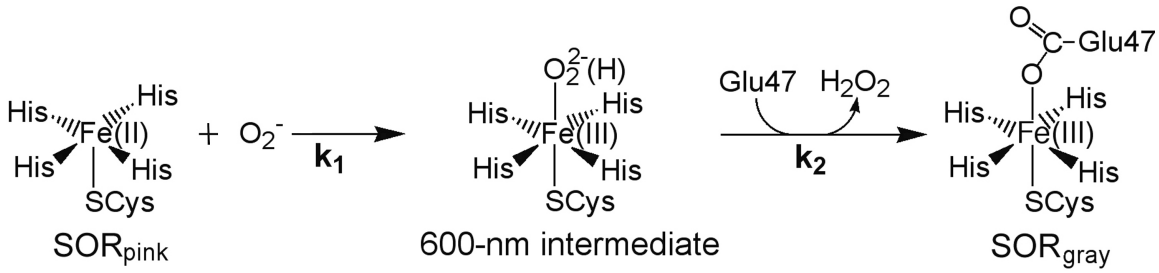
His
Fe(II)
His
His
His
SCys
SOR$_{pink}$
+ O_2^-
k_1
O_2^{2-}(H)
His
Fe(III)
His
His
His
SCys
600-nm intermediate
Glu47 H_2O_2
k_2
O
C–Glu47
O
His
Fe(III)
His
His
His
SCys
SOR$_{gray}$

Scheme 3.2.

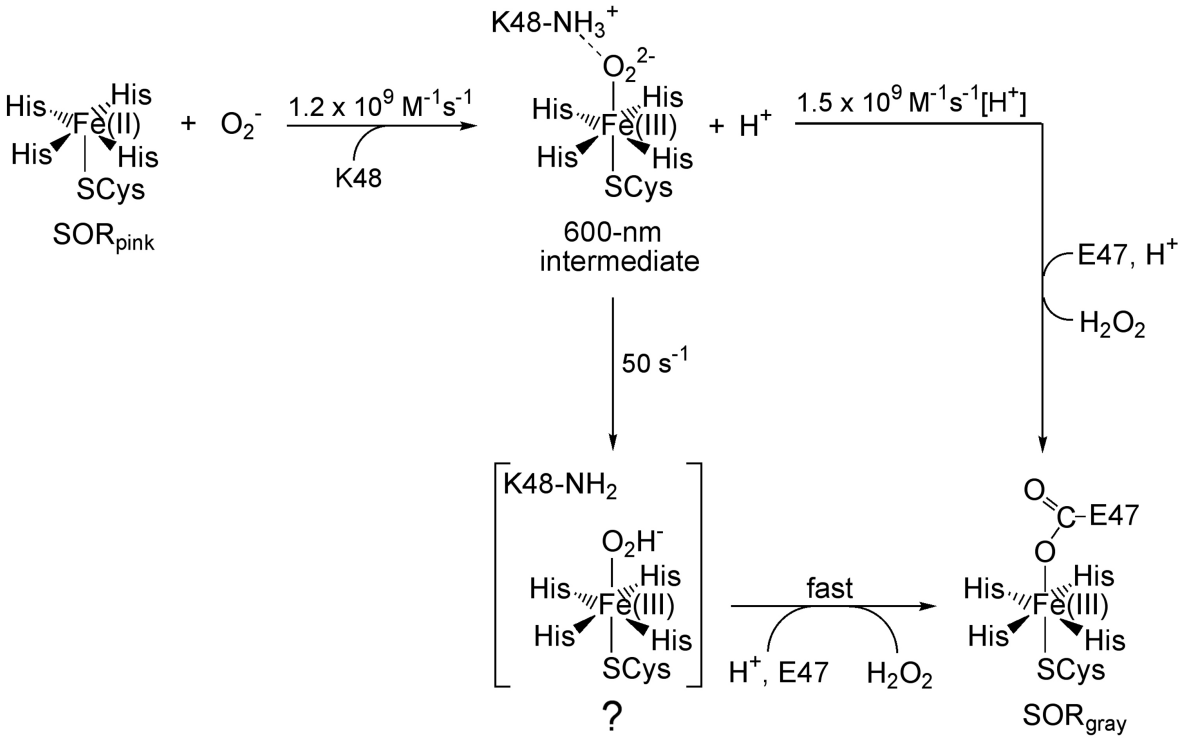
K48-NH3+
O2 2-
His
Fe(II)
His
His
His
SCys
SORpink
+ O2-
1.2 x 10^9 M-1s-1
K48
Fe(III)
600-nm
intermediate
+ H+
1.5 x 10^9 M-1s-1[H+]
E47, H+
H2O2
50 s-1
K48-NH2
O2H-
?
fast
H+, E47
H2O2
O
C-E47
SORgray

CHAPTER 4

AN ENGINEERED TWO-IRON SUPEROXIDE REDUCTASE LACKING THE [Fe(SCys)$_4$] CENTER AND ITS REACTIVITY *IN VIVO* AND *IN VITRO*

4.A. Introduction

Several obligately anaerobic and microaerophilic bacteria and archaea contain a unique class of non-heme iron proteins called superoxide reductases (SORs) which catalyze reaction 4.1:

$$e^- + O_2^- + 2H^+ \quad \rightarrow \quad H_2O_2 \qquad (4.1)$$

SORs have been shown to play an alternative and/or complementary role to that of superoxide dismutases (SODs) in oxidative stress protection.[1-8] SORs have recently attracted a great deal of attention because of their novel activity and unique square-pyramidal ferrous [Fe(NHis)$_4$(SCys)] active site.[9-16] Due at least in part to its high reduction potential (≥ 200 mV vs. NHE), this ferrous site is remarkably stable to oxidation in air, yet it reacts with superoxide in an essentially diffusion-controlled fashion, as diagrammed in Figure 4.1.A.[17-22] At least one transient species forms

during this reaction, which has a characteristic visible absorption feature at ~ 600 nm, which has been formulated as either a ferric-peroxo or ferric-hydroperoxo species.

SORs can be sub-classified into 1Fe-SORs, which contain the $[Fe(NHis)_4(SCys)]$ active site as the only cofactor, and 2Fe-SORs, which, as shown in Figure 4.1.B., contain an additional N-terminal polypeptide domain with a $[Fe(SCys)_4]$ site, the role of which is presumed to be electron transfer. In fact, the reduction potential of the $[Fe(SCys)_4]$ site, ~ 2 mV vs. NHE[23] renders it thermodynamically capable of reducing the ferric $[Fe(NHis)_4(SCys)]$ site. The crystal structure of the 2Fe-SOR homodimer from *Desulfovibrio (D.) desulfuricans*,[24] however, shows both intra- (~ 22 Å) and inter-subunit (~ 32 Å) through-space distances between $[Fe(SCys)_4]$ and $[Fe(NHis)_4(SCys)]$ iron centers that seem beyond the range for efficient intra-protein electron transfer.[25] Thirty-eight- and 93-residue polypeptides corresponding to the N-terminal $[Fe(SCys)_4]$- and C-terminal $[Fe(NHis)_4(SCys)]$-containing domains, respectively, of *D. vulgaris* 2Fe-OR were genetically engineered and expressed separately in *E. coli*.[26] The isolated 2Fe-SOR domains largely retained their constituent iron sites with native-like absorption spectra and reduction potentials, but the recombinant 2Fe-SOR fragments, either separately or in combination, were reported to show no evidence for reaction with superoxide. These results imply that a functional 2Fe-SOR requires both domains and perhaps both constituent iron sites in a single native polypeptide. On the other hand, the fact that 1Fe-SORs are apparently fully functional with only an $[Fe(NHis)_4(SCys)]$ site [5, 27] implies that the $[Fe(SCys)_4]$ site is not essential for the superoxide reductase activity of 2Fe-SORs. In this work we address these alternative possibilities by

examination of an engineered *D. vulgaris* 2Fe-SOR variant in which one cysteine residue of the [$Fe(SCys)_4$] site was changed to serine. This single amino acid residue change was found to completely destroy the native [$Fe(SCys)_4$] site, but to leave the [$Fe(NHis)_4(SCys)$] site and the protein homodimer intact.

4.B. Materials and Methods

Reagents and General Procedures. Reagents and buffers were the highest grade commercially available and were used as received. Enzymes were purchased from Sigma Chemical Co. All reagent solutions and media were prepared in water purified using a Millipore Ultrapurification system to a resistivity of ~ 18 MΩ, in order to minimize trace metal-ion contamination. Standard procedures for molecular biology manipulations were followed.[28] The correctness of plasmid gene sequences was verified by nucleotide sequencing at the University of Georgia Molecular Genetics Instrumentation Facility. Recombinant rubredoxin and 2Fe-SOR both from *D. vulgaris* were prepared as described previously.[17, 20, 29] Except where noted, all *E. coli* strains harboring plasmids were cultured in media containing 100 mg/L of ampicillin.

Expression and Purification of the N-terminal Domain of D. vulgaris 2Fe-SOR. A protein fragment corresponding to residues 1-38 of *D. vulgaris* 2Fe-SOR, was expressed and purified using a protocol similar to that described by Ascenso et al.[26] A plasmid pRbo1-38 encoding the N-terminal 38 residues of *D. vulgaris* 2Fe-SOR, a polypeptide hereafter referred to as N-term 2Fe-SOR, was constructed by inserting a stop codon after the codon for residue 38 within the *D. vulgaris* 2Fe-SOR gene in pRbo (c.f.

Chapter 2 Section 2.B).[7] This insertion was accomplished using two complimentary oligonucleotide primers containing the desired mutation (underlined): 5′-CGTCAG-AAGTGCCTTACTTCATGAGCTTC-3′ and 5′-GAAGCTCATGAAGTAAGGCACT-CCTGACG-3′ with the QuikChange mutagenesis kit (Stratagene, Inc.) following procedures described in the product manual.

Overexpression and Isolation of the N-term 2Fe-SOR. The plasmid, pRbo1-38, was transformed into *E. coli* strain BL21 (DE3) CodonPlus (Stratagene Inc.). For overexpression of N-term 2Fe-SOR, cultures of *E. coli* BL21(DE3) CodonPlus [pRbo1-38] were grown with shaking at 37 °C in M9 minimal media, supplemented with 0.02 % Casamino acids and 1 x 10^{-4} % thiamine. The protocols for overexpression, and harvesting and lysing of cells were otherwise identical to those described below for the C13S 2Fe-SOR. The supernatant from the lysed cells was loaded onto a 1.6 x 2.5 HiTrap anion-exchange column (Amersham Pharmacia Biotech, Inc.) equilibrated with buffer and eluted at a flow rate of 2 mL/min. A red fraction that eluted when the column was washed with buffer containing 0.5 M NaCl was collected and concentrated to ~ 2 mL/L culture. The concentrated fractions were loaded onto a HiPrep 16/60 Sephacryl S-100 column (Amersham Pharmacia Biotech, Inc.) equilibrated with buffer containing 250 mM NaCl and eluted at a flow rate of 0.5 mL/min. A deep red eluting fraction was adjudged to be pure N-term 2Fe-SOR by sodium dodecylsulfate-polyacrylamide gel electrophoresis. The pure N-term 2Fe-SOR, had an absorbance ratio (A_{280}/A_{502}) = 3. Approximately 0.3 mg of pure N-term SOR was isolated per liter of culture. The purified protein was stored at -80^{o} C.

Preparation of C13S 2Fe-SOR. A plasmid encoding the *D. vulgaris* 2Fe-SOR, but replacing the codon for cysteine-13 with that for serine, was generated from the plasmid, pRbo [17], using two complimentary oligonucleotide primers containing the desired C13S codon change (underlined bases indicate changed residue): 5′-CAAATGCATCCACTCTGGCAACATCGTCG-3′ and 5′-CGACGATGTTGCC-AGAGTGGATGCATT-3′ and the QuikChange mutagenesis kit (Stratagene, Inc.) following procedures described in the product manual. The resulting plasmid, pC13Rbo, was transformed into *E. coli* strain QC774 (*sodAsodB*).[30] Procedures for overexpression, isolation and purification of the C13S 2Fe-SOR variant from *E. coli* QC774 [pC13SRbo] were similar to those previously described for isolation of the corresponding wild type 2Fe-SOR [17, 20] and are described below.

Overexpression and Isolation of the Recombinant D. vulgaris C13S 2Fe-SOR Variant. A single colony of *E. coli* QC774 [pC13SRbo] was selected and transferred to 6 mL of Luria-Bertani medium, and grown for approximately 3 hours at 37 ^{o}C with shaking. One-milliliter aliquots of this 6-mL culture were then used to inoculate six 50-mL volumes of M9 minimal media. After overnight incubation at 37 ^{o}C with shaking, these 50-mL cultures were used to inoculate 1-L volumes of M9 media. The 1-L cultures were grown with shaking at 37 ^{o}C to an OD_{600} of ~ 0.6, at which point isopropyl-β-D-thiogalactoside (100 mg/L) was added to induce protein expression. The cultures were also supplemented with 25 mg ferrous sulfate per liter at the time of induction, and incubated with shaking for a further 3 hrs at 37 ^{o}C, after which the cells were harvested by centrifugation. The buffer used throughout protein purification was 50 mM MOPS pH

7.5. After a – 80 ^{o}C freeze-thaw cycle the harvested cells from 6 to 8 L of culture were resuspended in 50 mL of buffer/L culture and lysed by sonication. The supernatant was loaded onto a 1.6 x 2.5 HiTrap anion-exchange column (Amersham Pharmacia Biotech, Inc.) equilibrated with buffer and eluted at a flow rate of 2 mL/min. A colorless fraction that eluted upon washing the column with buffer (no added salt) was concentrated to ~ 2 mL/L culture. The concentrated fraction was loaded onto a HiPrep 16/60 Sephacryl S-100 column (Amersham Pharmacia Biotech, Inc.) equilibrated with 50 mM MOPS, 250 mM NaCl and eluted with the same buffer at flow rate of 0.5 mL/min. A colorless to pale blue eluting fraction was adjudged to be pure C13S 2Fe-SOR by sodium dodecyl sulfate polyacrylamide gel electrophoresis. Approximately 5 mg of pure C13S 2Fe-SOR was isolated per liter of culture. The colorless, as-isolated protein was stored at - 80 ºC.

Metal and Protein Analyses. Metal contents of proteins were determined by inductively coupled plasma-atomic emission (ICP-AE) at the University of Georgia Chemical Analysis Laboratory. Protein concentrations were determined using the Bio-Rad protein assay with bovine serum albumin (BSA) as standard for wild type 2Fe-SOR and wild type 2Fe-SOR for C13S 2Fe-SOR and N-term 2Fe-SOR. Native molecular weights were determined by calibrated elution times from a HiPrep 16/60 Sephacryl S-100 column (Amersham Pharmacia Biotech, Inc.). Concentrations of non-heme iron proteins were determined spectrophotometrically using the previously reported molar absorptivities: rubredoxin, ε_{490} = 8,700 $M^{-1}cm^{-1}$ [29]; 2Fe-SOR$_{pink}$, ε_{502} = 4,300 $M^{-1}cm^{-1}$ (protein monomer basis) [20]; C13S 2Fe-SOR, ε_{645} = 1,900 $M^{-1}cm^{-1}$ (protein monomer basis, determined in this work for the chemically oxidized protein from the iron analysis).

Oxidations of [Fe(NHis)$_4$(SCys)] Sites. Recombinant *D. vulgaris* wild type and C13S 2Fe-SORs containing ferric [Fe(NHis)$_4$(SCys)] sites were prepared by adding a five-fold molar excess of potassium hexachloroiridate from a buffered stock solution. The excess oxidant was then removed by repetitive concentration/re-dilution in a Centricon YM5 filter (Amicon, Inc.) or by passage through a 5-mL HiTrap desalting column (Amersham Pharmacia Biotech, Inc.).

Reduction Potentials. A spectrophotometric, dye-mediated, electrochemical titration method similar to those described for other SORs was used.[31-33] All measurements were conducted at room temperature (~ 23 ºC) in 500 mM Tris-sulfate pH 7. A platinum/glass combination microelectrode (Brinkmann, Inc.) attached to a potential meter (World Precision Instruments, Inc.) was inserted through a tight-fitting rubber septum into a specially designed quartz cuvette containing 4 mL of anaerobic SOR solution under an argon atmosphere. Freshly prepared 10 mM stock solutions of anaerobic redox dyes were individually added by gas-tight syringe to make a redox mediator cocktail containing 0.5 μM each of: hydroquinone, 2,6-dichloroindophenol, 1,2-naphthaquinone, phenazine methosulfate, toluidine blue, duroquinone, and anthraquinone 2,6-disulfonic acid. Small aliquots (1-10 μl) of either 12 mM sodium dithionite (starting from the oxidized 2Fe-SOR) or 4.7 mM sodium hexachloroiridate in 500 mM Tris-sulfate pH 7.0, were injected into the reaction mixture. After each addition, the solution was thoroughly mixed by rocking the cuvette back and forth. After the potential reading had stabilized (approximately 30 seconds after mixing), the UV-visible absorption spectrum and the potential of the solution were measured. The absorption was corrected for

dilution by hexachloroiridate or dithionite additions. For the apparatus used here, the experimentally measured, uncorrected potential is the negative of the reduction potential, due to reverse polarization of the electrode. The uncorrected, measured potentials were therefore multiplied by -1. Using this apparatus, multiple spectro-electrochemical titrations were conducted on 200 μM *D. vulgaris* rubredoxin (~0 mV vs. NHE),[34] and 200 μM horse heart cytochrome c (+251 mV vs. NHE).[35] These data were fit to the Nernst equation (c.f. below) and a correction factor of + 174 mV for this apparatus was determined. For the 2Fe-SOR titrations 174 mV was therefore added to the measured potentials (E_{meas}) to arrive at the corrected potentials (E_{corr}) which is relative to the normal hydrogen electrode (NHE), as shown in equation 4.2. The corrected potentials were then fit using the Nernst equation (4.3).

$$E_{corr}(mV) = -1(E_{meas}) + 174 \quad (4.2)$$

$$E_{corr} = E_0 + (RT/nF)\ln([A_o]/[A_r]) \quad (4.3)$$

$[A_o]$ and $[A_r]$ represent concentrations of oxidized and reduced A, E_{corr} is the corrected measured potential after each addition of oxidant or reductant, E_0 is the derived mid-point reduction potential of the A_o/A_r redox couple, n is the number of electrons exchanged, and all constants have their normal values. The solutions for 2Fe-SOR titrations contained either 120 μM wild type or 320 μM C13S 2Fe-SOR [$Fe(NHis)_4(SCys)$] sites and the redox dye cocktail listed above. The fractional absorption (at 502 and 650 nm for wild type, and 650 nm for C13S) were plotted versus corrected potential, and the data

was least-squares fit to equation 4.3 assuming a one-electron process, from which the E_0 values listed in Section 4.C were derived. Further experimental details are supplied in the legend to Figure 4.3.

Growth Complementation. The aerobic growth rates of the superoxide-deficient *E. coli* strain QC774 [30] harboring plasmids individually for wild type *D. vulgaris* 2Fe-SOR (pRbo),[17] C13S 2Fe-SOR (pC13SRbo),[this work], N-term 2Fe-SOR (pRbo1-38), *E. coli* Mn-SOD (pDT1-5),[30] or the empty control plasmid, pCYB1 (New England Biolabs, Inc.) were conducted as follows. Each strain was cultured aerobically at 37 ^{o}C to stationary phase in M63 minimal medium supplemented with 0.02 % Casamino acids and 1 x 10^{-4} % vitamin B1. Eight 3-μL aliquots of each of the above cultures were used to inoculate eight 200-μL volumes of aerobic M63 medium without added supplements or antibiotics in individual wells of a 96-well plate. The cultures in the 96-well plate, which had initial OD_{600}'s of 0.05 - 0.07, were then incubated with shaking at 37 ^{o}C, and growths were monitored by periodic measurements of OD_{600} in a microplate reader (Molecular Devices, Inc.).

Pulse Radiolysis. The rates of reaction of as-isolated *D. vulgaris* wild-type 2Fe-SOR_{pink} and as-isolated C13S 2Fe-SOR with superoxide were measured at 25^{o} C by pulse radiolysis using the 2-MeV Van de Graaff accelerator at Brookhaven National Laboratory, as described previously.[17, 20] Additional experimental details are provided in the Figure 4.5. and 4.6. legends. The data were analyzed using the BNL Pulse Radiolysis Program.

SOR Assay. This coupled assay measures SOR-dependent consumption of NADPH by superoxide, and was conducted as described previously.[29] To 1 ml of 50 mM phosphate buffer pH 7.5 containing 100 μM EDTA were added aliquots of stock solutions of xanthine, *D. vulgaris* rubredoxin, 2Fe-SOR, catalase, and NADPH to achieve concentrations of approximately 500 μM, 1 μM, 1 μM, 200 U/mL and 100 mM, respectively. The relatively high catalase activity was needed to minimize consumption of NADPH by hydrogen peroxide, a by-product of the xanthine/xanthine oxidase superoxide generating system (data not shown). The rate of NADPH consumption was followed by its absorbance decrease at 340 nm ($\varepsilon_{340} \sim 6220\ M^{-1}cm^{-1}$). After 20 seconds spinach ferredoxin:$NADP^+$ oxidoreductase (FNR) was added to achieve a concentration of 1 μM FNR in assay mixture. Twenty seconds after the FNR addition, a pre-calibrated amount of xanthine oxidase was added to initiate the generation of superoxide. The flux of superoxide was independently calibrated using the same amount of xanthine and xanthine oxidase and measuring the rate of reduction of horse heart cytochrome c.[29] The superoxide flux and other experimental conditions are listed in the text and Figure 4.8 caption.

4.C. Results and Discussion

Characterization of N-term 2Fe-SOR. The N-term 2Fe-SOR, when purified as described above, was determined to contain 0.6 ± 0.1 mol iron/mol protein monomer and no detectable zinc above background levels. Liquid chromatography-electrospray

ionization mass spectrometry of the N-term 2Fe-SOR showed that the major chromatographic peak corresponded to a 4065-Da species, which is within one mass unit of that calculated (4,064 Da) for residues 2-38 of *D. vulgaris* 2Fe-SOR. This result indicated that the N-terminal methionine residue had been processed off during overexpression. The native molecular weight of N-term 2Fe-SOR could not be established by gel filtration, apparently due to the same aggregation phenomenon reported by Ascenso et al.[26] An extinction coefficient, ε_{502} = 4,300 $M^{-1}cm^{-1}$, was determined for the purified N-term 2Fe-SOR, based on its iron content. This value is somewhat lower than that reported by Ascenso et al.,[26] but agrees well with that reported previously for *D. vulgaris* 2Fe-SOR_{pink}.[20] The near UV-visible absorption spectrum of N-term 2Fe-SOR, as purified in this work, is shown in Figure 4.2. The absorption between 300 and 800 nm is due to the ferric $[Fe(SCys)_4]$ site.[26]

Physical, Spectroscopic and Redox Characterization of C13S 2Fe-SOR. Based on amino acid sequence alignment and high homology with the structurally characterized *D. desulfuricans* 2Fe-SOR,[24] cysteine 13 in *D. vulgaris* 2Fe-SOR supplies a ligand to the $[Fe(SCys)_4]$ site. The recombinant *D. vulgaris* wild type 2Fe-SOR and C13S 2Fe-SOR variant, when expressed in *E. coli* grown in minimal medium supplemented with iron, were determined to contain 2.1 ± 0.3 and 1.2 ± 0.3 mol iron/mol protein monomer. These values indicated full occupancy of both $[Fe(SCys)_4]$ and $[Fe(NHis)_4(SCys)]$ sites for wild type 2Fe-SOR, but only approximately one iron per C13S 2Fe-SOR monomer. Zinc and other transition metal contents were negligible (<0.05 mol metal/mol monomer) for both proteins. Gel filtration verified that both wild type and C13S 2Fe-SOR are

dimeric. Under the assay conditions used in this work, wild type 2Fe-SOR is known to remain dimeric.[36]

Figure 4.3 shows the near UV-visible absorption spectra of both as-isolated C13S 2Fe-SOR, labeled $C13S_{clear}$, and hexachloroiridate-oxidized C13S 2Fe-SOR, labeled $C13S_{blue}$. An absorbance ratio, A_{280}/A_{645} = 17, for this chemically oxidized form was used as a standard of protein purity. The "clear" and "blue" subscripts in Figure 4.3 reflect the respective colors of the protein solutions and also correspond to ferrous and ferric oxidation states, respectively, of the $[Fe(NHis)_4(SCys)]$ site. These oxidation state assignments are based on the close similarity of the $C13S_{clear}$ and $C13S_{blue}$ spectra in Figure 4.3 to the corresponding as-isolated and chemically oxidized 1Fe-SORs from several sources.[5, 37, 38] The 645-nm absorption feature in the $C13S_{blue}$ spectrum (ε_{645} = 1,900 $M^{-1}cm^{-1}$) is also very similar to that of the wild type 2Fe-SOR,[17] which is labeled wild $type_{gray\text{-}pink}$ in the inset to Figure 4.3. The wild type 2Fe-SOR is isolated with ferric $[Fe(SCys)_4]$ and ferrous $[Fe(NHis)_4(SCys)]$ sites, a form referred to as $2Fe\text{-}SOR_{pink}$.[31] This form can be oxidized to $2Fe\text{-}SOR_{gray}$, in which both iron sites are ferric. The wild $type_{gray\text{-}pink}$ difference absorption spectrum shown in the inset to Figure 4.3, thus, subtracts the contribution of the ferric $[Fe(SCys)_4]$ site, and the remaining absorption, centered at ~ 645 nm, is, therefore, due to the ferric $[Fe(NHis)_4(SCys)]$ site. On the basis of magnetic circular dichroism (MCD) and resonance Raman spectroscopic studies on a 1Fe-SOR, the ~ 645 nm absorption feature has been assigned to a π-type cysteine sulfur → ferric charge transfer (CT) transition.[38, 39] The absorption corresponding to the shoulder at ~ 320 nm in the $C13S_{clear}$ spectrum has been similarly

assigned as the analogous higher-energy π-type cysteine sulfur → ferrous CT transition of the reduced [Fe(NHis)$_4$(SCys)] site. The absorption corresponding to the shoulder at ~ 330 nm in the C13S$_{blue}$ spectrum in Figure 4.3 also appears in all reported ferric 1Fe-SOR spectra and has not been definitively assigned.

The stronger visible and near-UV absorptions of the ferric [Fe(SCys)$_4$] site, with ε_{502} ~ 4,300 $M^{-1}cm^{-1}$ and ε_{375} ~ 8,000 $M^{-1}cm^{-1}$,(c.f. Figure 4.2),[26] are, thus, absent in both as-isolated and chemically oxidized C13S 2Fe-SOR. Engineered substitutions of a serine for a cysteine ligand residue are known to result in stable ferric [Fe(SCys)$_3$(OSer)] sites in rubredoxins and rubrerythrin with absorption features in the visible region that are blue-shifted from those of the [Fe(SCys)$_4$] sites.[40, 41] The absorption spectra of the C13S variant, however, showed no evidence of such blue-shifted features. Furthermore, formation of the [Fe(SCys)$_3$(OSer)] sites in rubredoxin and rubrerythrin required *in vitro* incorporation of iron. We have been unable to incorporate iron into the isolated C13S 2Fe-SOR above the approximately 1 per subunit cited above using the methods described for these other serine-substituted proteins. During isolation and purification, a small quantity of C13S 2Fe-SOR was eluted from the HiTrap-Q column, as a separate fraction that, based on its absorption spectrum, may have contained a small portion of ferric [Fe(SCys)$_3$(OSer)] sites. However, the visible absorption attributed to these sites bleached irreversibly after several minutes at room temperature following elution, whereas a much more intense blue color due to the ferric [Fe(NHis)$_4$(SCys)] sites could be generated by addition of oxidants.

The Nernst plots in Figure 4.4 were obtained by measuring 650-nm absorption intensities of wild type or C13S 2Fe-SORs at a series of poised redox potentials. Based on these data, the [Fe(NHis)$_4$(SCys)] site of C13S 2Fe-SOR underwent a reversible, one-electron redox process with a measured midpoint reduction potential of +285 ± 3 mV vs. NHE. This potential was very similar to that determined for the [Fe(NHis)$_4$(SCys)] center of wild type 2Fe-SOR, +272 ± 7 mV, under the same conditions. Midpoint reduction potentials of [Fe(NHis)$_4$(SCys)] sites in SORs have been reported over the range of +90 to +430 mV vs. NHE,[23, 42] depending on the technique used, but most of the reported values cluster within the range of 200 - 250 mV.[26, 31-33, 37, 38]

The spectroscopic, analytical and redox results together show that the *D. vulgaris* C13S 2Fe-SOR variant contains a [Fe(NHis)$_4$(SCys)] site as its only cofactor, and that this site in the C13S variant has very similar spectroscopic and redox properties to those in other SORs. Most notably, these characteristic properties of the [Fe(NHis)$_4$(SCys)] site in the C13S variant are not significantly perturbed from those of the corresponding wild type 2Fe-SOR. The fact that the C13S 2Fe-SOR remains soluble and dimeric also suggests that the polypeptide structure has not been drastically altered by the loss of the [Fe(SCys)$_4$] site.

*Complementation of E. coli(sodAsodB) by C13S 2Fe-SOR. E. coli sodAsod*B strains lack the genes encoding both MnSOD and FeSOD and are unable to grow in aerobic minimal media unless supplemented with amino acids.[30] This phenotype is attributed to superoxide damage to iron-sulfur cluster-containing enzymes, some of which are part of the branched-chain amino acid pathway, and to Fenton chemistry

resulting from elevated "free" iron levels in the cytoplasm.[43] The *E. coli* genome contains no SOR homolog. Pianzzola et al.[1] first showed that plasmid-borne expression of 2Fe-SORs, including that from *D. vulgaris*, can restore the aerobic growth phenotype to *sodAsodB* strains of *E. coli*. This complementation was subsequently shown to be due to lowering of intracellular superoxide levels,[2] presumably by SOR's catalysis of reaction 4.1 using an unidentified endogenous source of electrons.[4] Figure 4.5. shows that plasmid-borne expression of *D. vulgaris* C13S 2Fe-SOR also restores aerobic growth to the *E. coli sodAsod*B strain, QC774, in minimal medium without supplements and is indistinguishable from the behavior of the wild type 2Fe-SOR in this regard. As reported previously for the wild type protein, the background "leaky" expression was sufficient for complementation, i.e., no inducer of over-expression was necessary.[7] A plasmid containing a gene encoding the N-terminal fragment, residues 1-38 of *D. vulgaris* 2Fe-SOR, did not restore the aerobic growth phenotype to strain QC774 under the same conditions. These results show that a 2Fe-SOR lacking its native [$Fe(SCys)_4$] site is capable of lowering the superoxide levels below lethality in *E. coli*. Note that the spectroscopic and redox characterizations of C13S 2Fe-SOR described above were performed on protein isolated from the same *sodAsod*B strain, also grown in aerobic minimal medium (supplemented with iron.)

Pulse Radiolysis. Results of pulse radiolysis experiments, shown in Figure 4.6 indicate that as-isolated C13S 2Fe-SOR, which contains a predominantly ferrous [$Fe(NHis)_4(SCys)$] site, reacts with superoxide in a manner very similar to that of the wild type 2Fe-SOR_{pink} as outlined in Figure 4.1.A. Fits to the kinetic traces in Figure

4.6.A and 4.6.B resulted in a calculated second order rate constant of 1 x 10^9 $M^{-1}sec^{-1}$ for formation of a transient intermediate and 100 sec^{-1} for its decay. Figure 4.6.C shows a spectrum at 50 μsec after the pulse (at maximum absorbance of the transient) constructed from kinetic traces obtained at several wavelengths between 470 nm to 700 nm. This transient species with λ_{max} ~ 595 nm and ε_{595} = 3,500 $M^{-1}cm^{-1}$ is nearly superimposable on the 100-μsec spectrum of the intermediate previously reported for the wild type 2Fe-SOR_{pink}.[17,20] No other intermediate species were detected. The analogously constructed spectrum in Figure 4.6.C obtained 100 msec after the pulse (after apparently complete decay of the intermediate) has λ_{max} ~ 645 nm, ε_{595} = 2,700 $M^{-1}cm^{-1}$, which matches well with the spectrum of the chemically oxidized C13S 2Fe-SOR shown in Figure 4.3, except for a somewhat higher calculated molar absorptivity. The extinction coefficients in Figure 4.6.C were calculated assuming that the sub-stoichiometric amounts of superoxide generated in each pulse were quantitatively reduced by 1:1 mol:mol reaction with ferrous $[Fe(NHis)_4(SCys)]$ sites of the 2Fe-SOR. This somewhat higher calculated intensity was also previously reported for the 100-msec spectra obtained from pulse radiolysis of wild type 2Fe-SOR and can attributed to experimental uncertainty.[20]

SOD Activity. Ambiguities arise in interpreting apparent SOD activities of SORs when measured using the traditional SOD assay,[3] which is based on the inhibition of reduction of cytochrome *c* due to scavenging of superoxide.[44] However, using pulse radiolysis at pH 7.8, the dismutation rate of superoxide can be measured directly by the decrease in absorbance of superoxide at 260 nm (ε_{260} = 2,100 $M^{-1}cm^{-1}$).[45] Any increase

over the natural dismutation rate in the presence of a catalyst can be unambiguously interpreted as SOD activity. Classical SODs enhance superoxide dismutation rates by at least several thousand-fold under these conditions.[17, 46, 47] However, no significant increases over the spontaneous dismutation rates were observed at two different temperatures in the presence of either wild type or C13S 2Fe-SOR as shown in Figure 4.7. Destruction of the [Fe(SCys)$_4$] site, therefore, does not unmask latent SOD activity of *D. vulgaris* 2Fe-SOR.

NADPH:Superoxide Oxidoreductase Activity. An *in vitro* superoxide reductase assay has been reported in which NADPH reduces superoxide via the catalytic electron transport chain: NADPH → FNR → rubredoxin → 2Fe-SOR → superoxide.[29] In these experiments a pre-calibrated flux of superoxide was generated using the xanthine/xanthine oxidase catalyzed reduction of dioxygen, and the expected stoichiometry of 1 mol NADPH oxidized:2 mol superoxide reduced for reduction to hydrogen peroxide was confirmed, after correcting for the background NADPH consumption rate in the absence of SOR. A high level of catalase activity was added to ensure that the NADPH consumption is not due to its reduction of hydrogen peroxide. Figure 4.8 shows that the enhancement of the NADPH consumption rate by C13S 2Fe-SOR in this assay is similar to that of the wild type protein. The traces for wild type and C13S 2Fe-SOR correspond to NADPH consumption rates of 8.3 and 7.9 μM NADPH/minute, respectively. Subtracting the background (no SOR) consumption rate of 1.7 μM NADPH/minute gives corrected consumption rates, 6.6 and 6.2 μM NADPH/minute for wild type and C13S 2Fe-SORs, respectively, which are

approximately half of the pre-calibrated superoxide flux, 12 μM superoxide/min, i.e., the stoichiometry expected for reaction 4.1. The N-term 2Fe-SOR showed a background-corrected NADPH consumption rate of 1.2 μM NADPH/minute. No NADPH consumption above background was observed if any of the components were omitted from the reaction mixture.

The Role of the [Fe(SCys)$_4$] Site in 2Fe-SOR. The results described above demonstrate that the recombinant *D. vulgaris* C13S 2Fe-SOR variant contains approximately one iron per monomer, contains neither [Fe(SCys)$_4$] nor [Fe(SCys)$_3$(OSer)] sites, but retains a [Fe(NHis)$_4$(SCys)] site with spectroscopic and redox properties that are nearly indistinguishable from those of the wild type protein. The pulse radiolysis kinetics and SOR assays on C13S 2Fe-SOR show that destruction of the [Fe(SCys)$_4$] site neither affects superoxide reactivity nor unmasks latent SOD activity of the [Fe(NHis)$_4$(SCys)] site in 2Fe-SOR. The growth complementation results show that the native [Fe(SCys)$_4$] site is not necessary for *D. vulgaris* 2Fe-SOR to catalyze reaction 4.1 at a rate sufficient to reduce superoxide to non-lethal levels in *E. coli*; the [Fe(NHis)$_4$(SCys)] site in C13S 2Fe-SOR is apparently sufficient for this function even though non-native electron donors must supply the reducing equivalents. The SOR assay described in this work used *D. vulgaris* rubredoxin, a small electron transfer protein, as proximal electron donor to the 2Fe-SOR. C13S 2Fe-SOR was as active as the wild type protein in this assay, indicating that rubredoxin efficiently donates electrons directly to the [Fe(NHis)$_4$(SCys)] site. The native source(s) of reducing equivalents for SORs' catalysis of reaction 4.1 is(are) currently unknown, although both genetic and

biochemical evidence suggest rubredoxin as the prime candidate for proximal electron donor to *D. vulgaris* 2Fe-SOR.[29, 48] *In vitro* experiments have shown that *D. vulgaris* rubredoxin catalyzes reduction of both the [Fe(SCys)$_4$] and [Fe(NHis)$_4$(SCys)] sites of *D. vulgaris* 2Fe-SOR, but that reduction of the latter site is at least four-fold faster than the former.[29] The results presented here also indicate that the [Fe(SCys)$_4$] site does not "tune" the redox properties of the [Fe(NHis)$_4$(SCys)] site in 2Fe-SOR and argues against the recent proposal that a conserved tyrosine residue participates in a superexchange electron transfer pathway between the [Fe(SCys)$_4$] and [Fe(NHis)$_4$(SCys)] sites.[39] A role for this tyrosine in facilitating electron transfer between rubredoxin (or other exogenous electron donors) and the [Fe(NHis)$_4$(SCys)] site of 2Fe-SOR remains a possibility.

Since the [Fe(SCys)$_4$] site apparently does not participate in the superoxide reductase activity of 2Fe-SOR, alternative functions must be considered. The stability and full occupancy of the [Fe(SCys)$_4$] sites in 2Fe-SORs argues against an iron uptake/delivery function. The lack of apparent interactions with the [Fe(NHis)$_4$(SCys)] site does not favor an intramolecular redox signaling function for the [Fe(SCys)$_4$] site. Although the isolated C13S 2Fe-SOR is somewhat less stable than the wild type protein to long term storage, a purely structural role for the [Fe(SCys)$_4$] site seems inconsistent with the wild type-like homodimer and activities of the C13S variant. The properties of a 1Fe-SOR from *Treponema pallidum* further argue against a structural role for the [Fe(SCys)$_4$] site. The *T. pallidum* SOR contains an N-terminal domain with significant amino acid sequence homology to that of *D. vulgaris* 2Fe-SOR, but the *T. pallidum* SOR

lacks three of the four cysteine residues that supply ligands to the [Fe(SCys)$_4$] site in 2Fe-SORs and contains no metal or other cofactors in its N-terminal domain.[5, 33] In fact, the N- and C-terminal domains of *D. vulgaris* 2Fe-SOR have even higher sequence homologies to two distinct proteins from *Desulfovibrio gigas*: the N-terminal domain is homologous to the small [Fe(SCys)$_4$]-containing protein, desulforedoxin, and the C-terminal domain to a 1Fe-SOR called neelaredoxin.[26, 27, 48] Notably, the *D. gigas* desulforedoxin and neelaredoxin have never been demonstrated to be redox partners. The possibility of an as yet undiscovered physiological redox partner for the [Fe(SCys)$_4$] site in 2Fe-SORs cannot, however, be ruled out. Another possible role for the [Fe(SCys)$_4$] site, for which we know of no precedent, is catalytic one-electron reduction of dioxygen to generate superoxide, which, if rapidly scavenged by the ferrous [Fe(NHis)$_4$(SCys)] site, would circumvent the unfavorable redox potential difference between the [Fe(SCys)$_4$] site and the O_2/O_2^- couple. The 2Fe-SOR could, thus, lower not only the intracellular superoxide, but also the dioxygen concentration.

4.D. References

1. Pianzzola, M. J., Soubes, M., Touati, D. (1996) *J. Bacteriol. 178*, 6736-6742.
2. Liochev, S. I., Fridovich, I. (1997) *J. Biol. Chem. 272*, 25573-5.
3. Jenney, F. E., Jr., Verhagen, M. F. J. M., Cui, X., Adams, M. W. W. (1999) *Science 286*, 306-309.
4. Lombard, M., Fontecave, M., Touati, D., Niviere, V. (2000) *J. Biol. Chem. 275*, 115-21.
5. Lombard, M., Touati, D., Fontecave, M., Niviere, V. (2000) *J. Biol. Chem. 275*, 27021-6.
6. Kurtz, D. M., Jr., Coulter, E. D. (2001) *Chemtracts, Inorg. Chem. 14*, 407-435.
7. Lumppio, H. L., Shenvi, N. V., Summers, A. O., Voordouw, G., Kurtz, D. M., Jr (2001) *J. Bacteriol. 183*, 101-108.
8. Fournier, M., Zhang, Y., Wildschut, J. D., Dolla, A., Voordouw, J. K., Schriemer, D. C., Voordouw, G. (2002) *J. Bacteriol.*, *185*, 71-79.
9. Kurtz, D. M., Jr., Coulter, E. D. (2002) *J. Biol. Inorg. Chem. 7*, 653-658.
10. Adams, M. W. W., Jenney, F. E., Jr., Clay, M. D., Johnson, M. K. (2002) *J. Biol. Inorg. Chem. 7*, 647-652.
11. Imlay, J. A. (2002) *J. Biol. Inorg. Chem. 7*, 659-663.
12. Auchère, F., Rusnak, F. (2002) *J. Biol. Inorg. Chem. 7*, 664-667.
13. Abreu, I. A., Xavier, A. V., LeGall, J., Cabelli, D. E., Teixeira, M. (2002) *J. Biol. Inorg. Chem. 7*, 668-674.

14. Shearer, J., Nehring, J., Lovell, S., Kaminsky, W., Kovacs, J. A. (2001) *Inorg. Chem. 40*, 5483-5484.

15. Shearer, J., Scarrow, R. C., Kovacs, J. A. (2002) *J. Am. Chem. Soc. 124*, 11709-11717.

16. Mathe, C., Mattioli, T. A., Horner, O., Lombard, M., Latour, J.-M., Fontecave, M., Niviere, V. (2002) *J. Am. Chem. Soc. 124*, 4966-4967.

17. Coulter, E. D., Emerson, J. P., Kurtz, D. M., Jr., Cabelli, D. E. (2000) *J. Am. Chem. Soc. 122*, 11555-11556.

18. Niviere, V., Lombard, M., Fontecave, M., Houee-Levin, C. (2001) *FEBS Lett. 497*, 171-173.

19. Lombard, M., Houee-Levin, C., Touati, D., Fontecave, M., Niviere, V. (2001) *Biochemistry 40*, 5032-5040.

20. Emerson, J. P., Coulter, E. D., Cabelli, D. E., Phillips, R. S., Kurtz, D. M., Jr. (2002) *Biochemistry 41*, 4348-4357.

21. Yeh, A. P., Hu, Y., Jenney, F. E., Jr., Adams, M. W., Rees, D. C. (2000) *Biochemistry 39*, 2499-2508.

22. Abreu, I. A., Saraiva, L. M., Soares, C. M., Teixeira, M., Cabelli, D. E. (2001) *J. Biol. Chem. 276*, 38995-9001.

23. Verhagen, M. F. J. M., Voorhorst, W. G., Kolkman, J. A., Wolbert, R. B., Hagen, W. R. (1993) *FEBS Lett. 336*, 13-18.

24. Coehlo, A. V., Matias, P., Fülop, V., Thomson, A., Gonzalez, A., Carrondo, M. A. (1997) *J. Biol. Inorg. Chem. 2*, 680-689.

25. Page, C. C., Moser, C. C., Chen, X., Dutton, P. L. (1999) *Nature 402*, 47-52.

26. Ascenso, C., Rusnak, F., Cabrito, I., Lima, M. J., Naylor, S., Moura, I., Moura, J. J. G. (2000) *J. Biol. Inorg. Chem. 5*, 720-729.

27. Silva, G., LeGall, J., Xavier, A. V., Teixeira, M., Rodrigues-Pousada, C. (2001) *J. Bacteriol. 183*, 4413-20.

28. Ausubel, F. A., Brent, R., Kingston, R. E., Moore, D. D., Seidman, J. G., Smith, J. A., Struhl, K. (1990) *Current Protocols in Molecular Biology* (Green Publishing and Wiley-Interscience, New York, N.Y.).

29. Coulter, E. D., Kurtz, D. M., Jr. (2001) *Arch. Biochem. Biophys.* 394, 76-86.

30. Carlioz, A., Touati, D. (1986) *EMBO J. 5*, 623-630.

31. Tavares, P., Ravi, N., Moura, J. J. G., LeGall, J., Huang, Y.-H., Crouse, B. R., Johnson, M. K., Huynh, B. H., Moura, I. (1994) *J. Biol. Chem. 269*, 10504-10510.

32. Abreu, I. A., Saraiva, L. M., Carita, J., Huber, H., Stetter, K. O., Cabelli, D., Teixeira, M. (2000) *Mol. Microbiol.* 38, 322-334.

33. Jovanovic, T., Ascenso, C., Hazlett, K. R., Sikkink, R., Krebs, C., Litwiller, R., Benson, L. M., Moura, I., Moura, J. J., Radolf, J. D., Huynh, B. H., Naylor, S., Rusnak, F. (2000) *J. Biol. Chem. 275*, 28439-28448.

34. Eidsness, M. K., Burden, A. E., Richie, K. E., Kurtz, D. M., Jr., Scott, R. A., Smith, E. T., Ichiye, T., Beard, B., Min, T.-P., Kang, C. H. (1999) *Biochemistry 38,* 14803 – 14809.

35. *The Merck Index, 10*, #2785, Windholz, M., Ed., Merck & Co., Inc., New Jersey, 1983.

37. Chen, L., Sharma, P., Le Gall, J., Mariano, A. M., Teixeira, M., Xavier, A. (1994) *Eur. J. Biochem. 226*, 613-618.

38. Clay, M. D., Jenney, F. E., Jr., Hagedoorn, P. L., George, G. N., Adams, M. W. W., Johnson, M. K. (2002) *J. Am. Chem. Soc. 124*, 788-805.

39. Clay, M. D., Jenney, F. E., Jr., Noh, H. J., Hagedoorn, P. L., Adams, M. W., Johnson, M. K. (2002) *Biochemistry 41*, 9833-9841.

40. Xiao, Z., Lavery, M. J., Ayhan, M., Scrofani, S. D. B., Wilce, M. C. J., Guss, J. M., Tregloan, P. A., George, G. N., Wedd, A. G. (1997) *J. Am. Chem. Soc. 120*, 4135-4150.

41. Coulter, E. D., Shenvi, N. V., Beharry, Z., Smith, J. J., Prickril, B. C., Kurtz, D. M., Jr. (2000) *Inorg. Chim. Acta 297*, 231-234.

42. Berthomieu, C., Dupeyrat, F., Fontecave, M., Vermeglio, A. & Niviere, V. (2002) *Biochemistry* 41, 10360-8.

43. Touati, D. (2000) *Arch. Biochem. Biophys. 373*, 1-6.

44. McCord, J. M., Fridovich, I. (1969) *J. Biol. Chem. 244*, 6049-6055.

45. Bielski, B. H. J., Cabelli, D. E., Arudi, R. L. (1985) *J. Phys. Chem. Ref. Data 14*, 1041-1100.

46. Goto, J. J., Gralla, E. B., Valentine, J. S., Cabelli, D. E. (1998) *J. Biol. Chem. 273*, 30104-30109.

47. Fisher, C. L., Cabelli, D. E., Tainer, J. A., Hallewell, R. A., Getzoff, E. D. (1994) *Proteins: Struct., Funct., Genet. 19*, 24-34.

48. Brumlik, M. J., Voordouw, G. (1989) *J. Bacteriol. 171*, 4996-5004.

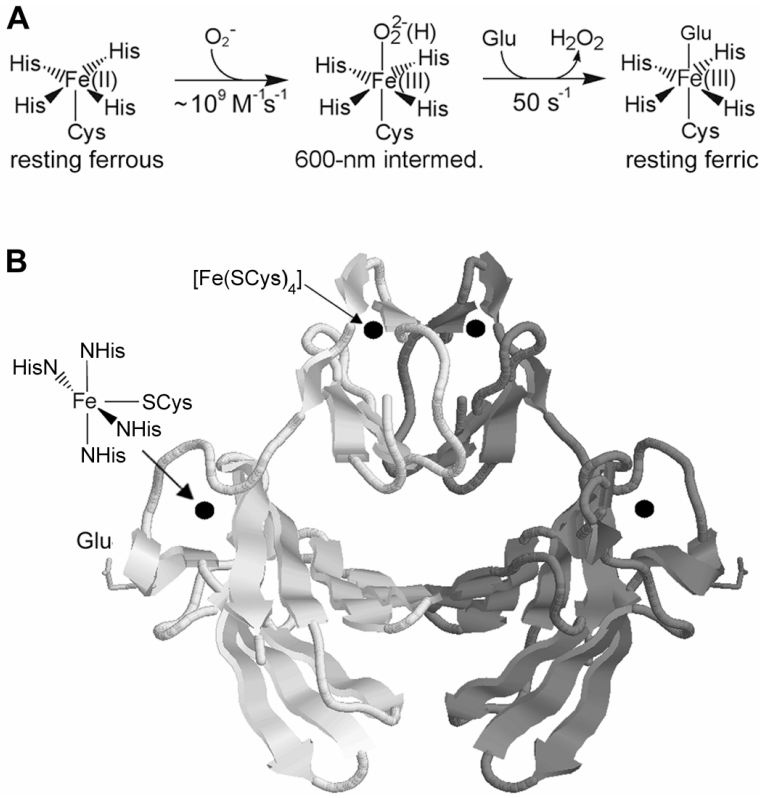

Figure 4.1. **A**, Scheme for the SOR reaction with superoxide. **B**, Ribbon drawing of the *D. desulfuricans* 2Fe-SOR homodimer (PDB ID 1DFX) [24] with darker and lighter-shaded subunits. Iron centers are represented as spheres.

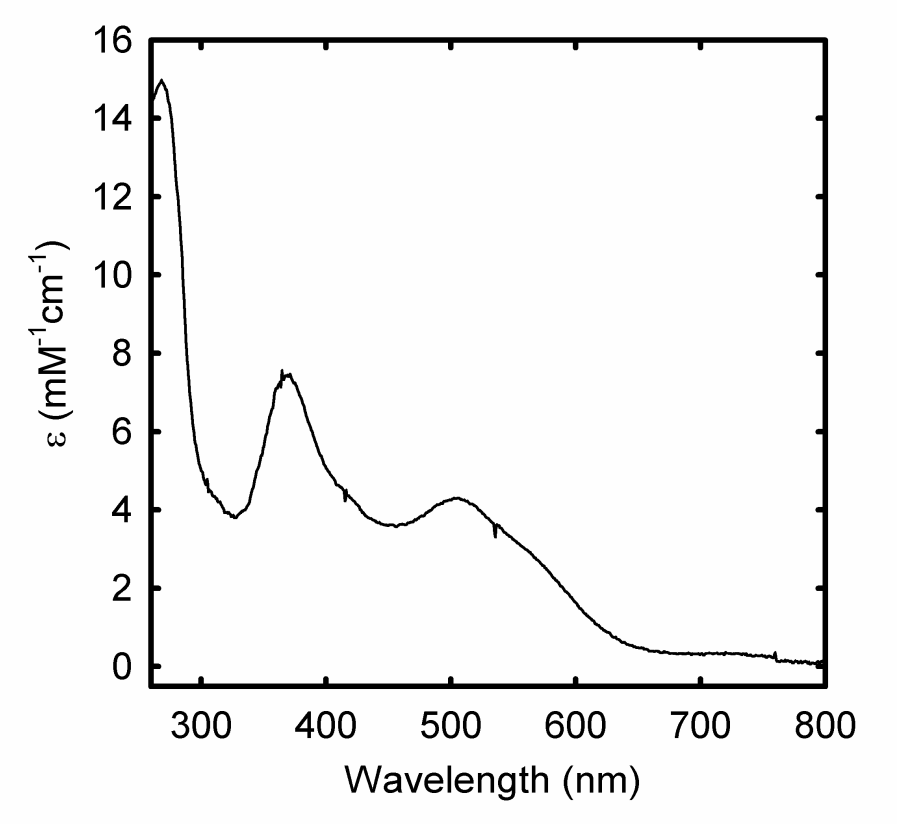

Figure 4.2. Absorption spectrum of the *D. vulgaris* N-term 2Fe-SOR in 50 mM MOPS, pH 7.5.

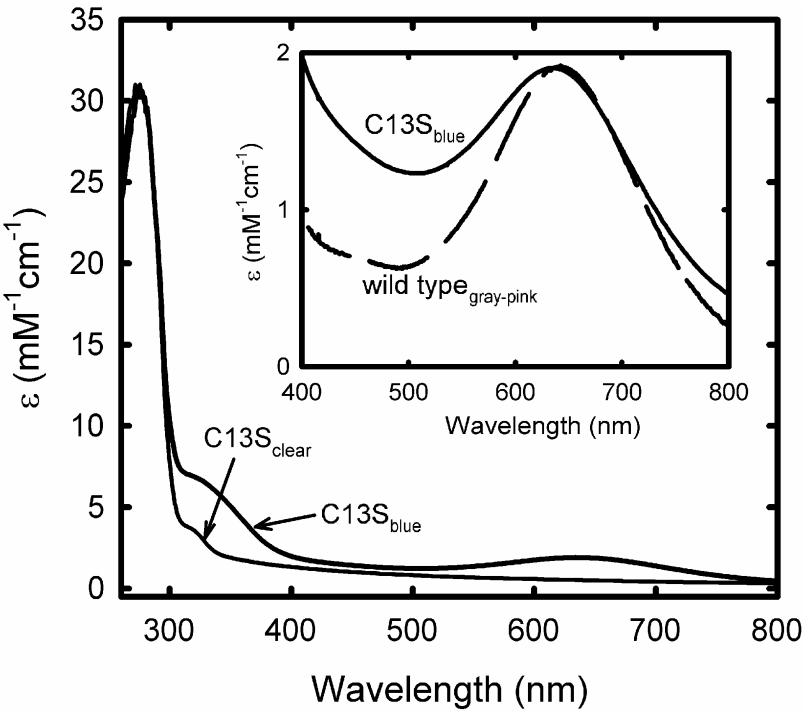

Figure 4.3. Absorption spectra of *D. vulgaris* C13S 2Fe-SOR in 50 mM MOPS pH 7.5. Shown are spectra of as-isolated C13S 2Fe-SOR (thin trace labeled "$C13S_{clear}$") and hexachloroiridate-oxidized C13S 2Fe-SOR (thick trace labeled "$C13S_{blue}$"). The inset compares the ~ 645-nm absorption feature in the C13S 2Fe-SOR_{blue} spectrum (solid trace) with that of the wild type 2Fe-$SOR_{gray\text{-}pink}$ difference absorption spectrum (dashed trace).

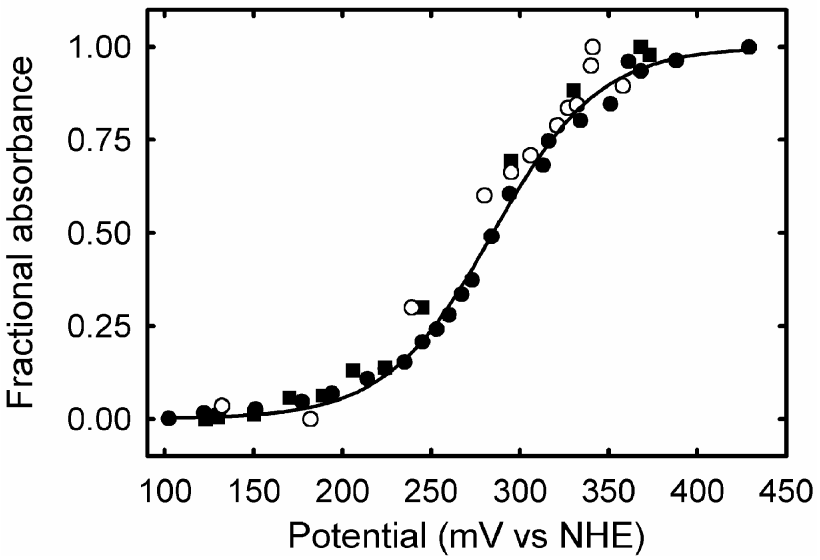

Figure 4.4. Nernst plot of fractional 650-nm absorbance change vs. potential data (corrected to NHE) for wild type and C13S 2Fe-SOR in 500 mM Tris-sulfate, pH 7 at room temperature. C13S 2Fe-SOR was titrated with either sodium dithionite (filled squares) or potassium hexachloroiridate (filled circles). Open circles are analogously obtained data for the wild type 2Fe-SOR titrated with sodium dithionite. The solid curve is a least-squares fit of the C13S 2Fe-SOR data to the Nernst equation assuming a one-electron process with the midpoint potential cited in the text.

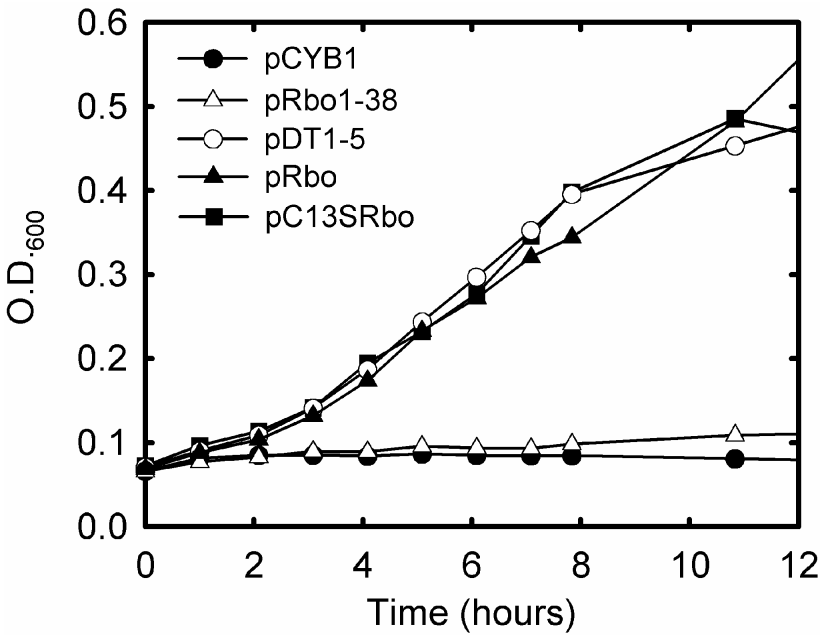

Figure 4.5. Aerobic growth versus time of *E. coli* QC774 (*sodAsodB*) expressing plasmid-borne genes encoding *E. coli* MnSOD (pDT1-5), *D. vulgaris* 2Fe-SOR (pRbo), C13S 2Fe-SOR (pC13SRbo), N-term 2Fe-SOR (pRbo1-38) or the control plasmid, pCYB1 with no inserted gene. Freshly inoculated cultures in M63 medium were incubated with shaking at 37 ^{o}C and growths were monitored as OD_{600} periodically for 24 hours; data points for the first 12 hours are shown (with connecting lines extrapolating towards the 24-hour data). Symbols are defined within the figure and represent the averages (range ± 12%) for 8 duplicate cultures.

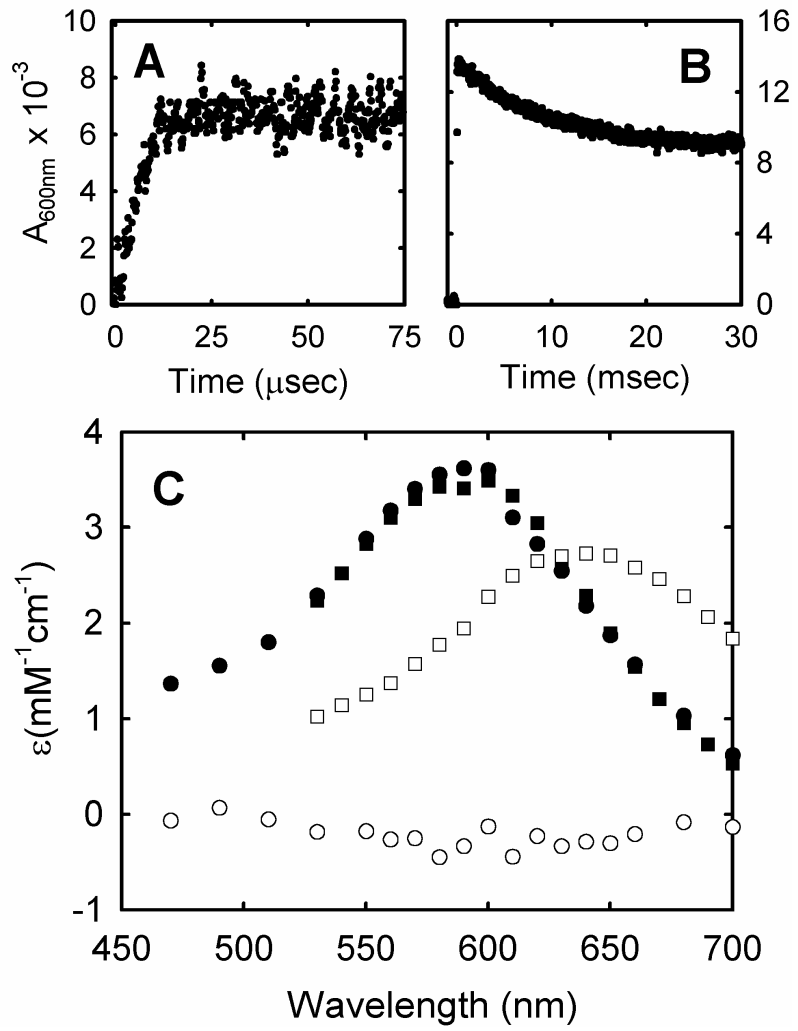

Figure 4.6. Time courses for the formation (Panel A) and decay (Panel B) of the 600-nm absorbing transient species and spectra constructed from the absorbance transients (Panel C) following pulse radiolysis of as-isolated *D. vulgaris* C13S 2Fe-SOR in 100 μM Tris-sulfate, 10 mM sodium formate pH 7.8 at 25 °C. The trace in Panel A was obtained following pulse radiolysis of the C13S 2Fe-SOR solution (200 μM in iron sites) to generate 1.0 μM superoxide and was best fit to a first-order rate constant of 1.9 x 10^5 sec^{-1}. The trace in Panel B was measured for the same solution as for Panel A following pulse radiolysis to generate 2.0 μM superoxide and was best fit to a first-order rate constant of 100 sec^{-1}. The absorption spectra in Panel C were constructed from pulse radiolysis absorbance vs time traces analogous to those shown in Panels A and B for a solution of C13S 2Fe-SOR (100 μM in iron sites) pulsed with 1.5-2.0 μM superoxide. Open circles: initial absorbances before the pulse; closed circles: absorbances at ~ 50 μsec after the pulse; closed squares: initial absorbances after the pulse using millisecond detector; open squares: 100 msec after the pulse.

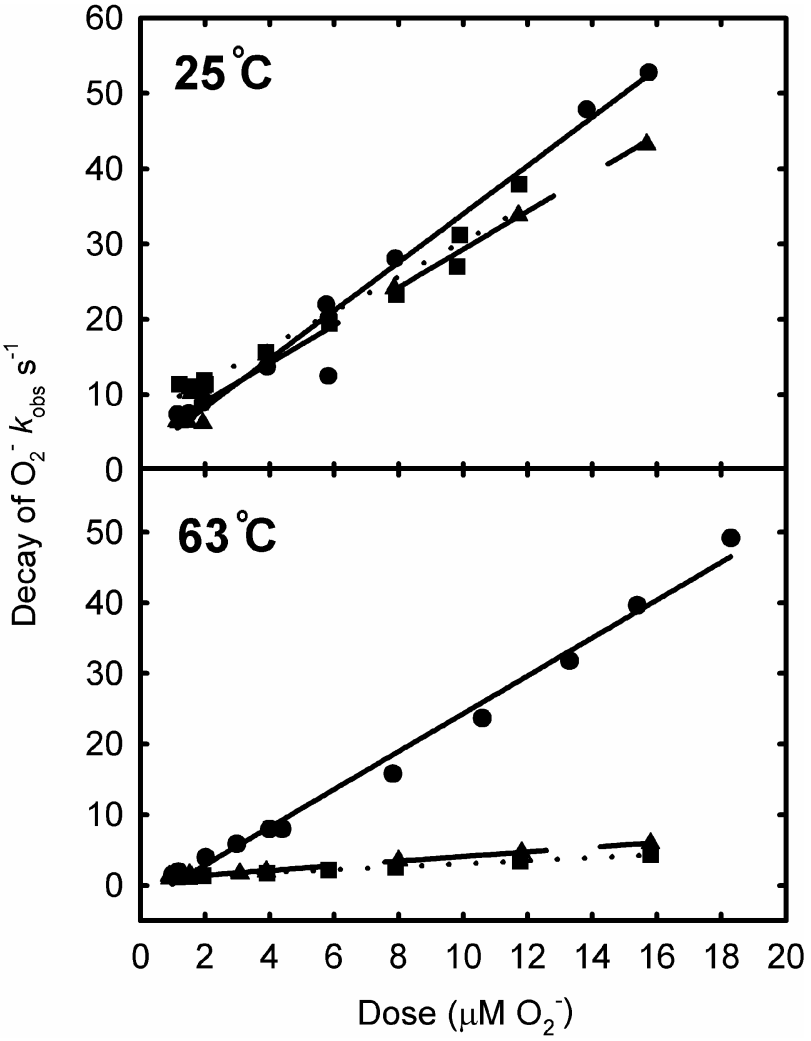

Figure 4.7. Rates of superoxide decay in either the presence or absence of catalytic concentrations (1 μM in [Fe(NHis)$_4$(SCys)] sites) of as-isolated *D. vulgaris* wild type or C13S 2Fe-SOR. Rates were monitored as the decrease in absorbance at 260 nm following pulse radiolysis to generate the indicated doses of superoxide in 120 μM Tris-sulfate containing 10 mM sodium formate, 5 μM EDTA, pH 7.8 (adjusted with sulfuric acid and sodium hydroxide). For both panels the data points are represented as: circles for controls with no SOR, squares for wild type 2Fe-SOR and triangles for C13S 2Fe-SOR. The data in the top panel were obtained at 25 ^{o}C, and the data in the bottom panel were obtained at 63 ^{o}C. The reason for the slower superoxide decay rates in the presence of SOR at 63 ^{o}C is unknown.

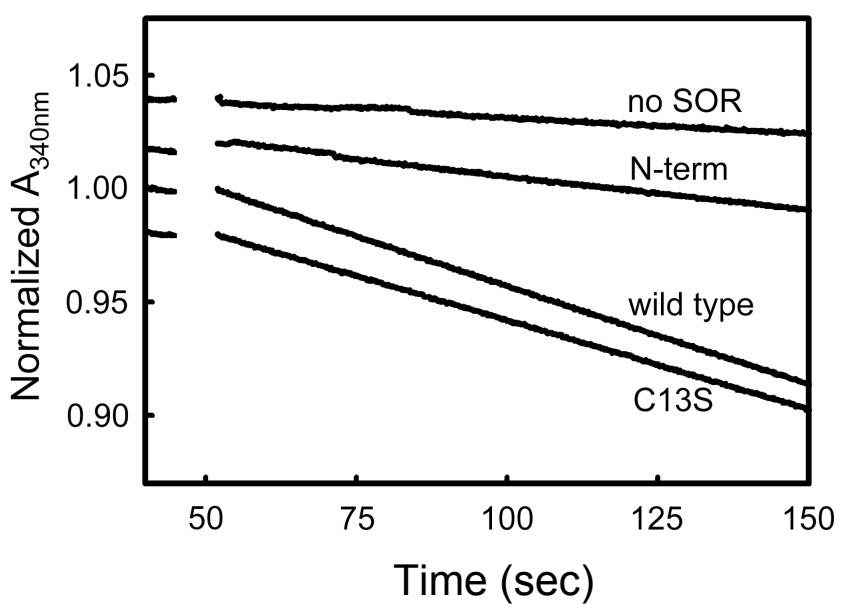

Figure 4.8. NADPH:superoxide oxidoreductase activities of *D. vulgaris* wild type, C13S and N-term 2Fe-SORs. Rates of NADPH consumption were monitored at room temperature in a 1-mL cuvette as decreases in absorbance at 340 nm (NADPH ε_{340} = 6,220 $M^{-1}cm^{-1}$) in solutions containing (in the added order) 500 μM xanthine, 100 μM NADPH, 186 U/mL of catalase, 1 μM Rub, 1 μM FNR, and either wild type or C13S 2Fe-SOR (1 μM in $[Fe(NHis)_4(SCys)]$ sites) or N-term 2Fe-SOR (1 μM in iron sites). After recording a "baseline" NADPH consumption rate for 50 sec, a pre-calibrated amount of xanthine oxidase was added to produce a flux of 12 μM superoxide/minute, and NADPH consumption was monitored for several minutes. Absorbance spikes caused by the various additions and mixing were omitted, and the traces obtained with each SOR are offset vertically by an arbitrary amount for clarity.

CHAPTER 5

REACTIONS OF THE FULLY REDUCED TWO-IRON SUPEROXIDE REDUCTASE WITH DIOXYGEN, SUPEROXIDE, AND HYDROGEN PEROXIDE: A STOPPED-FLOW KINETIC APPROACH

5.A. Introduction

The cytoplasm of anaerobically growing *D. vulgaris* is likely to be a highly reducing environment. Therefore, both the [Fe(NHis)$_4$(SCys)] and [Fe(SCys)$_4$] sites (~270 mV and ~2 mV vs. NHE, respectively) [1-3] of 2Fe-SOR should be predominantly ferrous, a form termed 2Fe-SOR$_{clear}$, due to its lack of visible absorption. 2Fe-SOR$_{clear}$ should, thus, be the most pertinent form to study its interaction with superoxide. Such studies, however, have not been reported. A major hurdle in studying this reactivity is that 2Fe-SOR$_{clear}$ reacts with both dioxygen and hydrogen peroxide.[4] This dioxygen reactivity requires that anaerobic solutions of 2Fe-SOR$_{clear}$ can be reacted with superoxide. However, pulse radiolysis uses aerobic solutions to generate superoxide.[5] In this chapter, an alternative stopped-flow method for monitoring the reaction of SOR with superoxide is described.

Depending on the coordination sphere, ferrous iron can undergo autoxidation in the presence of dioxygen to produce a ferric complex and superoxide, reaction 5.1.[6, 7]

$$Fe^{2+} + O_2 \rightarrow Fe^{3+} + O_2^- \quad (5.1)$$

Evidence that autoxidation of the ferrous [Fe(SCys)$_4$] center of rubredoxin produces superoxide, reaction 5.2, has also been reported.[8] The ferrous [Fe(SCys)$_4$] site of 2Fe-SOR could also react with dioxygen according to reaction 5.2 but, as pointed out in Chapter 4 Section 4.C, this reaction is thermodynamically unfavorable unless a subsequent reaction removes the superoxide. An intriguing possibility for this subsequent reaction is reduction of superoxide by the ferrous [Fe(NHis)$_4$(SCys)] site, which has been shown to react rapidly with superoxide.[9-11]

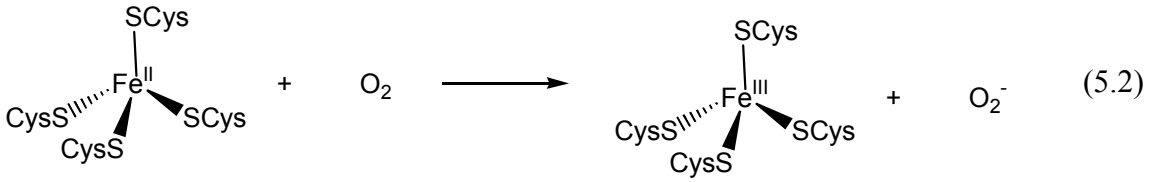

(5.2)

We and others [10, 12] have shown that hydrogen peroxide oxidizes the ferrous [Fe(NHis)$_4$(SCys)] site of 2Fe-SOR$_{pink}$. Recently, a proposed ferric-(hydro)peroxo species was reported during the reaction of excess hydrogen peroxide with the E47A variant of *D. baarsii* 2Fe-SOR.[13] This transient species was reportedly trapped by manual mixing and freezing within 5 seconds of mixing. Our observations, however, suggest that 2Fe-SOR$_{pink}$ is somewhat unstable in the presence of excess hydrogen peroxide.[10] No reports of 2Fe-SOR$_{clear}$ reactions with hydrogen peroxide have appeared. Therefore, the reactivity of 2Fe-SOR with hydrogen peroxide remains unclear.

This chapter reports preliminary stopped-flow studies of 2Fe-SOR_{clear} with dioxygen, superoxide, and hydrogen peroxide. The biological and biophysical significance of these reactions are discussed.

5.B. Materials and methods.

Reagents, Proteins, and General Procedures. Reagents and buffers were the highest grade commercially available. Bovine catalase was purchased from Sigma Chemical Co. Recombinant *D. vulgaris* wild type 2Fe-SOR and the variant E47A was expressed in *E. coli*, isolated and purified as described previously. [9, 10] Concentrations of wild type and E47A 2Fe-SOR stock solutions were calculated using ε_{502} = 4,300 $M^{-1}cm^{-1}$ (monomer basis).[10]

Stopped-Flow Spectroscopy. All stopped-flow runs were conducted using a RSM-1000 stopped-flow spectrophotometer fitted with a rapid scanning monochromator (OLIS, Inc.). These experiments were conducted at 25 °C in triplicate and also repeated with fresh solutions to verify their reproducibility. Concentrations of 2Fe-SOR, superoxide, hydrogen peroxide and dioxygen immediately after stopped-flow mixing are listed in the figure legends.

Reactions of 2Fe-SOR with superoxide were conducted using 5-mL and 0.5-mL volume drive syringes, to achieve a 10:1 (v/v) mixing ratio. Stock solutions of 2Fe-SOR_{clear} and 2Fe-SOR_{pink} were prepared in 250 mM Tris-sulfate, pH 7, containing 150 units/mL catalase, typically in ~5-mL volumes containing 38-60 μM [$Fe(SCys)_4$] sites. Anaerobic solutions were made by diluting a concentrated stock solution of 2Fe-SOR_{pink}

into the anaerobic Tris-sulfate/catalase buffer listed above in a septum-sealed plastic tube, then purging the head space with argon for ~ 20 minutes. Solutions of 2Fe-SOR_{clear} were prepared by careful titration of anaerobic 2Fe-SOR_{pink} solutions with ~ 10 mM sodium dithionite solutions added through a gas-tight syringe. This reduction was monitored visually until addition of 1 μL of the sodium dithionite solution resulted in a colorless 2Fe-SOR solution. Approximately 1.1 reducing equivalents of sodium dithionite per $[Fe(SCys)_4]$ site were required to achieve this endpoint. A portion (typically 2 mL) of the 2Fe-SOR_{pink} or 2Fe-SOR_{clear} solutions were loaded into the 5-mL drive syringe of the stopped-flow spectrophotometer, under a stream of argon gas in the case of 2Fe-SOR_{clear}. An aqueous potassium superoxide solution at pH 13 was prepared by adding ~10 mg of potassium superoxide to ~10 mL of 0.1 M sodium hydroxide, resulting in a rapidly bubbling solution. Within one minute of preparation, the concentration of superoxide in these stock solutions was determined to be ~ 2 mM using ε_{260} = 2,000 $M^{-1}cm^{-1}$.[5] A portion of this stock superoxide solution was immediately loaded into the 0.5-mL drive syringe of the stopped-flow spectrophotometer. The stopped-flow reactions were then initiated and monitored by changes in absorbance between 450 and 700 nm using the rapid scanning mode. The post-mixing pH of these solutions was determined to be 7.8.

Stopped-flow reactions of 2Fe-SOR_{clear} and 2Fe-SOR_{pink} with dioxygen or hydrogen peroxide were conducted similarly to those with superoxide described above, except using two equal-volume drive syringes, with volumes of either 2.5 or 5.0 mL. 2Fe-SOR solutions, 30-100 μM in each iron site, were prepared in 50 mM Tris-sulfate pH 7.5 (anaerobically in the case of 2Fe-SOR_{clear}). Aqueous solutions containing dissolved

O_2 at ~ 1.2 mM (dioxygen-saturated), or ~ 250 μM (air-saturated), were prepared in the same buffer containing 200 U/mL of catalase. Hydrogen peroxide solutions were made by diluting a 9 M stock (Aldrich Chemical Co.) with 50 mM Tris-sulfate pH 7.5. The above solutions were individually loaded into the drive syringes. The stopped-flow reactions were then initiated and monitored by changes in absorbance between 450 nm and 750 nm in the rapid scanning mode.

Dioxygen Titration of 2Fe-SOR$_{clear}$. A 1-mL solution of 56 μM (in each iron sites) solution of 2Fe-SOR$_{clear}$ containing 100 U/mL of catalase was prepared in a 1-mL quartz cuvette as described above, except that the buffer was 50 mM phosphate, pH 7.5, and the dithionite titration was stopped when less than 2% of the initial 502-nm absorbance remained. Various volumes (45 to 400 μL) of dioxygen-saturated solutions were manually added to the 2Fe-SOR$_{clear}$ solution. The extent of oxidation of [Fe(NHis)$_4$(SCys)] and [Fe(SCys)$_4$] sites was monitored by the absorbance increases at 502 nm (using the molar absorptivity listed above) for the [Fe(SCys)$_4$] site and 650 nm (ε_{650} = 1,900 $M^{-1}cm^{-1}$) for the ferric [Fe(NHis)$_4$(SCys)(OGlu)] site.[2] The reactions were monitored at room temperature for ~ 300 seconds, or until no further changes in the absorption were noted.

5.C. Results

Stopped-flow Reactions of Superoxide with 2Fe-SOR. Stopped-flow reactions of superoxide with SODs have traditionally mixed DMSO solutions of superoxide with the aqueous SOD solutions, using either large aqueous:DMSO volume ratios (≥ 25:1) or a

rapid pre-mix of the DMSO solution with a buffered aqueous solution prior to stopped-flow mixing with the SOD [14 - 16] We found that a convenient and workable alternative for the 2Fe-SOR stopped-flow studies was to mix a well-buffered, pH 7, 2Fe-SOR solution with an aqueous pH 13 potassium superoxide solution in a 10:1 (v/v) ratio. One millimolar superoxide at pH 13 has a half life of ~ 23 minutes at 25 ºC.[5] Similar stopped-flow methodology has been reported on other metalloproteins using lower concentrations of superoxide and higher pH.[17]

Stopped-flow reactions of 2Fe-SOR_{pink}, the form containing ferric [$Fe(SCys)_4$] and ferrous [$Fe(NHis)_4(SCys)$] sites, with superoxide are shown in Figure 5.1. Spectra of the same 2Fe-SOR_{pink} solutions, stopped-flow mixed with an aqueous 0.1 M sodium hydroxide solution 10:1 (v/v), were subtracted from the corresponding superoxide reaction time course spectra, and the resulting difference spectra are shown in Figure 5.1. These spectra show that 2Fe-SOR_{pink} reacted with superoxide within the mixing dead time (~2 msec) to form a transient species with an absorption maximum at ~600 nm (Figure 5.1, spectrum **a**). Over the next 40 msec the absorption maximum decreased in intensity and red-shifted to ~645 nm leading to the final spectrum (Figure 5.1, spectrum **b**). The initial absorption spectrum and its subsequent time course, closely match those for the same reaction conducted by pulse radiolysis.[3, 12] As discussed in Chapters 2 and 3, the pulse radiolysis studies showed a transient 600-nm absorbing species resulting from a nearly diffusion-controlled reaction with superoxide (c.f. Scheme 5.1), which is consistent with its appearance within the stopped-flow mixing dead time in Figure 5.1. For these stopped-flow time courses, the 600-nm absorbance decreased with $k_{obs} = 44 \pm 1$

sec^{-1}, which was nearly the same within experimental error as that for the corresponding absorbance increase at 650 nm, 50 ± 4 sec^{-1}. These rate constants and the near isosbestic spectral interconversion once again closely match those previously reported for the same reaction conducted by pulse radiolysis. Using the estimated ε_{600} = 3,500 $M^{-1}cm^{-1}$ for the transient 600-nm intermediate[9-11] and the absorbances of the earliest obtainable stopped-flow spectra (represented by Figure 5.1, spectrum **a**), a maximum of 60-75 % of the $[Fe(NHis)_4(SCys)]$ sites was observed as the transient intermediate in multiple experiments; presumably the other 25 - 40 % had already decayed. This apparent percentage decay within the mixing time is somewhat higher than expected for a ~50 sec^{-1} decay. This discrepancy could be due to inefficient mixing and/or to competing disproportionation of superoxide. Even so, the absolute absorption of the 600-nm transient shown in Figure 5.1 is an order of magnitude higher than in the corresponding pulse radiolysis spectra,[9-11] consistent with our use of excess superoxide over $[Fe(NHis)_4(SCys)]$ sites in these stopped-flow experiments vs. sub-stoichiometric superoxide for the pulse radiolysis experiments. The close agreement of the stopped-flow and pulse radiolysis spectral time courses show that stopped-flow spectroscopy can be reliably used to monitor the reaction of 2Fe-SOR with superoxide.

$2Fe\text{-}SOR_{clear}$ showed a biphasic reaction upon stopped-flow mixing with superoxide. Figure 5.2.A shows difference absorption spectra for the first phase of this reaction, once again subtracting the spectra for the stopped-flow mixing of $2Fe\text{-}SOR_{clear}$ with 0.1 M sodium hydroxide. This portion of the spectral time course closely resembled that seen for the superoxide reaction with $2Fe\text{-}SOR_{pink}$. The initial spectrum obtained

within the mixing dead time (Figure 5.2.A, gray trace) had an absorption maximum at ~600 nm, and this species transformed over the next 40 msec to a less intensely absorbing species with a ~645-nm absorption maximum (Figure 5.2.A, bold black trace). The absorbance at 600 nm decreased and that at 650 nm increased with k_{obs} = 61 ± 1 sec^{-1}, 64 ± 4 sec^{-1} respectively, and the spectral time course once again showed near isosbestic behavior. The spectral time courses in Figures 5.1 and 5.2.A, thus, presumably represent the same process, namely, oxidation of the [$Fe(NHis)_4(SCys)$] site by superoxide according to Scheme 5.1.

In these stopped-flow reactions of 2Fe-SOR_{clear} with superoxide, a second phase, observed as an absorbance increase in the region of 500 nm occurred with k_{obs} = 1.8 ± 0.1 sec^{-1}, as shown in Figure 5.2.B (which depicts absolute, not difference absorption spectra). Given the known absorption spectra of the two ferric sites in 2Fe-SOR [11] and that the [$Fe(NHis)_4(SCys)$] site has already oxidized during the first phase, this 500-nm absorbance increase must be due to oxidation of the ferrous [$Fe(SCys)_4$] site. This absorbance increase at 500 nm also occurred during the control stopped-flow reaction of 2Fe-SOR_{clear} mixed with an aerobic pH 13 solution 10:1 (v/v) without superoxide, although the rate of absorbance increase was ~6-times slower, k_{obs} = 0.3 ± 0.1 sec^{-1}. The rate of ~ 2 sec^{-1} measured for this oxidation of the ferrous [$Fe(SCys)_4$] site upon mixing with superoxide, is very similar to that measured for the reaction of 2Fe-SOR_{clear} mixed 1:1 (v/v) with saturated dioxygen solutions discussed below (c.f. Figure 5.3.B). Spontaneous disproportionation of superoxide both prior to and after mixing with the 2Fe-SOR solution will significantly add to the concentration of dissolved dioxygen. In

fact, most of the superoxide should have disproportionated prior to the [Fe(SCys)$_4$] oxidation observed in Figure 5.3.B (the half-life of 1 mM O_2^- at pH 7.8 is ~ 2 msec). A significant activity of catalase (100 U/mL) in these solutions should have minimized the possibility that the absorbance changes in Figure 5.2 are due to reactions with the hydrogen peroxide that results from spontaneous disproportionation of superoxide. We, therefore, assign this second phase to oxidation of the ferrous [Fe(SCys)$_4$] site by dioxygen. The product of these stopped-flow oxidations of 2Fe-SOR$_{clear}$ mixed with superoxide is, as expected, 2Fe-SOR$_{gray}$, the form containing ferric [Fe(NHis)$_4$(SCys)] and [Fe(SCys)$_4$] sites. The absorption spectrum in Figure 5.2.A, thus, represents a previously undescribed form of 2Fe-SOR containing a ferric [Fe(NHis)$_4$(SCys)] site and a ferrous [Fe(SCys)$_4$] site.

Reactions of 2Fe-SOR$_{clear}$ with Dioxygen. Consistent with previous studies at room temperature, 2Fe-SOR$_{pink}$ showed no detectable reaction at dioxygen concentrations up to 600 μM. However, 1:1 (v/v) mixing of an anaerobic solution of 2Fe-SOR$_{clear}$ with either air- or dioxygen-saturated aqueous solutions resulted in complete oxidation to 2Fe-SOR$_{gray}$ but proceeding through 2Fe-SOR$_{pink}$. The absorption spectral time course for 2Fe-SOR$_{clear}$ mixed with dioxygen-saturated buffer is shown in Figure 5.3. The ferric [Fe(SCys)$_4$] site of 2Fe-SOR has an absorption feature with λ_{max} ~ 502 nm that partially overlaps the absorption spectrum of the ferric [Fe(NHis)$_4$(SCys)] site (λ_{max} ~ 645 nm), as shown in Chapter 1, Figure 1.10.[3,11] The time courses (c.f. Figure 5.3.A) of the absorbance increase at 502 nm were fit to a first-order oxidation of the [Fe(SCys)$_4$] site by excess dioxygen with a k_{obs} = 1.6 ± 0.5 sec^{-1}. This portion of the 502-nm absorbance

increase was complete in approximately 2 seconds under these conditions. After a ~ 3 second lag period and apparently complete oxidation of the [$Fe(SCys)_4$] site, an absorbance increase at 650 nm, attributed to oxidation of the [$Fe(NHis)_4(SCys)$] site occurred. The post lag-phase 650-nm absorbance increase occurred with a fitted k_{obs} = 2.6 ± 1 sec^{-1} and resulted in a final absorption spectrum that was indistinguishable from that of "resting" 2Fe-SOR_{gray} (c.f. Figure 5.3, spectrum b). After complete oxidation to 2Fe-SOR_{gray}, a slower decrease in absorption at 502 nm (k_{obs} ~ 0.40 ± 0.01 sec^{-1}) and at 650 nm (k_{obs} ~ 0.010 ± 0.001 sec^{-1}) occurred. This bleaching process ended after ~ 6 seconds, leaving ~ 90% of the ferric centers apparently intact. Attempts to globally fit these spectral time courses using sums of exponentials were unsuccessful. The same reaction, but mixing 2Fe-SOR_{clear} with air- rather than dioxygen-saturated solution 1:1 (v/v), resulted in k_{obs} = 0.40 ± 0.05 sec^{-1} for the absorbance increase at 502 nm and, after a nearly 25-second lag period, k_{obs} = 0.4 ± 0.1 sec^{-1} for the absorbance increase at 650 nm (c.f. Figure 5.3.B). Once again 2Fe-SOR_{gray} was the final product.

Table 1 reports the proportion of each ferrous site of 2Fe-SOR_{clear} that becomes oxidized upon manual mixing with various excesses of dioxygen. Addition of 1 equivalent of dioxygen per 2Fe-SOR monomer was sufficient to completely oxidize all [$Fe(SCys)_4$] sites, whereas, large excesses of dioxygen were required for complete oxidation of the [$Fe(NHis)_4(SCys)$] site, i.e., conversion to 2Fe-SOR_{gray}.

Reactions of Hydrogen Peroxide with 2Fe-SOR. Although rate constants for the reaction of 2Fe-SOR_{pink} with hydrogen peroxide have been reported,[10,12] time courses of the absorbance changes have not. Figure 5.4 shows such a time course for stopped-

flow mixing 5 equivalents of hydrogen peroxide with 2Fe-SOR$_{pink}$. The time course corresponds to oxidation of the [Fe(NHis)$_4$(SCys)] site. The absorbance of wild type 2Fe-SOR$_{pink}$ increased at 650 nm (k_{obs} of 0.10 ± 0.01 sec^{-1}) to a final spectrum that was identical to that of resting 2Fe-SOR$_{gray}$. The ferrous [Fe(NHis)$_4$(SCys)] site of the axial-glutamate free E47A 2Fe-SOR$_{pink}$ variant underwent an analogous oxidation with the same excess of hydrogen peroxide, as shown in Figure 5.5. The absorption at 610 nm (λ_{max} for the ferric [Fe(NHis)$_4$(SCys)] site) of E47A 2Fe-SOR$_{pink}$ increased with a fitted k_{obs} of 0.20 ± 0.04 sec^{-1} to the known fully oxidized spectrum.[9,10] These k_{obs} are consistent with the respective second order rate constants of 21 and 37 M^{-1}sec^{-1} previously reported for hydrogen peroxide oxidations of *D. vulgaris* 2Fe-SOR$_{pink}$ and its E47A variant.[10] No chromophores were detected during these reactions other than those associated with 2Fe-SOR$_{pink}$ and 2Fe-SOR$_{gray}$ or the corresponding E47A variant spectra. Varying the scan rates and scanning time to examine slower processes (up to ~ 60 scans/sec and 2 minutes, respectively) resulted in the appearance of no additional chromophores.

Once again in contrast to that of 2Fe-SOR$_{pink}$, reaction of 2Fe-SOR$_{clear}$ with excess hydrogen peroxide resulted in rapid oxidation of both iron sites. Using 20 equivalents of hydrogen peroxide per 2Fe-SOR$_{clear}$ monomer, the absorbances at 502 and 650 nm, presumably corresponding to oxidations of the [Fe(SCys)$_4$] and [Fe(NHis)$_4$(SCys)] sites, respectively, increased with k_{obs} of 14 ± 3 and 4.3 ± 1.5 sec^{-1}, respectively, as shown in Figure 5.6. The maximum absorbance increases at both wavelengths occurred within ~ 300 msec after mixing. The absorbance increase at 650

nm occurred ~ 100-times faster than for H_2O_2 oxidation of 2Fe-SOR_{pink}. Interestingly, the A_{502}/A_{600} absorbance ratio seemed to change as a function of time, although the kinetic absorbance trace at 502 nm seems to indicate some mixing problem early in this reaction (c.f. Figure 5.6 inset). The ~ 80 msec spectrum seems to show a broadly absorbing species with λ_{max} ~ 570 nm; however, by ~ 160 msec the A_{502}/A_{600} ratio had changed to that typically associated with 2Fe-SOR_{gray}. After these absorbance increases a bleaching of the spectrum was observed and fit to a two-exponential process at both 502 and 650 nm. The fitted k_{obs} for bleaching at 502 nm were 0.60 ± 0.04 and 0.03 ± 0.01 sec^{-1}, and for bleaching of 650 nm, 0.40 ± 0.01 and 0.06 ± 0.01 sec^{-1}. This bleaching processes stopped after ~ 30 seconds, leaving ~ 10% yield of 2Fe-SOR_{gray}. This irreversible bleaching presumably represents destruction of the oxidized metal centers by further reactions with hydrogen peroxide. The initial portion of this bleaching can be seen in the 502-nm kinetic trace in the inset to Figure 5.6.

5.D. Discussion

The kinetics of the reactions of 2Fe-SOR_{pink} with superoxide, as monitored by rapid-scanning stopped-flow spectroscopy, are fully consistent with our previously reported pulse radiolytic experiments and Scheme 5.1.[9-11] In the stopped-flow experiments the 600-nm intermediate formed within the dead time of mixing, confirming that the rate of its formation must be ≥300 sec^{-1}, and decayed at rates and to a final spectrum that are very similar to those published for the pulse radiolysis studies.[9-11] The scanned absorption spectra obtained in these stopped-flow experiments reinforce the

spectra reconstructed from a series of single-wavelength scans obtained in the earlier pulse radiolysis experiments.[9-11] Thus the transient 600-nm absorbing species, presumably a ferric-hydroperoxo, is not an artifact of pulse radiolysis.

The reaction of wild type 2Fe-SOR$_{clear}$ with superoxide is probably a better representation of the *in vivo* reaction. Given the reduction potentials of the iron sites [1-3] and the highly reducing environment of a *D. vulgaris* cell, it is likely that 2Fe-SOR will be completely reduced a majority of its lifetime. The results reported here show that the ferrous [Fe(NHis)$_4$(SCys)] site of 2Fe-SOR$_{clear}$ reacts rapidly with superoxide ($\geq$300 sec^{-1}) to generate the same 600-nm absorbing transient species as observed for the 2Fe-SOR$_{pink}$ reaction, which decays to a spectrum attributable to the ferric [Fe(NHis)$_4$(SCys)] site. Using the molar absorptivity determined from the pulse radiolysis studies, (ε_{600} ~ 3,500 M^{-1}cm^{-1}),[9,10] nearly 34 μM of the transient species was detected of the 44 μM [Fe(NHis)$_4$(SCys)] sites in solution in the first obtainable spectrum after mixing (c.f. Figure 5.2.A gray spectrum). A slower oxidation of the ferrous [Fe(SCys)$_4$] site was then observed. This oxidation occurred at a k_{obs} ~ 2 sec^{-1}, which is consistent with oxidation by dioxygen rather than superoxide (c.f. Figures 5.2.B and 5.3).

There is no doubt that the ferrous [Fe(SCys)$_4$] site in 2Fe-SOR reacts with dioxygen and that the [Fe(NHis)$_4$(SCys)] site does not. The vast majority of aerobically isolated 2Fe-SOR has a ferric [Fe(SCys)$_4$] site and ferrous [Fe(NHis)$_4$(SCys)] site. Similarly, aerobically purified C13S 2Fe-SOR is air stable, maintaining a ferrous [Fe(NHis)$_4$(SCys)] site (c.f. Chapter 4). The ferrous [Fe(SCys)$_4$] site of 2Fe-SOR$_{clear}$ presumably reacts with dioxygen according to reaction 5.2. This reaction occurs ~ 24 Å

from a superoxide reactive center, namely the ferrous [Fe(NHis)$_4$(SCys)] site. Immediately after its production, the O_2^- would have to be relatively close to the [Fe(SCys)$_4$] center, thereby creating a locally high concentration of superoxide close to the [Fe(NHis)$_4$(SCys)] site. Using the assumption that the added catalase in solution is removing any hydrogen peroxide, superoxide must be oxidizing the ferrous [Fe(NHis)$_4$(SCys)] site. Table 5.1 shows one ferrous [Fe(SCys)$_4$] site is oxidized for every one dioxygen added, but nearly 8 equivalents of dioxygen are needed for full oxidation of 2Fe-SOR$_{clear}$ to 2Fe-SOR$_{gray}$. This result indicates that, even when superoxide is generated within ~ 24 Å of the [Fe(NHis)$_4$(SCys)] site, it does not necessarily react with the ferrous [Fe(NHis)$_4$(SCys)] center. The rate of [Fe(SCys)$_4$] oxidation seems to be dioxygen-dependent, which at lower concentrations of dioxygen limits the transient burst of superoxide (c.f. Figure 5.3 insets A and B). Thus as the dioxygen concentration is increased, the reaction becomes exponentially faster, producing a higher transient [O_2^-], some or all of which reacts with the ferrous [Fe(NHis)$_4$(SCys)] site.

This argument, however, does not explain the "lag" phase between oxidation of the [Fe(SCys)$_4$] and [Fe(NHis)$_4$(SCys)] sites. The reaction of the ferrous [Fe(NHis)$_4$(SCys)] site with superoxide has been shown to be diffusion-controlled.[9-11] If the production of superoxide at the [Fe(SCys)$_4$] center is rate limiting, the diffusion of superoxide should be very rapid and either the [Fe(NHis)$_4$(SCys)] site should oxidize at almost the same time as the [Fe(SCys)$_4$] center (i.e., without a lag phase), or the superoxide should disproportionate (50 μM O_2^- has a $t_{½}$ ~ 40 msec at pH 7.0). Therefore,

another process must be occurring to slow the oxidation of the ferrous [Fe(NHis)$_4$(SCys)] site by superoxide. One possibility may be that the anionic superoxide ion is prevented from rapidly diffusing away from the protein by positively charged residues along the surface of 2Fe-SOR. Figure 5.7 shows the electrostatic charge associated with the surface of the *D. desulfurican* 2Fe-SOR dimer.[18] The generated superoxide would presumably be repelled by the negative charges in the immediate vicinity of the [Fe(SCys)$_4$] site. The [Fe(NHis)$_4$(SCys)] site is positively charged; however, another positively charged region is positioned between the two iron centers within the 2Fe-SOR monomer. This pocket of positive charge, which can be seen in Figure 5.7, may act as an electrostatic guide for funneling superoxide to the [Fe(NHis)$_4$(SCys)] site. The [Fe(NHis)$_4$(SCys)] site would be temporarily shielded from superoxide by this positively charged region between the two centers of 2Fe-SOR.

Dioxygen reduction may not be the physiological role of the [Fe(SCys)$_4$] site of 2Fe-SOR, but could occur within a cell or after cell death and/or lysis. Assuming that the 2Fe-SOR concentration is approximately 1 μM within a *D. vulgaris* cell and that, when *D. vulgaris* cells encounter aerobic conditions, dioxygen diffuses into the cell at nearly diffusion controlled rates,[19] the intracellular dioxygen concentration would reach nearly 200 μM. 2Fe-SOR$_{clear}$ would then be exposed to much higher than 8 equivalents of dioxygen, which our experimental data suggests, would lead to the reactions shown in Scheme 5.2. Dioxygen is reduced to superoxide at the [Fe(SCys)$_4$] site, producing superoxide, which then diffuses along the protein surface to the ferrous

[Fe(NHis)$_4$(SCys)] center, where it gets reduced to hydrogen peroxide, thereby resulting in the resting ferric [Fe(NHis)$_4$(SCys)(OGlu)] site.

We have confirmed that high concentrations of hydrogen peroxide damage the metal centers of 2Fe-SOR. No transient chromophoric intermediate species was detected in stopped-flow reaction of 2Fe-SOR (or the E47A variant) with hydrogen peroxide. The lack of a detectable intermediate species upon mixing 5 equivalents of hydrogen peroxide with 1 equivalent of 2Fe-SOR, is not consistent with the transient ferric-(hydro)peroxo species reported by Mathe *et al*. upon manual mixing of 2Fe-SOR with excess hydrogen peroxide.[13] The ferric-peroxo species reported by Mathe *et al.* may be due to an intermediate along the destruction pathway of the iron centers by excess hydrogen peroxide.

The rapid reaction of 2Fe-SOR$_{clear}$ with hydrogen peroxide is not easily explainable. The concentration of hydrogen peroxide used in our experiments is likely to be much higher than *D. vulgaris* 2Fe-SOR would ever be exposed to *in vivo*. Intracellular levels of hydrogen peroxide are likely to be very low, especially in the presence of reducing equivalents and rubrerythrin, a peroxidase also found in *D. vulgaris*.[20] Low levels of hydrogen peroxide could oxidize the ferrous [Fe(NHis)$_4$(SCys)] site of intracellular 2Fe-SOR, but at a much slower rate than oxidation by superoxide. Finally, experimental evidence from Voordouw and co-workers suggests that the *in vivo* level of 2Fe-SOR is depleted when *D. vulgaris* is artificially exposed to hydrogen peroxide.[21] This depletion may be due to the destruction of 2Fe-SOR iron centers by hydrogen peroxide.

5.E. Reference

1. Verhagen, M. F., Voorhorst, W. G., Kolkman, J. A., Wolbert, R. B., Hagen, W. R. (1993) *FEBS Lett. 336*, 13-18.
2. Tavares, P., Ravi, N., Moura, J. J., LeGall, J., Huang, Y. H., Crouse, B. R., Johnson, M. K., Huynh, B. H., Moura, I. (1994) *J. Biol. Chem. 269*, 10504-10510.
3. Ascenso, C., Rusnak, F., Cabrito, I., Lima, M. J., Naylor, S., Moura, I., Moura, J. J. G. (2000) *J. Biol. Inorg. Chem. 5*, 720-729.
4. Emerson, J. P., Coulter, E. D., Kurtz, D. M., Jr., unpublished results
5. Bielski, B. H. J., Cabelli, D. E. (1991) *Int. J. Rad. Biol. 59*, 291-319.
6. Urbanski, N. K., Beresewicz, A. (2000) *Acta Biochim. Pol. 4*, 951-962.
7. Welch, K. D., Davis, T. Z., Aust, S. D., (2002) *Arch. Biochem. Biophys. 397*, 360-369.
8. May, S. W., Abbott, B. J., Felix, A. (1973) *Biochem. Biophys. Res. Com. 54*, 1540-1545.
9. Coulter, E. D., Emerson, J. P., Kurtz, D. M., Jr., Cabelli, D. E. (2000) *J. Am. Chem. Soc. 122*, 11555-11556.
10. Emerson, J. P., Coulter, E. D., Cabelli, D. E., Phillips, R. S., Kurtz, D. M., Jr. (2002) *Biochemistry 41*, 4348-4357.
11. Emerson, J. P., Cabelli, D. E., Kurtz, D. M., Jr. (2003) *Prot. Nat. Acad. Sci. 100*, 3802-3807.

12. Lombard, M., Touati, D., Fontecave, M., Niviere, V. J., (2000) *J. Biol. Chem*. *275*, 115-121.

13. Mathe, C., Mattioli, T. A., Horner, O., Lombard, M., Latour, J. M., Fontecave, M., Niviere, V., (2002) *J. Am. Chem. Soc. 124*, 4966-4967.

14. McClune, G. J., Fee, J. A. (1978) *Biophys J. 24*, 65-69.

15. Marklund, S. (1976) *J. Biol. Chem. 251*, 7504-7504.

16. Valentine, J. S., Curtis, A. B. (1975) *J. Am. Chem. Soc. 97*, 224-226.

17, Bradic, Z., Wilkins, R. G., (1984) *J. Am. Chem. Soc. 106*, 2236-2239.

18. Silaghi-Dumitrescu, R., unpublished results.

19. Imlay, J. A. (2002) *J. Biol. Inorg. Chem. 7*, 659-663.

20. Lumppio, H. L., Shenvi, N. V., Summers, A. O., Voordouw, G., Kurtz, D. M., Jr., (2001) *J. Bacteriol*. *183*, 101-107.

21. Fournier, M., Zhang, Y., Wildschut, J. D., Dolla, A., Voordouw, J. K., Schriemer, D. C., Voordouw, G., (2003) *J Bacteriol. 185*, 71-79.

Table 5.1. Proportion of 2Fe-SOR$_{clear}$ iron sites oxidized by dioxygen.[a]

			iron sites oxidized	
[2Fe-SOR$_{clear}$][b] (μM)	[O_2][b] (μM)	mol ratio O_2:2Fe-SOR	[$Fe(SCys)_4$][c] (μM)	[$Fe(NHis)_4(SCys)$][d] (μM)
30	30	1:1	28	0.8
30	100	3:1	29	2.3
25	200	8:1	24	6.0
22	340	16:1	21	9.0
28	600	21:1	28	27
2.5	200	80:1	2.7	2.4

[a]All reactions at room temperature in 50 mM phosphate, pH 7.5, containing ~100 U/mL of catalase. [b]Initial concentrations resulting from dilutions of a 2Fe-SOR$_{clear}$ stock solution with various volumes of 1.2 mM dioxygen solution. 2Fe-SOR concentrations are listed as protein monomer. [c]Calculated from the change in absorbance at 502 nm (ε_{502} = 4,300 $M^{-1}cm^{-1}$) following mixing with dioxygen. [d]Calculated from the change in absorbance at 650 nm (ε_{650} = 2,300 $M^{-1}cm^{-1}$) following mixing with dioxygen.

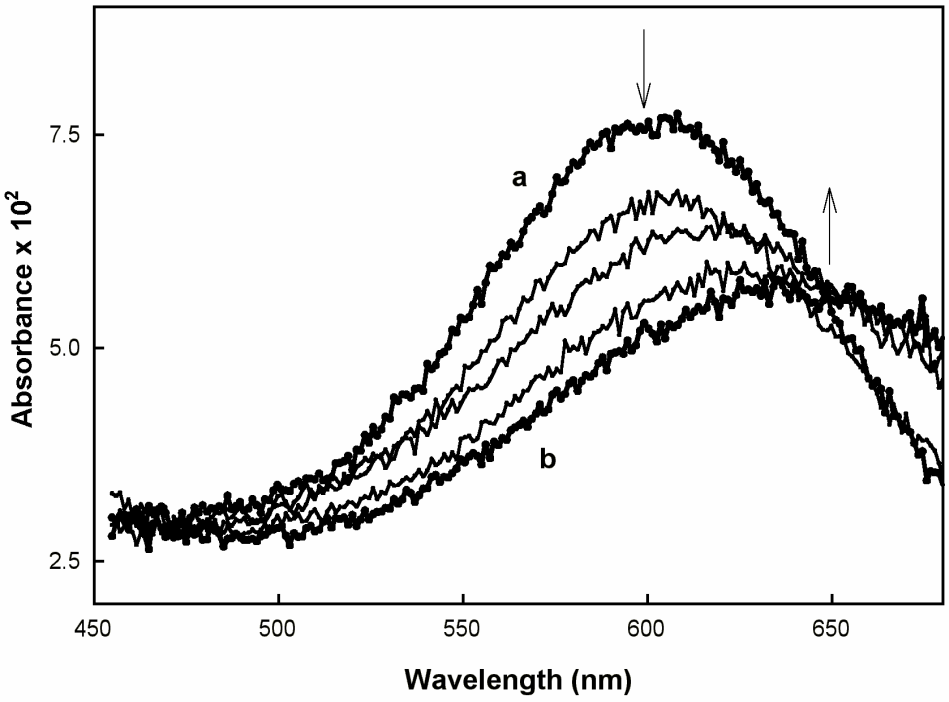

Figure 5.1. Rapid-scanning spectroscopy following stopped-flow mixing of 2Fe-SOR_{pink} solutions with superoxide solutions. 2Fe-SOR_{pink}, 51 μM in $[Fe(NHis)_4(SCys)]$ sites, in 250 mM Tris-sulfate, pH 7.0, was mixed 10:1 (v/v) with a pH 13 solution of ~2 mM superoxide. The dilution factor would result in 46 μM 2Fe-SOR_{pink} [Fe(NHis)4(SCys)] sites and ~180 μM superoxide immediately after mixing. (**A**) difference absorption spectra (reaction with pH 13 superoxide solution minus reaction with an aerobic pH 13 solution (0.1 M sodium hydroxide)) recorded at ~1 msec, **a**, and 40 msec, **b**, after the mixing dead times, and every 10 msec in between (thinner traces). Arrows show directions of absorbance changes.

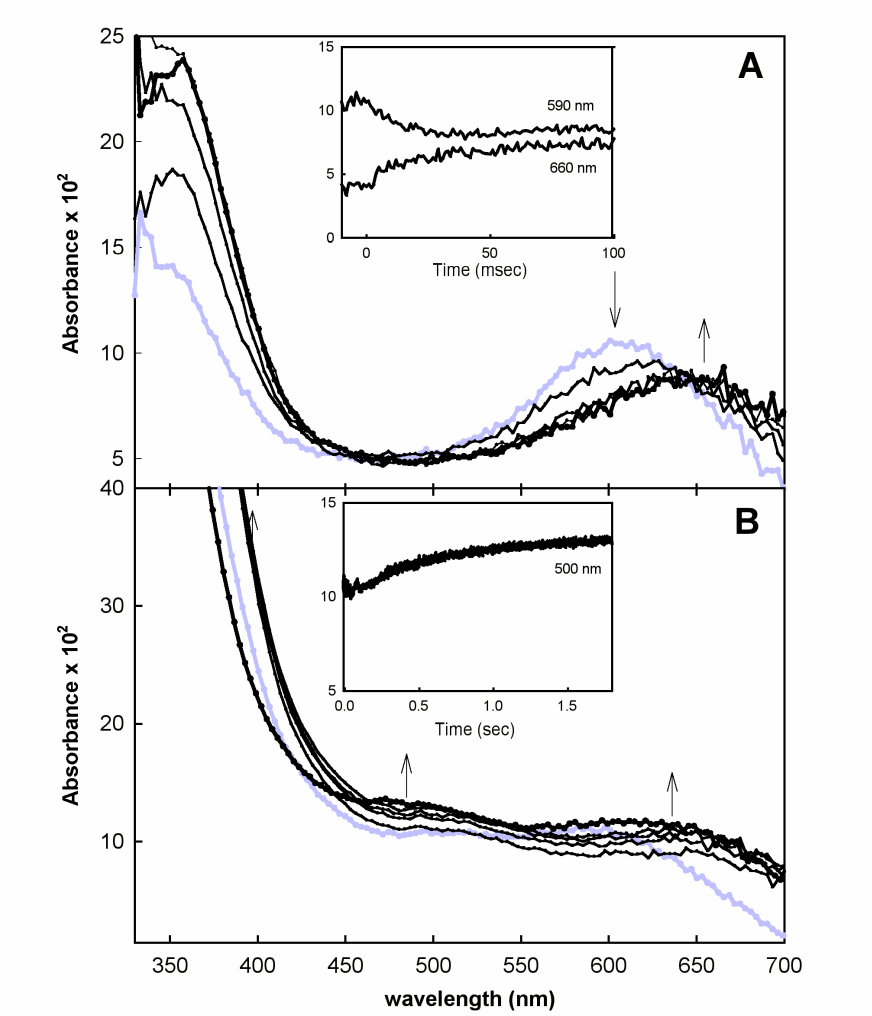

Figure 5.2. Rapid-scanning spectroscopy following stopped-flow mixing of 2Fe-SOR_{clear} solutions with superoxide solutions. Ten volumes of an anaerobic solution containing 48 μM in 2Fe-SOR_{clear} [$Fe(NHis)_4(SCys)$] sites in 250 mM Tris-sulfate, pH 7.0, containing 100 U/mL catalase was stopped-flow mixed with 1 volume of a freshly prepared pH 13 solution of ~2 mM potassium superoxide. The dilution factor would result in 44 μM 2Fe-SOR_{clear} [$Fe(NHis)_4(SCys)$] sites and ~180 μM superoxide immediately after mixing. The post-mixing pH was measured to be 7.8. (**A**) difference absorption spectra (reaction with pH 13 superoxide solution minus reaction with an aerobic pH 13 solution (0.1 M sodium hydroxide)) recorded at ~1 msec, gray trace, and 40 msec, bold black trace, after the mixing dead times, and every 10 msec in between (thinner traces). Inset shows corresponding time courses measured by the absolute absorbance changes at 590 nm and 660 nm. (**B**) Absolute absorption spectra recorded ~1 msec, gray trace, and 1,800 msec, bold black trace, after the mixing dead times and every 200 msec in between (thinner traces). Inset shows the corresponding kinetic trace at 500 nm. Arrows show directions of absorbance changes with time.

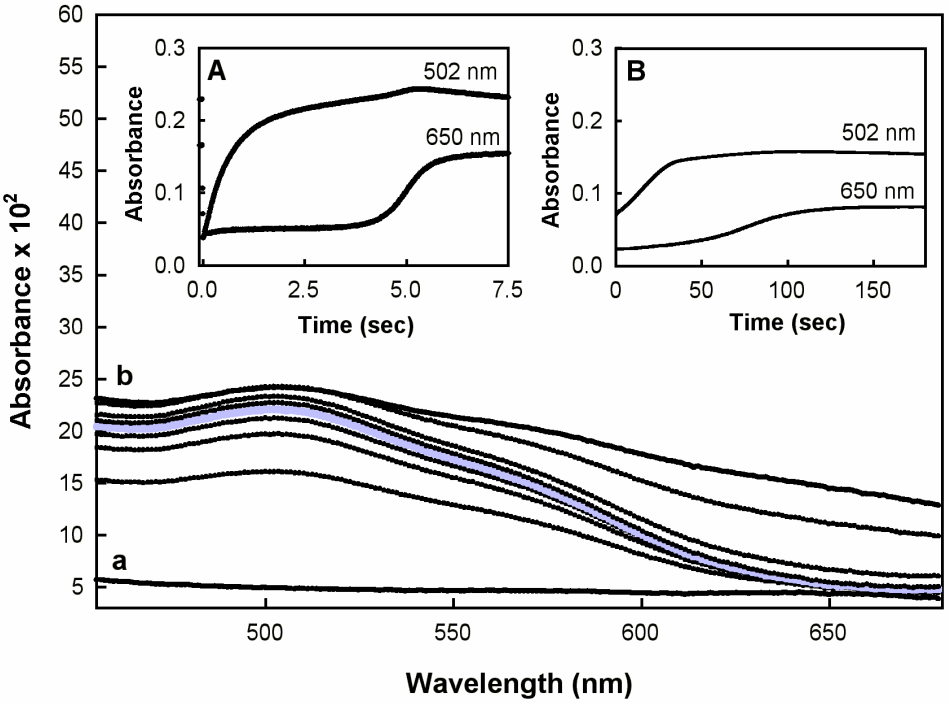

Figure 5.3. Rapid-scanning spectroscopy following stopped-flow mixing of 2Fe-SOR$_{clear}$ with dioxygen solutions. Buffer used for all solutions was 50 mM MOPS, pH 7.5, 200 U/mL catalase. An anaerobic solution of 2Fe-SOR$_{clear}$, 100 μM in [Fe(NHis)$_4$(SCys)] sites, was stopped-flow mixed 1:1 (v/v) with dioxygen-saturated solution, resulting in 50 μM 2Fe-SOR$_{clear}$ [Fe(NHis)$_4$(SCys)] sites and 0.6 mM dioxygen immediately after mixing. Spectral scans from 450 nm to 700 nm obtained ~ 1 msec, **a**, and 250 seconds, **b**, after the mixing dead time, as well as every 500 msec in between (thinner traces). The gray trace, recorded 2 sec after the mixing dead time most closely resembles that of "resting" 2Fe-SOR$_{pink}$, and trace **b**, that of "resting" 2Fe-SOR$_{gray}$. Insets: (**A**) kinetic traces at 500 nm and 650 nm for the spectra shown in the main figure, to which k_{obs} were fit to 1.6 ± 0.5 and 2.6 ± 0.5 sec^{-1}, respectively. (**B**) kinetic traces at 500 nm and 650 nm for the same reaction but mixing with air-saturated buffer ([2Fe-SOR$_{clear}$] = 38 μM and [O_2] = 125 μM immediately after mixing), to which k_{obs} of 0.40 ± 0.05 and 0.4 ± 0.1 sec^{-1}, respectively, were fit. The k_{obs} for the 650 nm traces do not include the "lag" phase (see text).

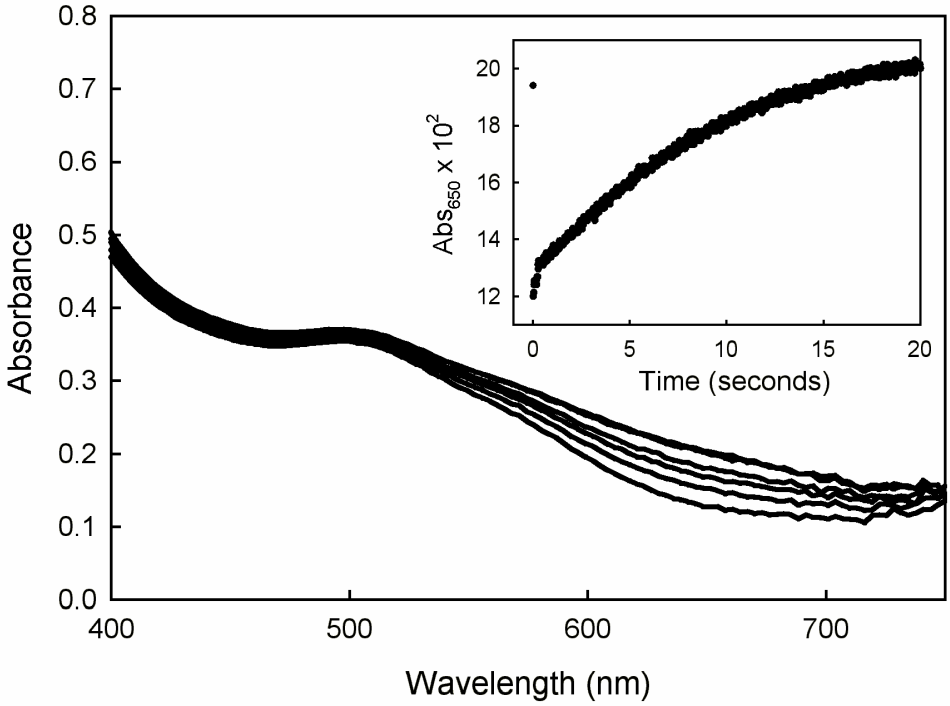

Figure 5.4. Rapid-scanning spectroscopy following stopped-flow mixing of *D. vulgaris* 2Fe-SOR_{pink} with excess H_2O_2. A solution of 150 μM in [$Fe(NHis)_4(SCys)$] sites 2Fe-SOR_{pink} in 50 mM sodium phosphate, 100 μM EDTA, at pH 7.5 was mixed (1:1 v/v) with a 900 mM (6 equivalents) H_2O_2 solution in 50 mM sodium phosphate, 100 μM EDTA, pH 7.5, resulting in 75 μM [$Fe(NHis)_4(SCys)$] sites and 450 μM H_2O_2 immediately after mixing. Spectral scans from 400 to 700 nm are shown, the first (having the lowest absorption) recorded 2 msec after the mixing dead time, and every 3.2 seconds thereafter until ~ 20 seconds. The inset shows the corresponding kinetic trace at 650 nm, to which a k_{obs} of 0.10 ± 0.01 sec^{-1} was fit.

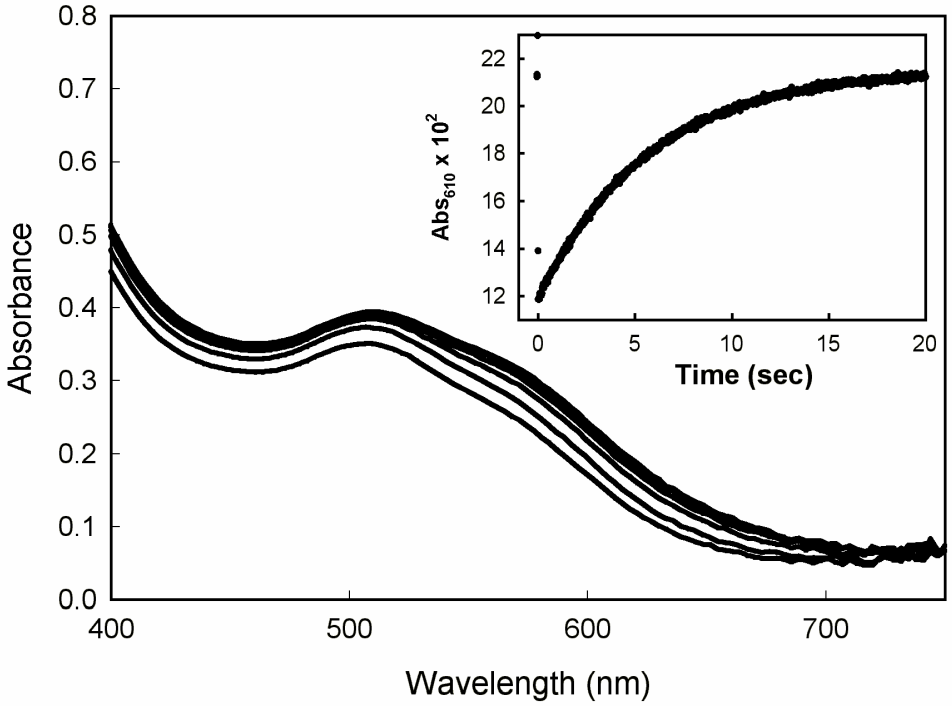

Figure 5.5. Rapid-scanning stopped-flow spectroscopy following stopped-flow mixing of *D. vulgaris* E47A 2Fe-SOR_{pink} with H_2O_2. A solution of 150 μM in [$Fe(NHis)_4(SCys)$] sites E47A 2Fe-SOR_{pink} in 50 mM sodium phosphate, 100 μM EDTA, at pH 7.5 was mixed (1:1 v/v) with a 900 mM (6 equivalents) H_2O_2 solution in 50 mM sodium phosphate, 100 μM EDTA, pH 7.5, resulting in 75 μM [$Fe(NHis)_4(SCys)$] sites and 450 μM H_2O_2 immediately after mixing. Spectral scans from 400 to 700 nm are shown, the first (having the lowest absorption) recorded 2 msec after the mixing dead time, and every 3.2 seconds thereafter until ~ 20 seconds. The inset shows kinetic traces at 650 nm, to which a k_{obs} of 0.20 ± 0.04 sec^{-1} was fit.

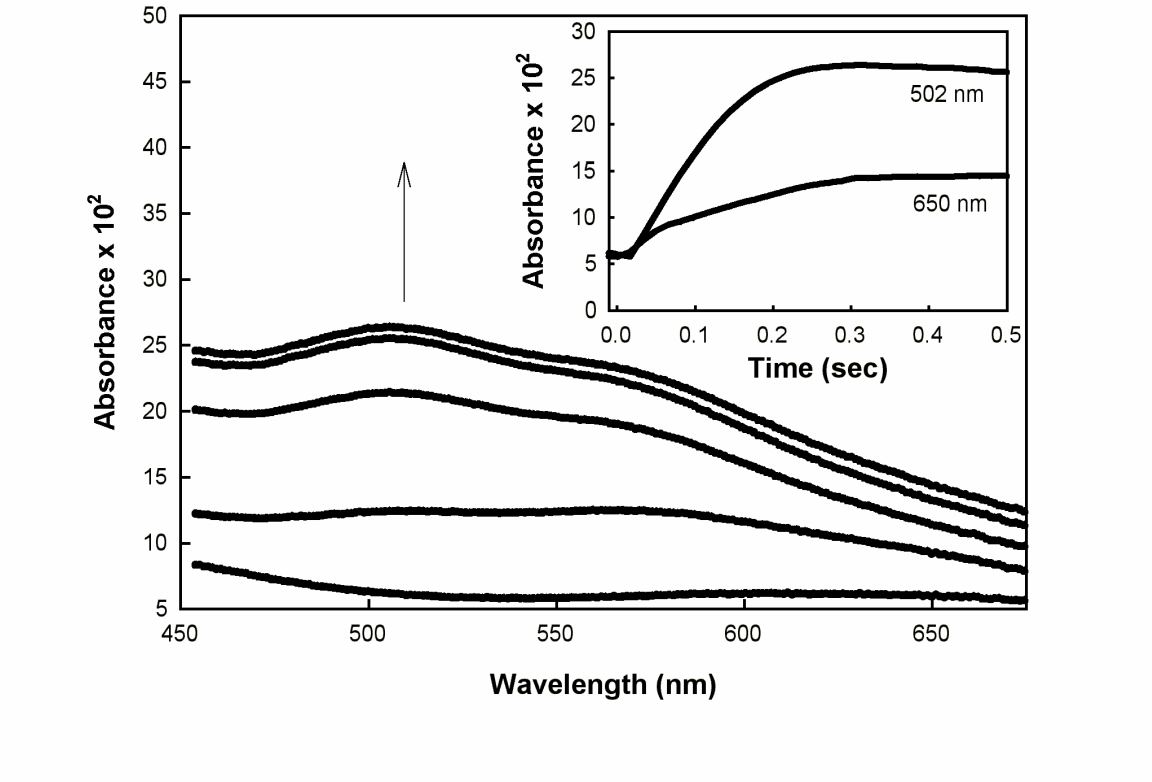

Figure 5.6. Rapid-scanning spectroscopy following stopped-flow mixing of *D. vulgaris* 2Fe-SOR$_{clear}$ with hydrogen peroxide. An anaerobic solution of 52 μM in both [Fe(NHis)$_4$(SCys)] and [Fe(SCys)$_4$] sites 2Fe-SOR$_{clear}$ in 50 mM sodium phosphate, 100 μM EDTA pH 7.5 was mixed (1:1 v/v) with an aerobic 1 mM hydrogen peroxide solution in the same buffer, resulting in 26 μM in 2Fe-SOR$_{clear}$ and 500 μM hydrogen peroxide immediately after mixing. Spectral scans from 450 to 680 nm are shown, the first one scan recorded 2 msec after the mixing dead time, and every 80 msec thereafter until ~ 0.5 seconds. Arrow shows direction of absorption change with time. The inset shows kinetic traces at 502 and 650 nm, to which k_{obs} of 14 ± 3 and 4.3 ± 1.5 sec^{-1}, respectively, were fit.

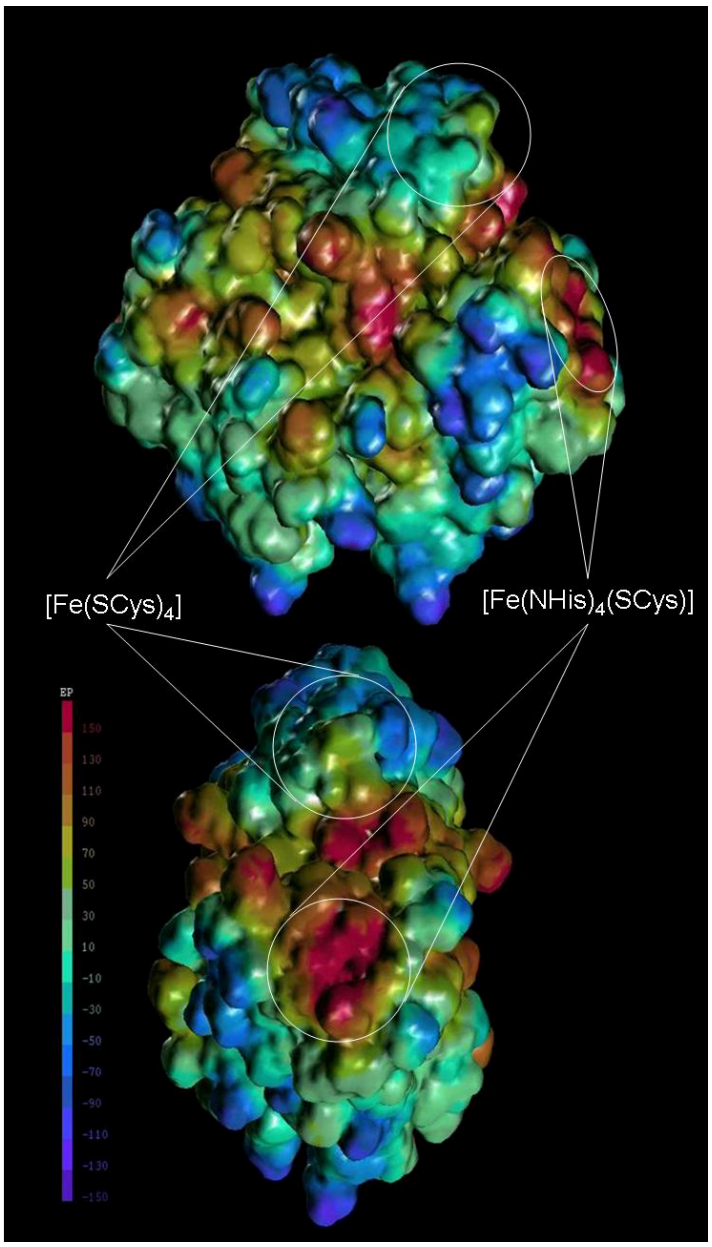

Figure 5.7. Electrostatic potential surfaces of *D. desulfuricans* 2Fe-SOR generated within the Sybyl (version 6.7) software package at the UGA SVMGL facility by Radu Silaghi-Dumitrescu. *D. desulfuricans* 2Fe-SOR coordinate file, 1DFX, was retrieved from the Protein Data Bank and prepared as follows: water molecules were removed, protons were added, Gasteiger-Huckel charges were added. Red and blue indicate positively and negatively charged regions, respectively.

Scheme 5.1.

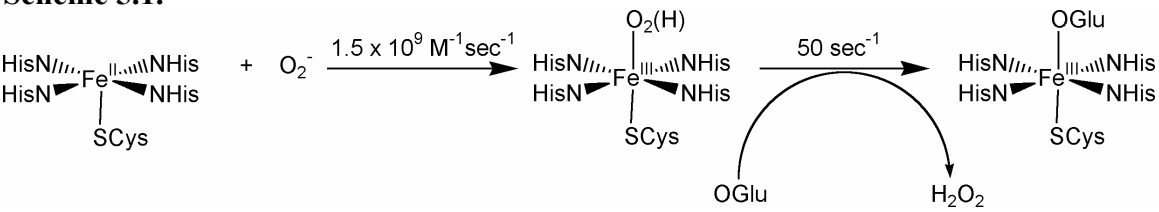
HisN
HisN
Fe
NHis
NHis
SCys
+
O_2^-
1.5 x 10^9 $M^{-1}sec^{-1}$
O_2(H)
50 sec^{-1}
OGlu
H_2O_2

Scheme 5.2.

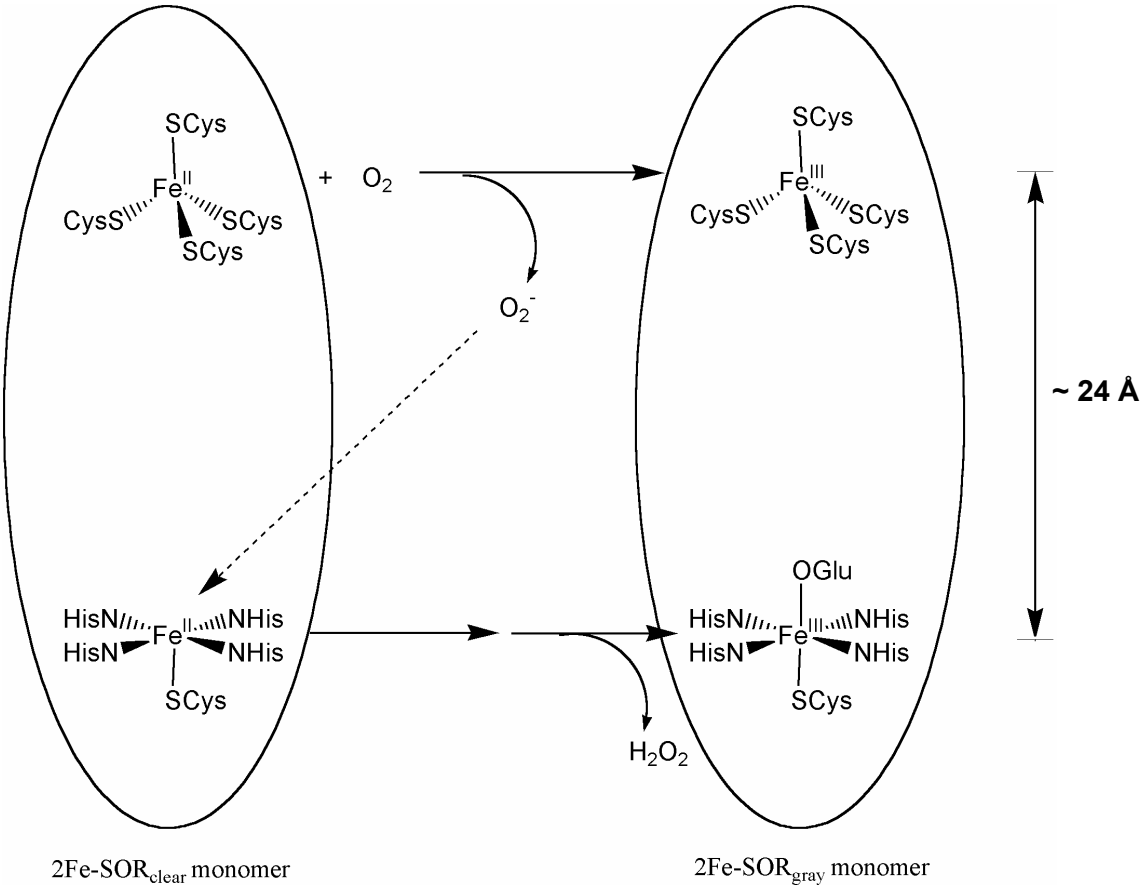
SCys
Fe II
CysS
SCys
SCys
+ O2
O2-
SCys
Fe III
CysS
SCys
SCys
~ 24 Å
HisN
HisN
Fe II
NHis
NHis
SCys
OGlu
HisN
HisN
Fe III
NHis
NHis
SCys
H2O2
2Fe-SORclear monomer
2Fe-SORgray monomer